REPORT NO.
EERC 76-8
MAY 1976

EARTHQUAKE ENGINEERING RESEARCH CENTER

CYCLIC SHEAR TESTS OF MASONRY PIERS
VOLUME 1 - TEST RESULTS

by
RONALD L. MAYES
YUTARO OMOTE
RAY W. CLOUGH

Report to the National Science Foundation

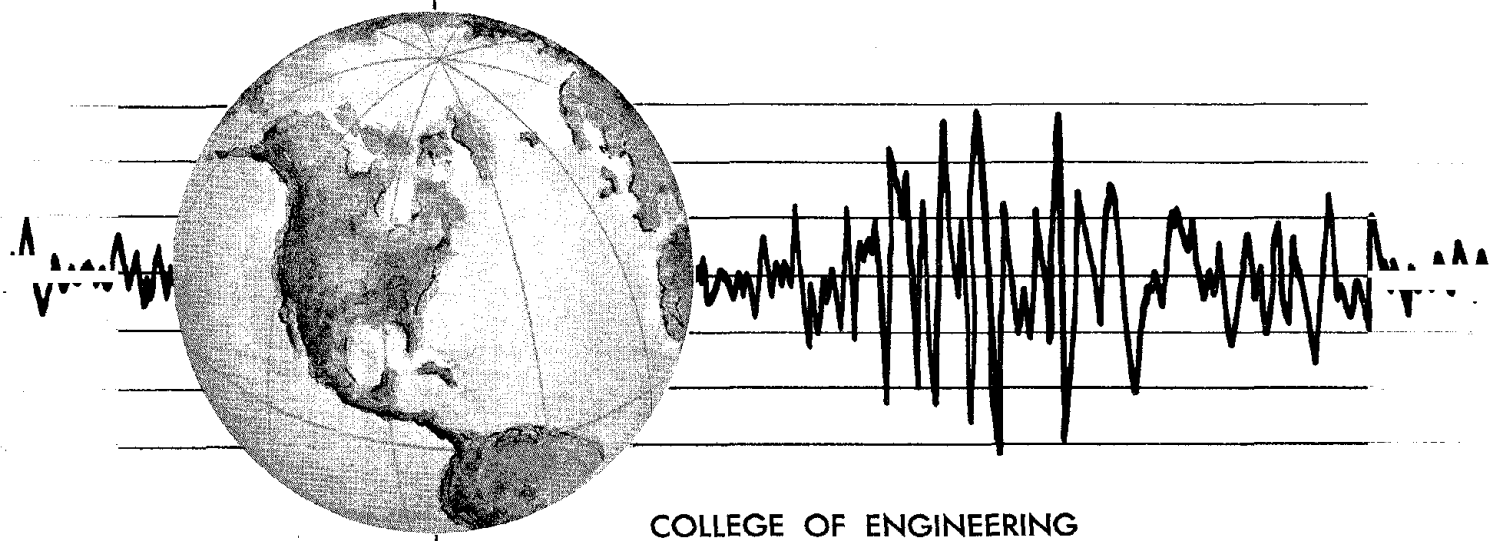

COLLEGE OF ENGINEERING

UNIVERSITY OF CALIFORNIA • Berkeley, California

For sale by the National Technical Information Service, U. S. Department of Commerce, Springfield, Virginia 22161.

See back of report for up to date listing of EERC reports.

BIBLIOGRAPHIC DATA SHEET	1. Report No. EERC 76-8	2. [illegible] Accession No.

4. Title and Subtitle
"Cyclic Shear Tests of Masonry Piers, Volume I - Test Results"

PB 264 424

5. Report Date
May 1976

7. Author(s)
Ronald L. Mayes, Yutaro Omote, Ray W. Clough

8. Performing Organization Rept. No. 76-8

9. Performing Organization Name and Address
Earthquake Engineering Research Center
University of California, Berkeley
1301 S. 46th Street
Richmond, California 94804

10. Project/Task/Work Unit No.

11. Contract/Grant No.
NSF AEN 73-07732

12. Sponsoring Organization Name and Address
National Science Foundation
1800 G Street, N.W.
Washington, D. C. 20550

13. Type of Report & Period Covered

14.

15. Supplementary Notes

16. Abstracts

This report presents the results of cyclic in-plane shear tests on a variety of fixed ended masonry piers. The test set-up is designed to simulate insofar as possible the boundary conditions the piers would experience in a perforated shear wall of a complete building. Each test specimen was a full scale panel about 15 feet (3 meters) square consisting of two piers and a top and bottom spandrel. The panels were constructed from 6" wide x 8" high x 16" long hollow concrete block units. The variables included in the investigation were the quantity and distribution of reinforcement including joint reinforcement, the rate of load application, partial grouting and the vertical bearing stress.

The results are presented in the form of hysteresis envelopes, graphs of stiffness degradation properties and tabulated data on the ultimate strength and ductility indicators. Part II of this report, EERC Report No. 76-16, provides a comparison of the results obtained from the double-pier tests with those obtained from a simple diagonal test and with other investigations, as well as a correlation of the test results with theoretically predicted results and comments on the design implications of the test results.

17b. Identifiers/Open-Ended Terms

17c. COSATI Field/Group

18. Availability Statement	19. Security Class (This Report)	21. No. of Pages
Release Unlimited	UNCLASSIFIED	108
	20. Security Class (This Page) UNCLASSIFIED	22. Price

CYCLIC SHEAR TESTS OF MASONRY PIERS
VOLUME I - TEST RESULTS

by

Ronald L. Mayes
Yutaro Omote
and
Ray W. Clough

Proposed under the sponsorship of the
National Science Foundation
Grant NSF AEN 73-07732

EERC Report No. 76-8
Earthquake Engineering Research Center
College of Engineering
University of California
Berkeley, California

May 1976

ia

SUMMARY

This report presents the results of cyclic in-plane shear tests on a variety of fixed ended masonry piers. The test set-up is designed to simulate insofar as possible the boundary conditions the piers would experience in a perforated shear wall of a complete building. Each test specimen was a full scale panel about 15 feet (3 meters) square consisting of two piers and a top and bottom spandrel. The panels were constructed from 6" wide x 8" high x 16" long hollow concrete block units. The variables included in the investigation were the quantity and distribution of reinforcement including joint reinforcement, the rate of load application, partial grouting and the vertical bearing stress.

The results are presented in the form of hysteresis envelopes, graphs of stiffness degradation properties and tabulated data on the ultimate strength and ductility indicators. Part II of this report, EERC Report No. 76-16, provides a comparison of the results obtained from the double-pier tests with those obtained from a simple diagonal test and with other investigations, as well as a correlation of the test results with theoretically predicted results and comments on the design implications of the test results.

ACKNOWLEDGEMENTS

This investigation was partly sponsored by the National Science Foundation under Grant No. AEN 73-07732 and the Masonry Institute of America. The authors wish to thank Mr. W. L. Dickey, a consulting Structural Engineer of the Masonry Institute of America for the help and encouragement he has given as an industry consultant throughout the test program. The authors also wish to thank S. W. Chen, J. Kubota, A. Shaban and A. Agarwal for their help in performing the tests and reducing the test data, and Mrs. B. Bolt for reviewing the manuscript.

The typing was done by Shirley Edwards and the drafting by Ms. Gale Feazell.

TABLE OF CONTENTS

LIST OF TABLES

LIST OF FIGURES

1. INTRODUCTION

In spite of its being the oldest building material, the technological development of masonry in earthquake engineering has lagged behind that of other structural materials. The paucity of knowledge on the subject has led to a lack of confidence by engineers in its use in seismic resistant structures. This attitude has been accentuated by a history of poor earthquake performance for "nonengineered" masonry structures.

Most of the experimental evidence obtained to date on the shear strength of masonry structural elements has been obtained under the condition of monotonic loading[1-14]. The three major studies known to the authors on the post-elastic cyclic behavior of masonry cantilever shear walls were performed by Williams[15], Meli and Esteva[16] and Priestley and Bridgeman[17]. Meli concluded that there are two possible modes of failure for cantilever masonry shear walls, (a) shear (diagonal tension) (b) flexure (yield or secondary compression). The shear failure is characterized by diagonal cracks, and the flexure failure by yielding of the tension steel and crushing at the compressive toe of the wall. Williams compared the pseudo-static and dynamic cyclic behavior of four different cantilever shear walls and concluded that strain rate may be an important factor in their performance; thus, contrary to frequently accepted opinion, cyclic pseudo-static test results may be inappropriate for use as a conservative basis for seismic design in masonry. The most interesting result of Priestley and Bridgeman's research was the significant improvement observed in the inelastic characteristics of piers failing in the flexural mode when joint reinforcement was added. A summary and analysis of all the investigations

performed to data are presented in two reports by Mayes and Clough[18,19].

The primary shear resisting elements of multistory reinforced masonry buildings are vertical cantilever, coupled or perforated, shear walls such as those shown in Figure 1.1. The smallest structural components of interest in the perforated shear walls are the single or double-pier elements circled in Figure 1.1. A complete understanding of the earthquake behavior of these elements will be of great help in developing a more realistic model of an entire perforated shear wall and also will aid in understanding the behavior of the coupled and cantilever shear walls. The advantages of the double-pier element chosen for this investigation, Figure 2.1, are the realistic boundary conditions which are provided for the piers, and the ability of the panel to represent reversal of the overturning moment when subjected to a cyclic load. The major disadvantages of such test specimens are the time and cost involved in their construction and testing as compared with a single pier.

This report presents the results obtained from seventeen tests performed on double-pier specimens. An accompanying report -- EERC Report No. 76-16 provides a comparison of the results obtained from the double-pier tests with those obtained from a simple diagonal test and with other investigations, as well as a correlation of the test results with theoretically predicted results and comments on the design implications of the test results. In addition, this test program is being followed by an extensive single-pier test program (including approximately 80 tests) in which the boundary conditions of the piers in the double-pier panel are being simulated as closely as possible by the single-pier test set-up shown in Figure 1.2.

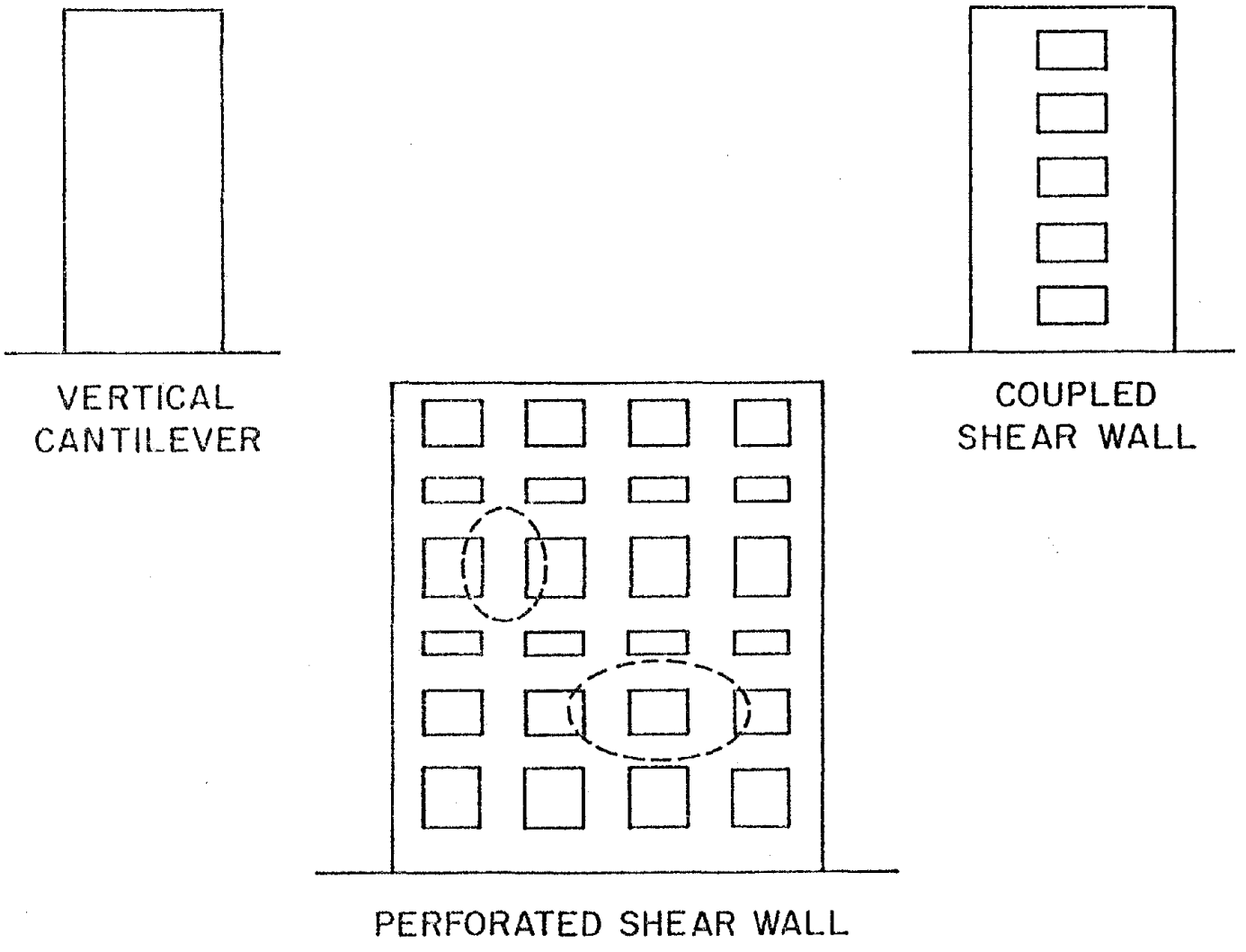

FIGURE 1.1 TYPICAL SHEAR WALLS

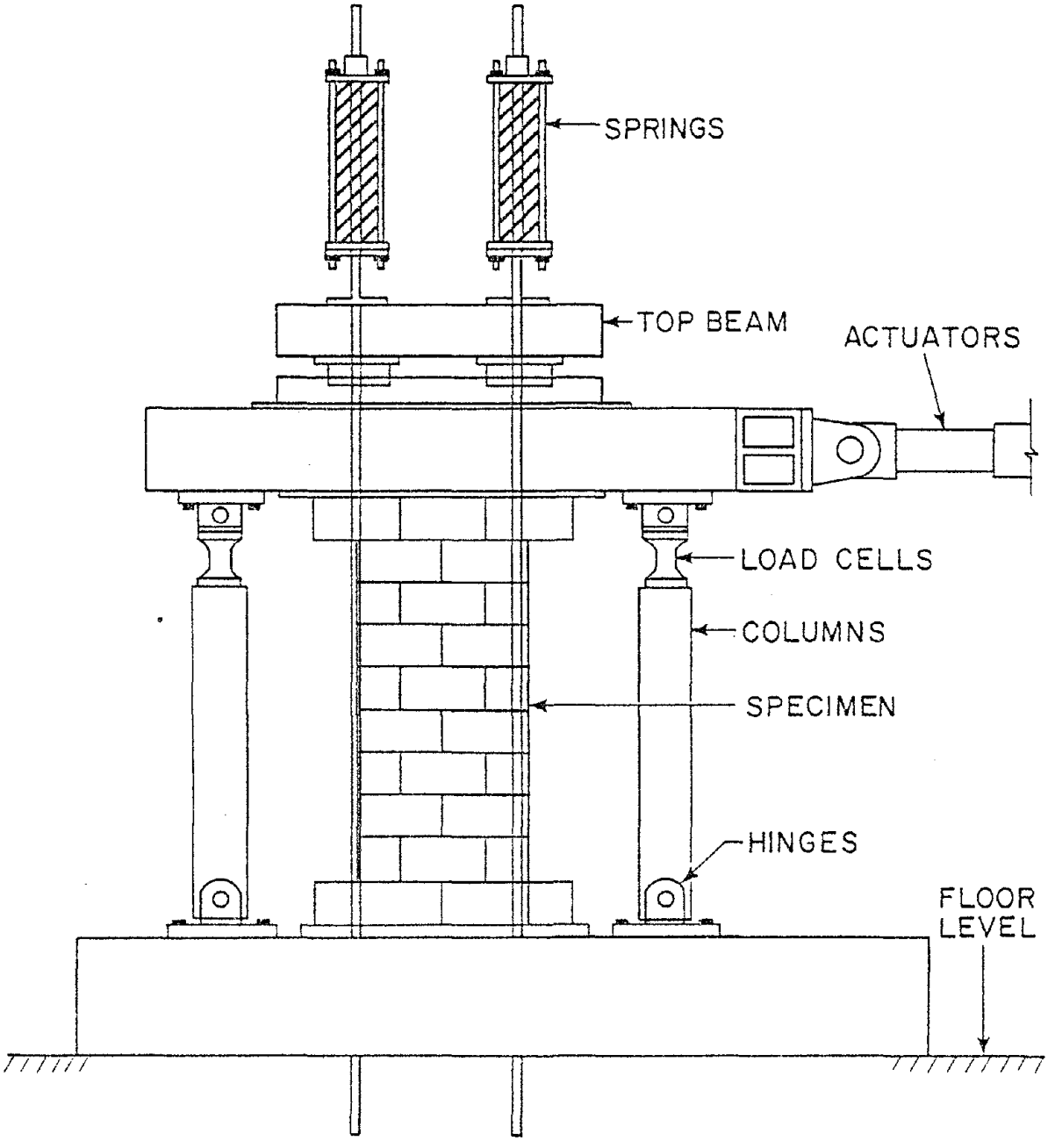

FIGURE 1.2 SINGLE PIER TEST SET-UP

2. DOUBLE-PIER TEST SPECIMEN

2.1 Design of Specimens

The overall dimensions of the seventeen (17) test specimens are the same and are shown in Fig. 2.1. The test specimens were designed to satisfy as closely as possible the boundary conditions of piers in a real structure. The piers, which had a height (5'-4") to width (2'-8") ratio of two, were the elements of interest. The top and bottom spandrels were heavily reinforced (using #7 re-bars as shown in Fig. 2.1) in an attempt to prevent their failure, although this objective was not achieved in all cases.

The panels were constructed from standard two-core reinforcible hollow concrete blocks, nominally 6" wide x 8" high x 16" long as shown in Fig. 2.2. The core of each block has an area of approximately 51.4 square inches with a ratio of net (concrete) to gross (block) area of 58%.

Both the piers and the top and bottom spandrels were fully grouted in fifteen (15) specimens, but only the cores containing the vertical re-bars were grouted in the piers of tests No. 11 and 12 (partially grouted).

The series of seventeen tests was planned to determine the effect of the bearing stress, the rate of loading, the quantity and distribution of reinforcement, and the effect of partial grouting on the strength and deformation properties of the piers, as shown in Table 2.1. In general, the specimens were constructed in identical pairs, one being tested dynamically, the other under pseudo-static conditions. Test specimens No. 1 and 2 were considered as the basic panel, while all other pairs of panels had variations of one or two major properties from those of

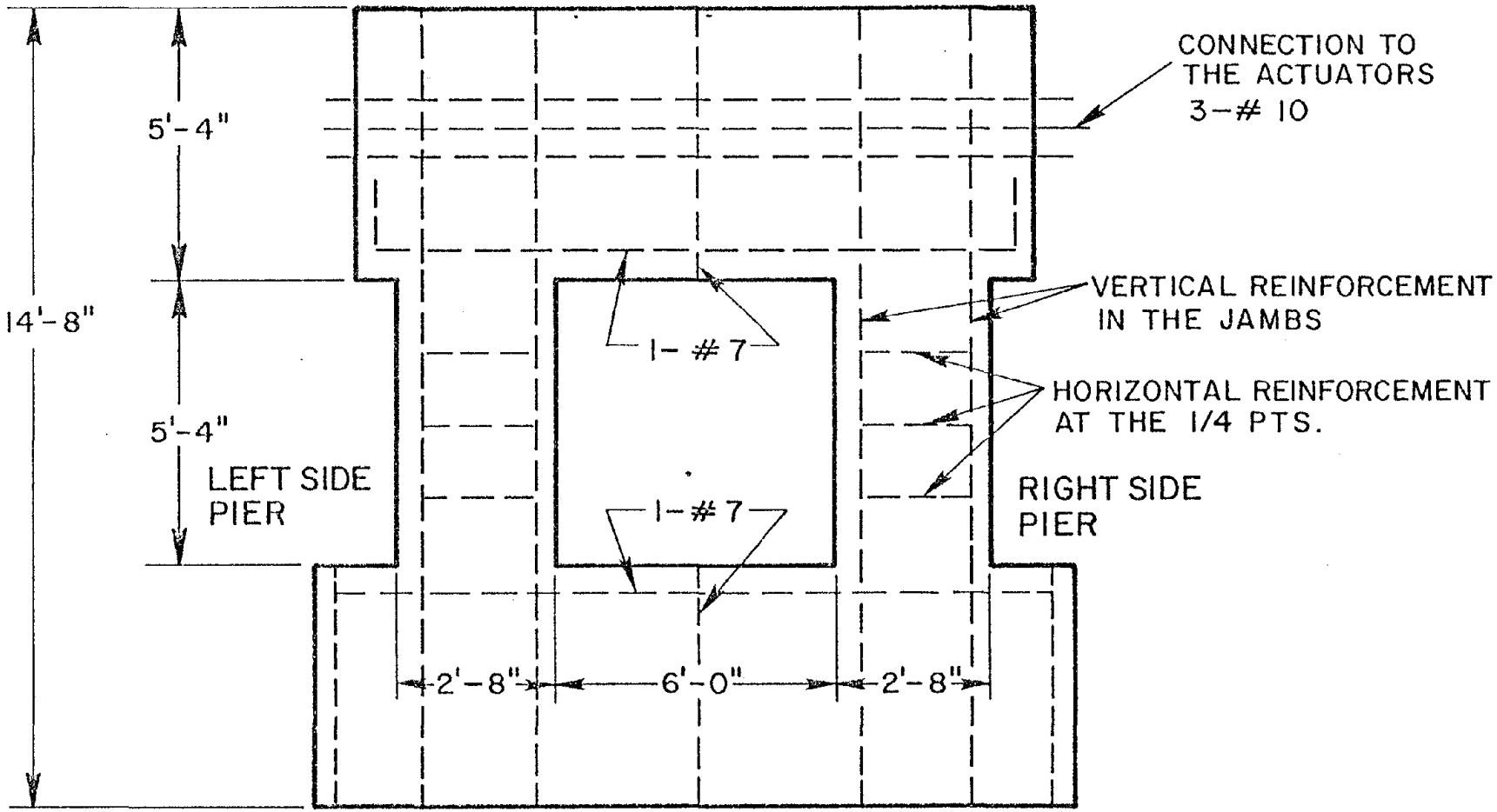

MATERIAL: HOLLOW CONCRETE BLOCKS 6" WIDE x 8" HIGH x 16" LONG.

FIGURE 2.1 TYPICAL DOUBLE-PIER TEST SPECIMEN

8" HIGH UNITS

6" WIDE WALL

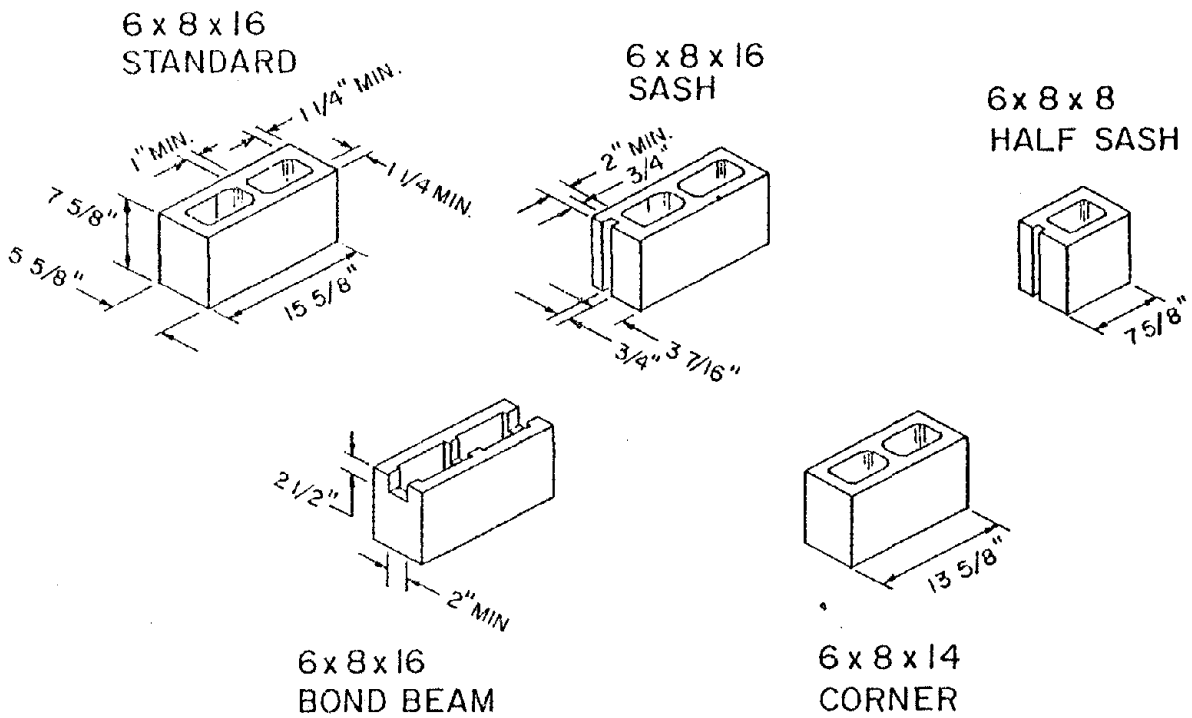

FIGURE 2.2 HOLLOW CONCRETE BLOCK UNIT

TABLE 2.1 MATERIAL AND PIER PROPERTIES

TEST NO.	Frequence[1] (cps)	Bearing Stress[2] (psi)	Vertical Reinforcement[3]	Horizontal Reinforcement[4]	Prism Strength (psi)	Mortar Strength (psi)	Grout Strength (psi)	Reinforcement Stresses[5] Horizontal (ksi)	Reinforcement Stresses[5] Vertical (ksi)	Average Ultimate Shear Strength[6] (psi)
1	0.02	250	2 - #6	--	2280	4955	4510	--	79. (111.)	125
2	3	250	2 - #6	--	2280	4955	4510	--	79. (111.)	161
3	0.02	125	2 - #4	--	2115	3985	3420	--	54.1 (83.4)	135
4	3	125	2 - #4	--	2115	3985	3420	--	54.1 (83.4)	119
5	0.02	0	2 - #6	--	2430	5260	6150	--	78.1 (108.8)	96
6	3	0	2 - #6	--	2430	5260	6150	--	78.1 (108.8)	113
7	0.02	250	2 - #6	1 - #5	2630	5610	4330	67.8 (94.6)	78.1 (108.8)	203
8	3	250	2 - #6	1 - #5	2630	5610	4330	67.8 (94.6)	78.1 (108.8)	229
9	0.02	500	2 - #6	--	2362	3568	3812	--	78.5 (117.5)	149
10	3	500	2 - #6	--	2362	3568	3812	--	78.5 (117.5)	170
11[7]	0.02	250	2 - #6	--	2253 (2587)	2302	2030	--	74.8 (112.6)	98 (126)
12[7]	3	250	2 - #6	--	2253 (2587)	2302	2030	-- -- --	74.8 (112.6)	107 (136)
13	0.02	125	2 - #4	3 - #7 2 - #5	1880	2554	3062	62.9 (89.7)	50.8 (74.9)	135
14	3	125	2 - #4	3 - #7 2 - #5	1880	2554	3062	62.9 (89.7)	51.7 (76.5)	125
15[8]	0.02	125	2 - #4	3 - #7 2 - #5 6 - H.	2105	1766	2450	64.0 (91.6)	51.8 (73.9)	175
16[8]	3	125	2 - #4	3 - #7 2 - #5 6 - H.	2105	1766	2450	64.0 (91.6)	51.3 (75.7)	169
17	3	250	--	--	1908	2760	4575	--	--	108

Notes:
1. Frequency of the sinusoidally applied actuator displacement.
2. Bearing stress based on the gross area (192 sq. in.).
3. Vertical Reinforcement in each jamb of the piers.
4. Horizontal Reinforcement as shown in Figure 2.3.
5. The top value is the yield stress, the value in brackets is the ultimate strength.
6. Average ultimate shear strength = $(P_1 + P_2)/(2 \times \text{gross area})$ where P_1 and P_2 are defined in Figure 4.41(1).
7. Groutad at Ma-Bars only. Values in parentheses are based on the net area.
8. Use the 1/8" plates as shown in Figure 2.4.

No. 1 and 2. Specimen 17 was unique; it did not have an identical mate.

The details of re-bar arrangement are shown in Figure 2.3 for each pair of specimens. Tests 1, 2, 5, 6 and 9 to 12 had 2-#6 vertical re-bars in each jamb of the pier, providing 0.92% of reinforcement based on the gross cross-sectional area. Tests 3 and 4 had 2-#4 vertical re-bars in each jamb and 3-#5 horizontal bars in each pier giving a total of 1.4% reinforcement. Tests 13-16 had a substantial amount of reinforcement (1.67%), arranged to ensure a flexural failure. In addition to the horizontal and vertical bar reinforcement, Tests 15 and 16 had steel plates inserted in the mortar joints at each of the three courses at the top and bottom of each pier[17]. The plate used is shown in Figures 2.4 and 2.5. The piers of Test 17 were completely unreinforced.

2.2 Unit Strength of Materials

The standard two-core reinforcible hollow concrete blocks, when tested as single units, had an average gross compressive strength of 1714 psi (2944 psi net strength) with a range from 1340 psi to 2040 psi over five samples. The average gross tensile strength of the unit was 267 psi with a range from 235 psi to 255 psi over five samples. The block test procedures followed the California Q-Block Quality Control Specification[20].

The joint mortar was specified as standard ASTM-Type M (i.e. 1 Cement: 1/4 Lime: 2 1/4 - 3 Sand), with a minimum strength of 2500 psi. The grout was also specified according to ASTM specifications. Because each of the nine sets of panels were built at different times, the grout and mortar strength for each set varied according to normal workmanship.

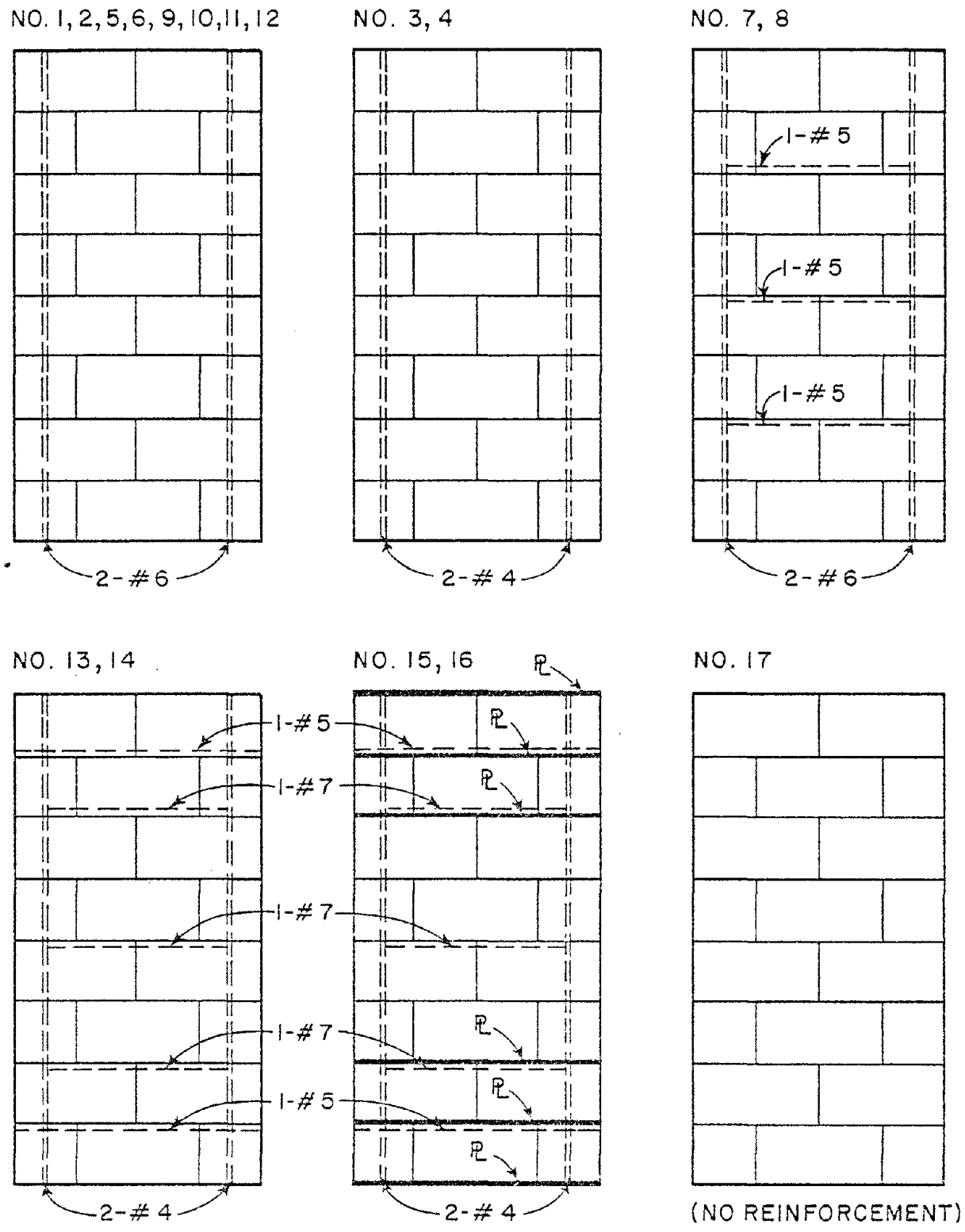

FIGURE 2.3 REINFORCING BAR ARRANGEMENT

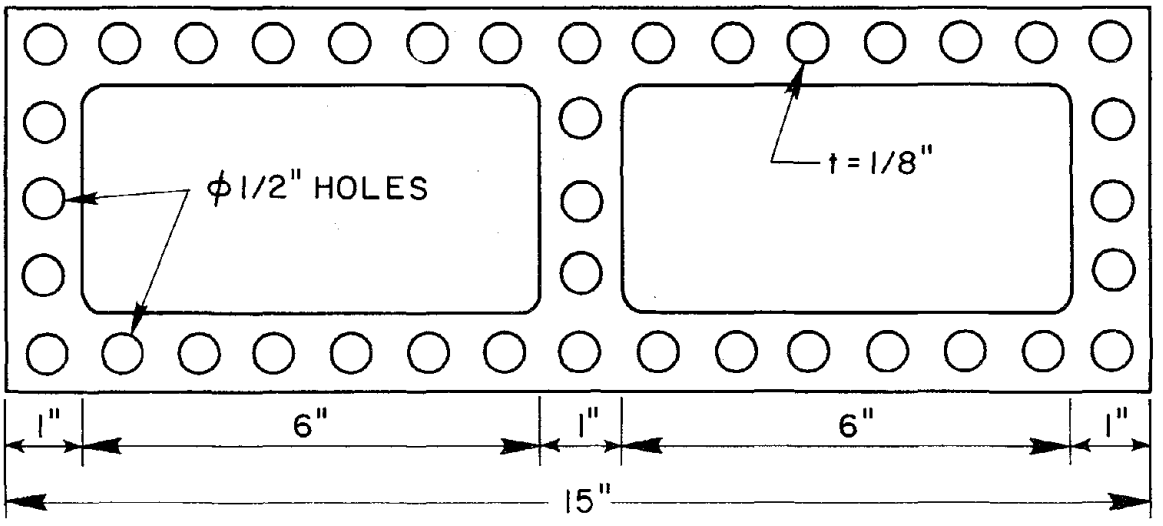

FIGURE 2.4 1/8" STEEL PLATE

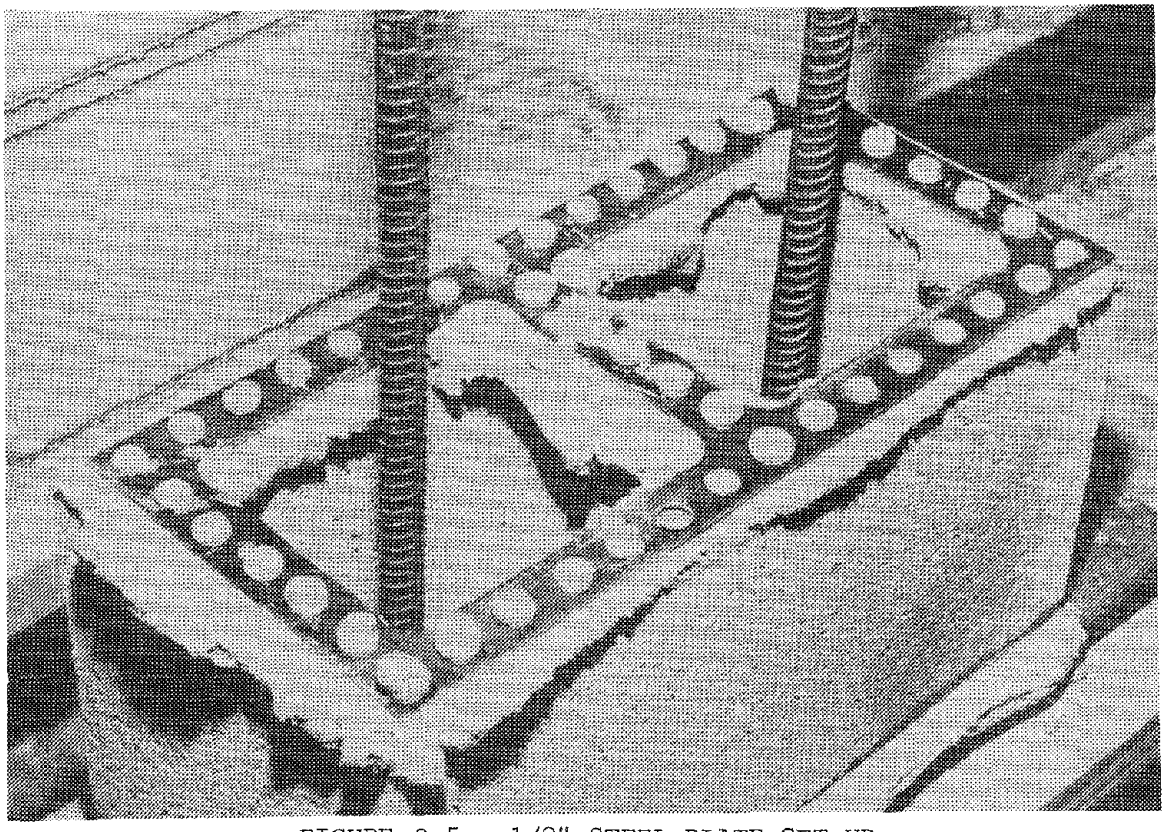

FIGURE 2.5 1/8" STEEL PLATE SET-UP

Five prisms (five blocks high and one long) for compression tests and two to four square panels (32" x 32") for diagonal tension tests were also constructed from the same mortar and grout as were used in each set of wall panels. The mortar, grout, prism and square panel samples were cured under normal atmospheric conditions and generally tested in the 14 days between the tests of the corresponding piers.

The mortar, grout and prism strengths are listed in Table 2.1; the square panel test results are discussed in EERC Report No. 76-16. The double-pier specimens were generally tested 2-3 months after construction.

3. DOUBLE-PIER TEST EQUIPMENT AND PROCEDURE

3.1 Test Equipment

The test equipment shown in Figures 3.1 and 3.2 permits lateral loads to be applied in the plane of the piers in a manner similar to which a floor diaphragm would load the piers during earthquake excitation. It consists of two, twenty-feet high, heavily-braced reaction frames supporting a pair of hydraulic actuators which act horizontally, a mechanism capable of applying vertical bearing loads similar to the gravity loads experienced by the piers in an actual structure, and a concrete base on which the panel is constructed and bolted to the test floor.

The maximum dynamic load which may be developed by the horizontal actuators is 60 kips each. The maximum stroke is ± 6 in., the maximum piston velocity is 26 in./sec. and the flow capacity of the servovalves is 200 gpm. The autuators can be controlled with regard to either displacement or load. The operational capabilities of the actuators are limited by the above mentioned force capacity, and also by a frequency limitation of about 5 Hz. The total load capacity of the test system necessitated the use of six inch thick blocks rather than eight inch thick units.

A vertical load of 160 kips can be applied to each pier through the springs and rollers shown in Figure 3.2. The Thomson Dual Roundway Bearings connecting the springs to the top of the panel allow the panel to move freely with minimal friction force. The coefficient of friction of the bearings is reputed to be 0.007.

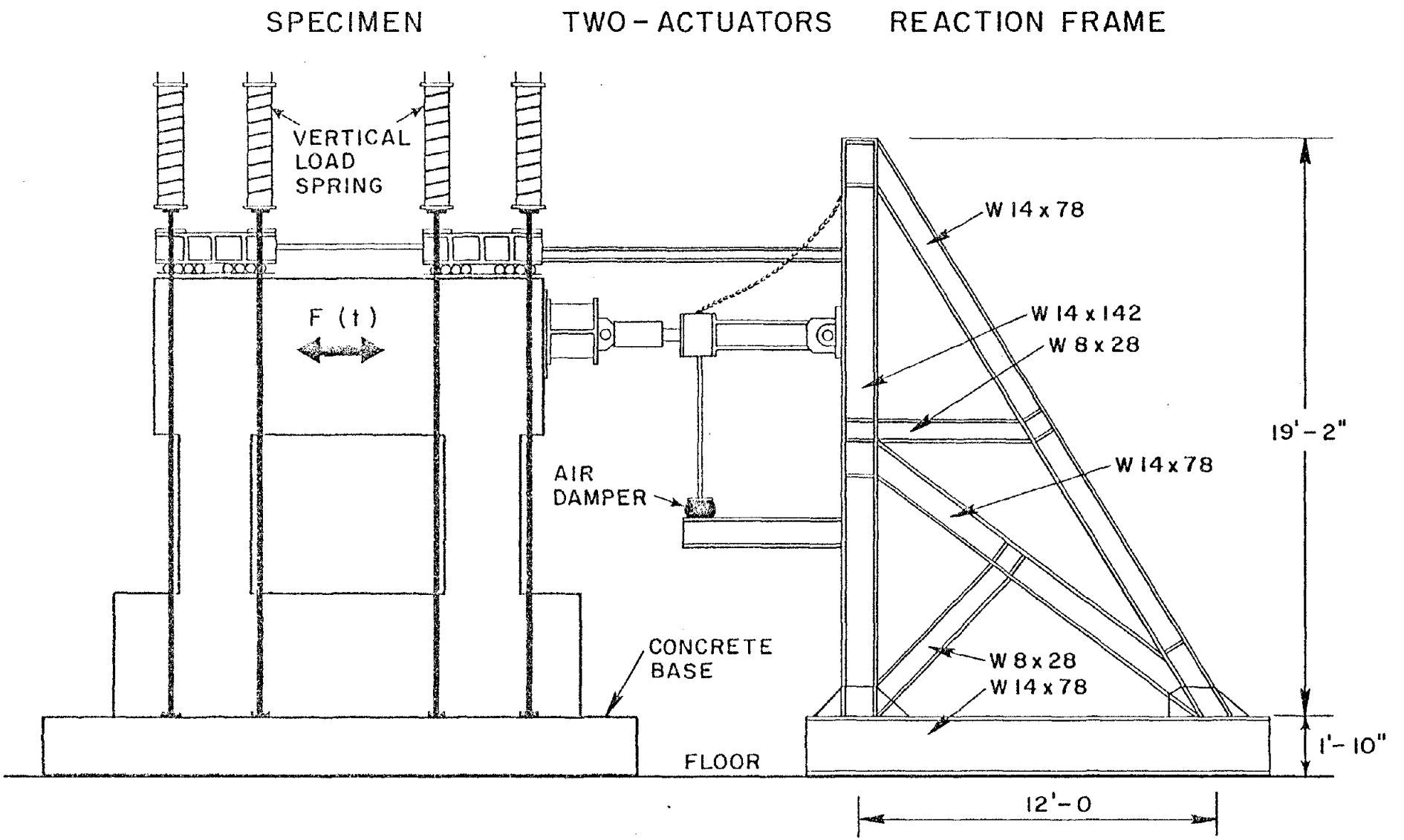

FIGURE 3.1 DOUBLE-PIER TEST SET-UP

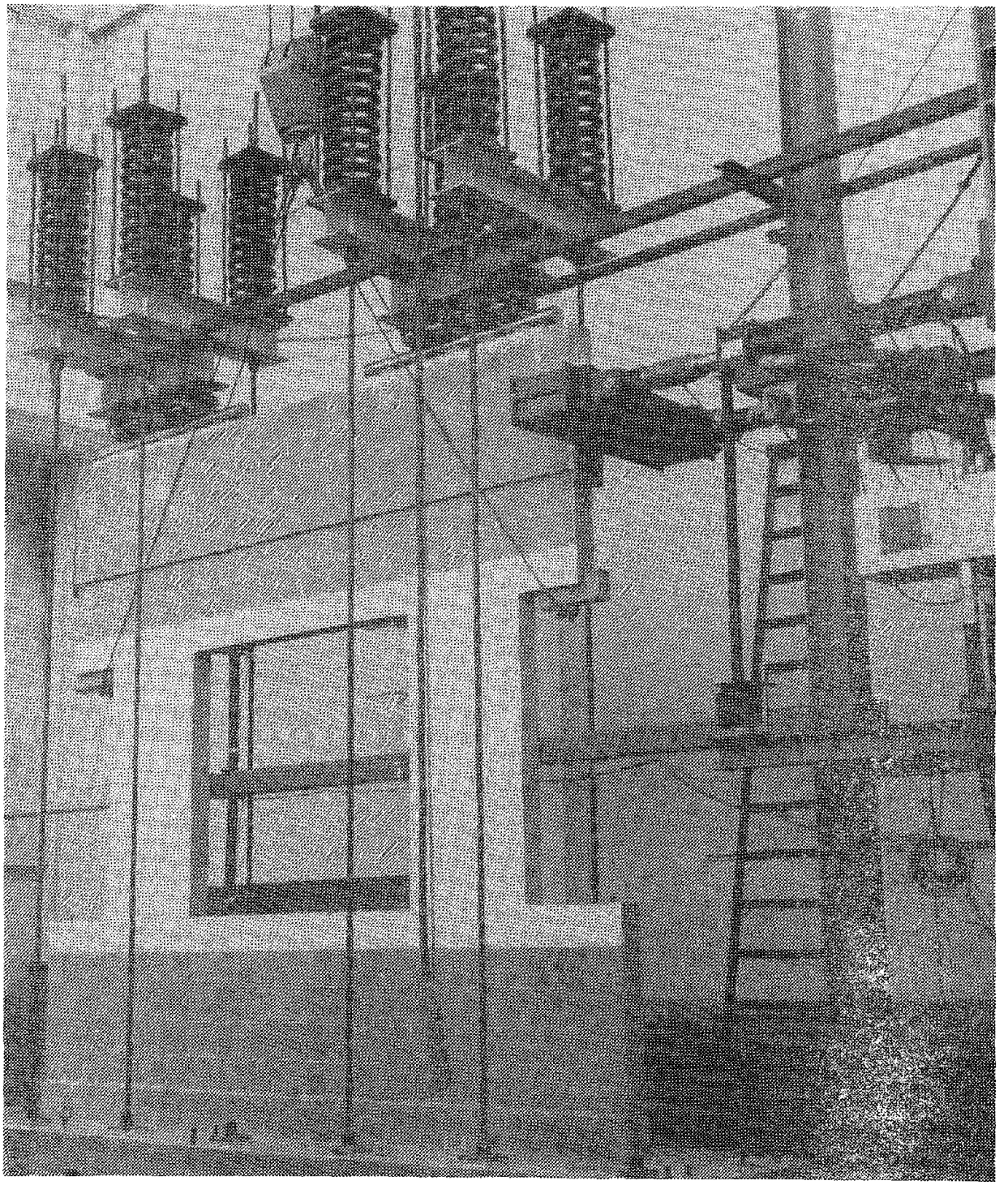

FIGURE 3.2 TEST EQUIPMENT

Each panel was constructed on a 20 ft x 4 ft x 2 ft concrete base which allowed the panels to be moved into place after construction and bolted to the test floor.

3.2 Loading Sequence

Each panel was loaded in an increasing amplitude sequence of simusoidal displacement cycles, with three cycles of each amplitude. The actuator displacements generally followed the sequence 0.02", 0.04", 0.06", 0.08", 0.12", 0.16", 0.20", 0.25", 0.30", --- 0.5", 0.6"----1.0" ----1.5". After each set of 3 displacement cycles, the walls were visually inspected and the crack pattern identified. The sinusoidal cycles were applied at the frequency of 3 Hz in dynamic tests, and at the rate of 0.02 Hz in the pseudo-static tests.

Panels No. 1 to 8 and 13 and 14 were subjected to a maximum input displacement of 1"; panels No. 9 to 12 completely failed at only 0.5"; whereas panels No. 15 and 16 (which had heavy shear reinforcement and 1/8" plates at the compression toes) were subjected to an input displacement of 1.5".

A problem was encountered in the loading procedure due to the fact that the displacement of the piers was controlled by the displacement of the actuators. When the actuators were pushing the panel away from the frame, deflections in the loading system included the effects of flexibility in the reaction frame and loading beam. In the reverse cycle, the actuators were pulling the panel towards the frame and additional deflections arose from tension placed on the bolting system. This resulted in larger deflections being applied to the panels in the pushing direction than while pulling, the effect being most pronounced at the higher load levels.

3.3 Instrumentation and Data Reduction

The total load applied by the hydraulic actuators was measured by a force transducer. The deflections at the center of the top and bottom of each pier were measured by either LVDT's (linear variable differential transformers) or DCDT's (direct current differential transformers) attached to the reference frame. The difference between the top and bottom measurements was used to indicate the relative deflection of each pier.

The force and displacement transducer outputs were amplified and recorded by a direct writing oscillograph (Visicorder). In Test No. 17, the data were also recorded in digital form on magnetic tape with the use of a high speed data acquisition system which became available at that time. This test served to verify the applicability of the digital system for future tests. The Visicorder traces had to be digitized manually, thus the potential advantage of the digitally recorded test data was obvious. In either case, the digitized displacement and load data were used to determine relative pier deflections, stiffness and energy absorption characteristics, and were plotted in the form of hysteresis loops.

4. DOUBLE-PIER TEST RESULTS

4.1 Introduction

The results of the seventeen (17) tests are presented in the form of hysteresis loops (Figs. 4.1 to 4.17), graphs of hysteresis envelopes (Figs. 4.37 to 4.40), stiffness degradation properties (Figs. 4.42 to 4.43) and a graph of the energy dissipation characteristics (Fig. 4.44). In addition, data on the maximum input displacement, the ultimate strength, and the ductility indicators for each test are listed in Table 4.1.

The measurements of the loads and displacements used for calculating the data presented are accurate to within $\pm$ 3%. The hysteresis loops, plotted in Figures 4.1 to 4.17 for the successive tests, were obtained by plotting half of the total actuator load against the relative displacement of each pier. The assumption that each pier resists half of the total applied shear force seems to be reasonable for the loading sequences of most tests. In tests 6 and 8 the validity of this assumption at input displacements above 0.25" is dubious because of the cracks developed in the top spandrel and the consequent cantilever type action of the left-side pier (Fig. 2.1). In addition when a large crack (or substantial cracking) developed in one pier and not in the other the assumption is also questionable. This was a rare occurrence as generally both piers developed large cracks at the same input displacement.

The last few displacement cycles are not included in several of the hysteresis loops because the displacement transducers had to be removed as failure was approached in order to avoid damaging them.

4.2 Mode of Failure

Photographs of the final failed state of each panel(*) are presented in Figs. 4.1 to 4.17, together with their corresponding hysteresis loops. The cracked state of the right-side piers (Fig. 2.1) at the working ultimate load (refer to section 4.3) are shown in Figs. 4.18(1) and 4.18(2) for Tests No. 1 to 17. Figures 4.19 to 4.35 show the successive crack formation and associated loads and displacements for all right-side piers. Four different failure modes can be identified in the photographs. Figure 4.36 presents schematic drawings of these four modes of failure. The first, diagonal tension or shear failure, is characterized by diagonal or X cracks similar to the tension failure of a square panel (Fig. 4.36A). This failure mode was observed in Tests 1, 2, 5, 6, 7, 8 and 17. The second diagonal tension and vertical splitting, is shown in Fig. 4.36A'. This was observed in cases of large vertical loadings (Tests 9, 10) and in the case of partially grouted piers (Tests 11, 12). The third mode of failure is combined shear and flexure yielding. It is characterized by a compressive failure at the toe of the pier due to substantial yielding of the tensile steel, combined with diagonal cracking (Fig. 4.36B for Tests 3 and 4). The fourth mode of failure, shown in Fig. 4.36C, is a flexure yielding mechanism characterized by compressive failure at the toe of the piers. Diagonal shear cracking is inhibited in these cases by the horizontal reinforcement (Tests 13-16).

4.3 Load-Displacement Characteristics

To interpret and compare the results of the hysteresis loops presented in Figures 4.1 to 4.17, several "indicators" were determined from the plots:

---

*Numbers indicated in the photographs (Figs. 4.13 to 4.17) are not correlated to the test numbers.

TABLE 4.1 SUMMARY OF TEST RESULTS

TEST NO.	Frequency[1] (cps)	Bearing Stress[2] (psi)	Vertical Reinforcement[3]	Horizontal Reinforcement[4]	$\frac{P_{u1}+P_{u2}}{2}$; $\frac{\tau_{u1}+\tau_{u2}}{2}$ [5] (kips)	(psi)	$\frac{P_1+P_2}{2}$; $\frac{\tau_1+\tau_2}{2}$ [6] (kips)	(psi)	P_3 ; τ_3 [7] (kips)	(psi)	$\frac{\delta_1+\delta_2}{2}$ [8]	$\frac{d_1+d_6}{2}$ [9] (in)	$\frac{\delta_3+\delta_4}{2}$ [10]	$\frac{d_1+d_5}{2}$ [11] (in)	Max. Input Stroke of Actuator (in) [12]
1	0.02	250	2 - #6	--	26.0	135	24	125	20	104	1.55	.095	3.5	.065	1.0
2	3	250	2 - #6	--	33.2	173	31	161	28	146	1.55	.130	2.4	.095	1.0
3	0.02	125	2 - #4	--	27.3	142	26	135	21	109	1.5	.180	4.1	.105	1.0
4	3	125	2 - #4	--	26.0	135	22.8	119	18	94	1.8	.165	5.6	.085	1.0
5	0.02	0	2 - #6	--	20.5	107	18.5	96	15	78	1.55	.180	5.6	.075	1.0
6	3	0	2 - #6	--	25.5	133	21.7	113	19	99	1.85	.105	5.3	.070	1.0
7	0.02	250	2 - #6	1 - #5	40.7	212	39	203	33	172	1.5	.235	4.4	.123	0.7
8	3	250	2 - #6	1 - #5	48.4	252	44	229	33	172	1.45	.350	3.0	.180	1.0
9	0.02	500	2 - #6	--	29.5	154	28.7	149	24	125	2.1	.080	4.1	.060	0.45
10	3	500	2 - #6	--	34.1	178	32.7	170	28	146	2.8	.130	5.6	.055	0.5
11[13]	0.02	250	2 - #6	--	20.0	104 (132)	18.9	98 (124)	17	89 (113)	3.8	.120	6.5	.055	0.5
12[13]	3	250	2 - #6	--	21.8	114 (143)	20.6	107 (136)	18	94 (119)	5.1	.065	8.1	.048	0.55
13	0.02	125	2 - #4	3 - #7, 2 - #5	29.1	151	26.0	135	18	94	1.8	.215	5.2	.075	1.0
14	3	125	2 - #4	3 - #7, 2 - #5	28.8	150	24.0	125	19	99	3.1	.160	6.6	.080	0.9
15	0.02	125	2 - #4	3 - #7, 2 - #5R	35.2	189	33.6	175	23	120	2.5	.320	9.2	.090	1.5
16	3	125	2 - #4	3 - #7, 2 - #5R	36.2	189	32.4	169	22	115	3.4	.190	10.5	.090	1.5
17	3	250	--	--	23.7	123	20.7	108	17	89	1.6	--	--	--	0.7

Notes of Table 4.1

1. Frequency of the sinusoidally applied actuator displacement.
2. Bearing Stress based on the gross area (192 sq. in.).
3. Vertical reinforcement in each jamb of the piers.
4. Horizontal reinforcement as shown in Figure 2.3.
5. P_{ul} and P_{u2} are the peak shear loads in either direction, and defined in Figure 4.41. τ_{ul} and τ_{u2} are the corresponding shear stresses based on the gross area.
6. P_1 and P_2 are the average ultimate shear strengths as defined in Figure 4.41. τ_1 and τ_2 are the corresponding shear stresses based on the gross area.
7. P_3 is a working ultimate shear strength defined in Figure 4.41. τ_3 is the corresponding shear strength based on the gross area.
8. δ_1 and δ_4 are approximate ductility ratios associated with P_1 and P_2 and defined in Figure 4.41.
9. Average value of deflection associated with P_1 and defined in Figure 4.41.
10. δ_3 and δ_4 are ductility indicators associated with P_3 and defined in Figure 4.41.
11. Average value of deflection associated with P_3 and defined in Figure 4.41.
12. Maximum input displacement of activator.
13. Grouted at Re-bars only. Values in parentheses are stresses based on net area. (152 sq. in.).

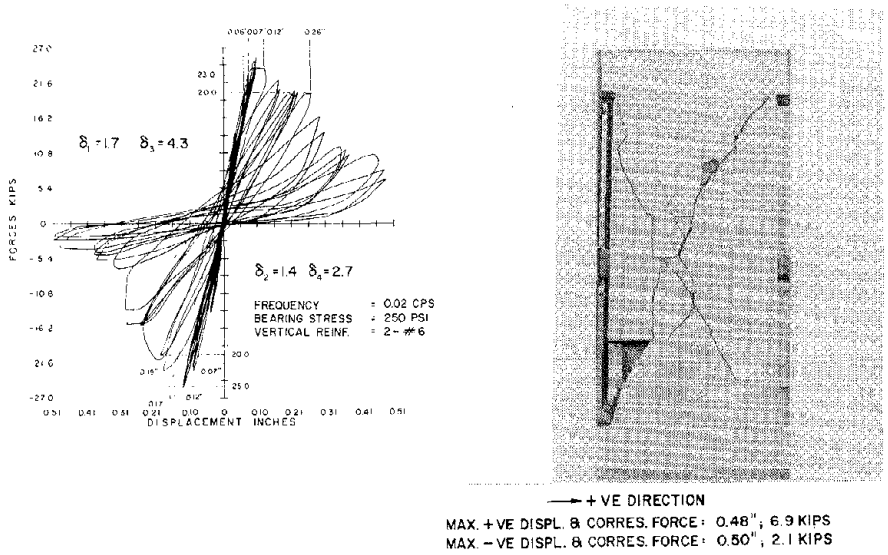

FIGURE 4.1 HYSTERESIS LOOP TEST 1. (RIGHT SIDE PIER)

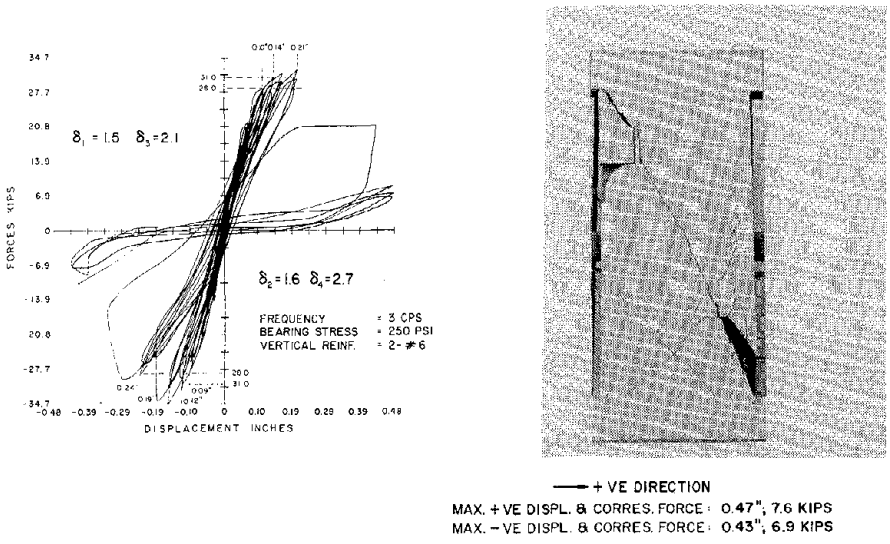

FIGURE 4.2 HYSTERESIS LOOP TEST 2. (RIGHT SIDE PIER)

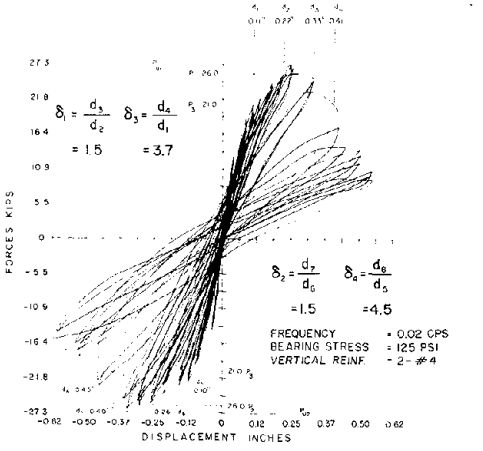

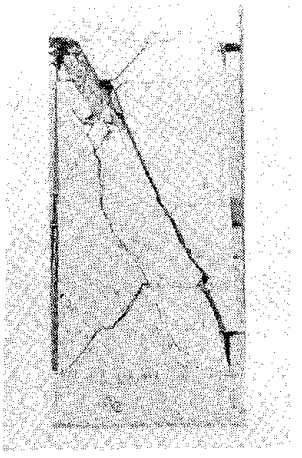

← + VE DIRECTION
MAX. + VE DISPL. & CORRES. FORCE : 0.55"; 11 KIPS
MAX. – VE DISPL. & CORRES. FORCE : 0.58"; 16 KIPS

FIGURE 4.3 HYSTERESIS LOOP TEST 3. (RIGHT SIDE PIER)

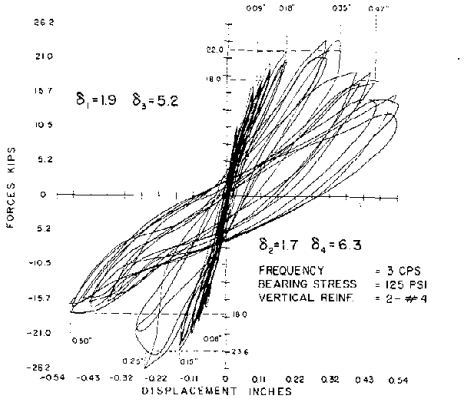

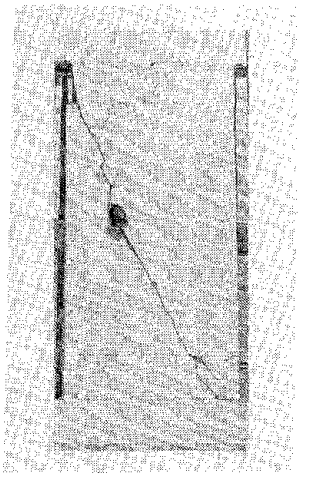

← + VE DIRECTION
MAX. + VE DISPL. & CORRES. FORCE : 0.54"; 16 KIPS
MAX. – VE DISPL. & CORRES. FORCE : 0.50"; 18 KIPS

FIGURE 4.4 HYSTERESIS LOOP TEST 4. (RIGHT SIDE PIER)

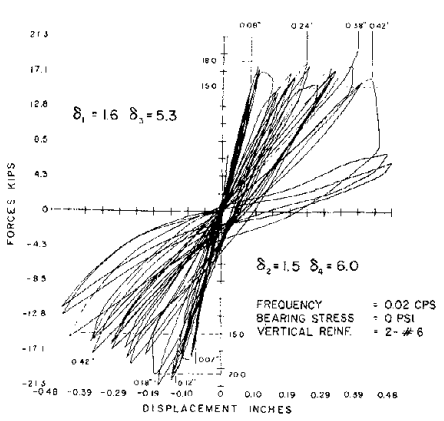

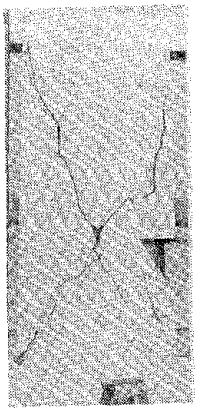

← + VE DIRECTION
MAX. + VE DISPL. & CORRES. FORCE : 0.48"; 6 KIPS
MAX. − VE DISPL. & CORRES. FORCE : 0.45"; 12 KIPS

FIGURE 4.5 HYSTERESIS LOOP TEST 5. (RIGHT SIDE PIER)

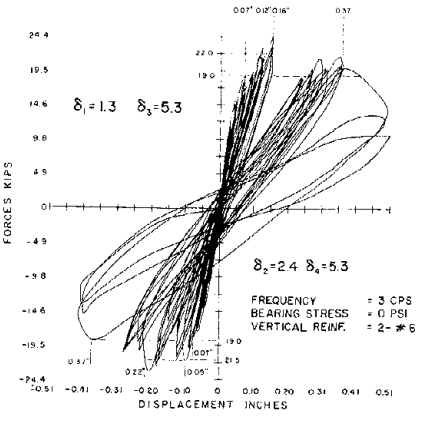

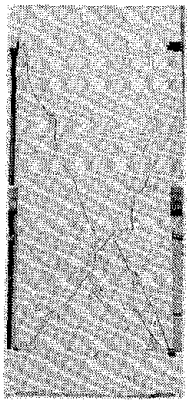

← + VE DIRECTION
MAX. + VE DISPL. & CORRES. FORCE : 0.52"; 10 KIPS
MAX. − VE DISPL. & CORRES. FORCE : 0.43"; 14 KIPS

FIGURE 4.6 HYSTERESIS LOOP TEST 6. (RIGHT SIDE PIER)

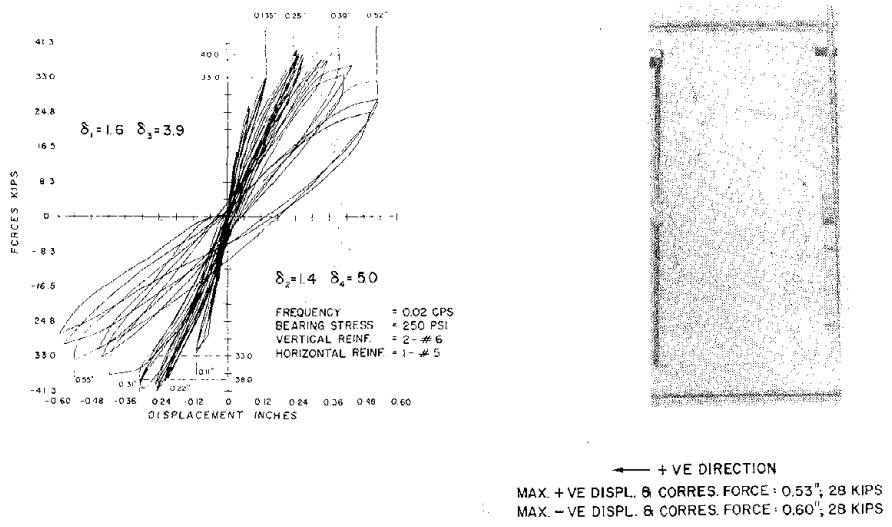

FIGURE 4.7 HYSTERESIS LOOP TEST 7. (RIGHT SIDE PIER)

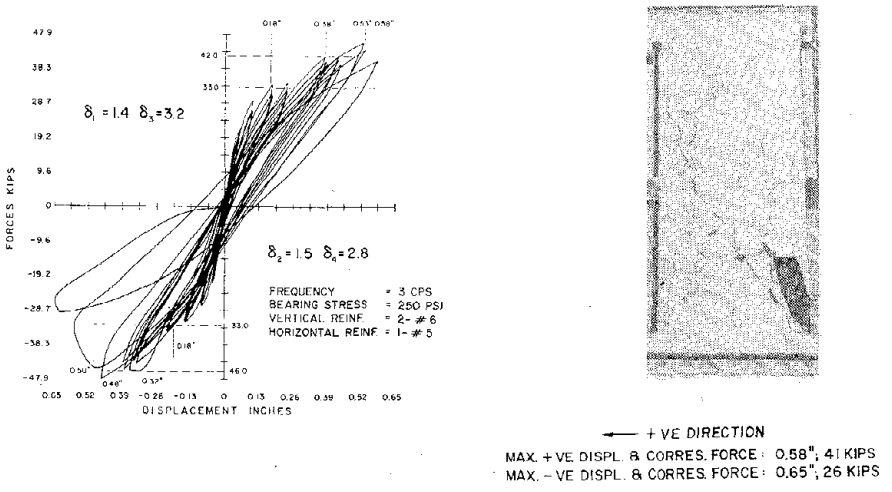

FIGURE 4.8 HYSTERESIS LOOP TEST 8. (RIGHT SIDE PIER)

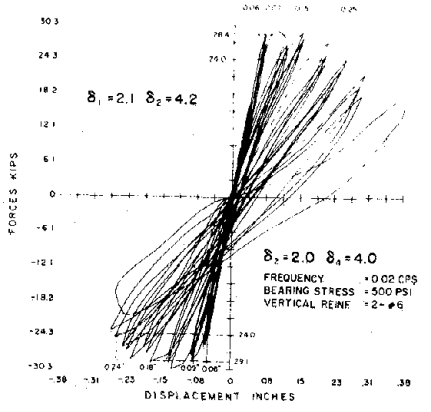

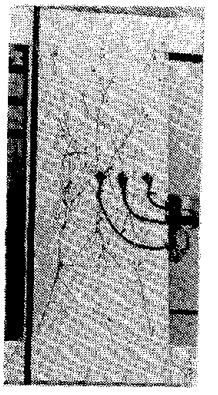

→ + VE DIRECTION
MAX. + VE DISPL. & CORRES. FORCE : 0.29"; 18 KIPS
MAX. − VE DISPL. & CORRES. FORCE : 0.27"; 24 KIPS

FIGURE 4.9 HYSTERESIS LOOP TEST 9. (RIGHT SIDE PIER)

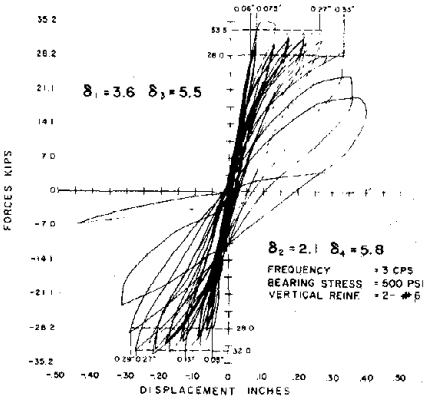

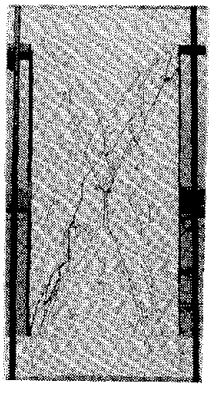

→ + VE DIRECTION
MAX. + VE DISPL. & CORRES. FORCE : 0.38"; 20 KIPS
MAX. − VE DISPL. & CORRES. FORCE : 0.31"; 24 KIPS

FIGURE 4.10 HYSTERESIS LOOP TEST 10. (RIGHT SIDE PIER)

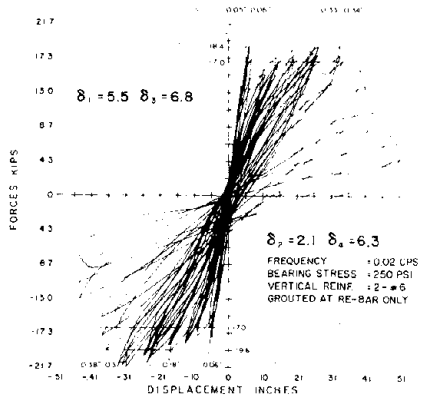

→ + VE DIRECTION
MAX. + VE DISPL. & CORRES. FORCE : 0.51", 4.7 KIPS
MAX. – VE DISPL. & CORRES. FORCE : 0.45", 7.0 KIPS

FIGURE 4.11 HYSTERESIS LOOP TEST 11.(RIGHT SIDE PIER)

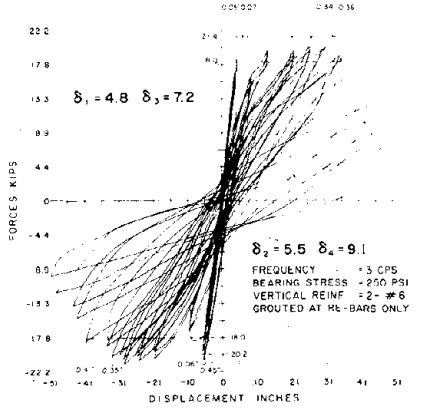

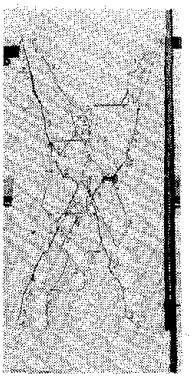

→ + VE DIRECTION
MAX. + VE DISPL. & CORRES. FORCE : 0.44", 10 KIPS
MAX. – VE DISPL. & CORRES. FORCE : 0.45", 14 KIPS

FIGURE 4.12 HYSTERESIS LOOP TEST 12.(RIGHT SIDE PIER)

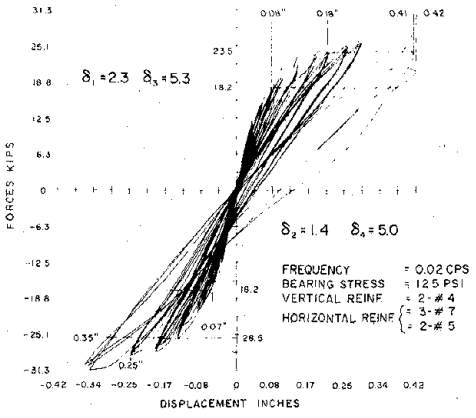

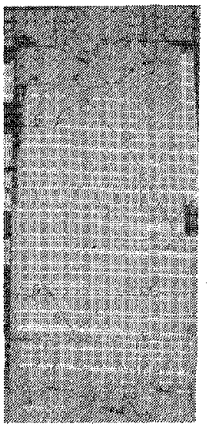

→ + VE DIRECTION
MAX + VE DISPL. & CORRES. FORCE: 0.42", 27 KIPS
MAX − VE DISPL. & CORRES. FORCE: 0.35", 31 KIPS

FIGURE 4.13 HYSTERESIS LOOP TEST 13. (RIGHT SIDE PIER)

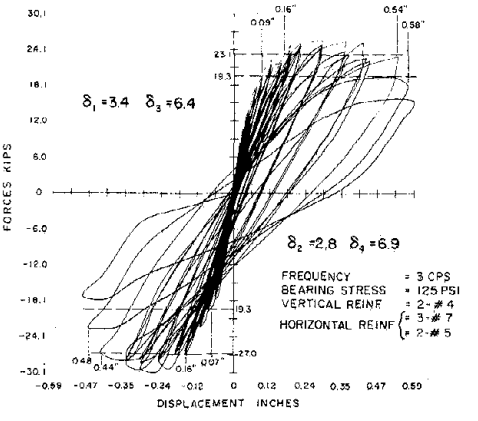

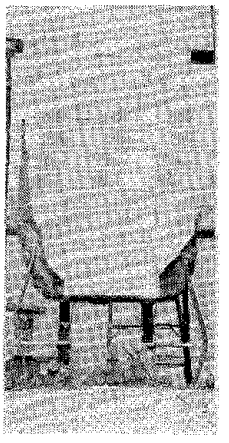

→ + VE DIRECTION
MAX. + VE DISPL. & CORRES. FORCE: 0.37", 26 KIPS
MAX. − VE DISPL. & CORRES. FORCE: 0.26", 30 KIPS

FIGURE 4.14 HYSTERESIS LOOP TEST 14. (RIGHT SIDE PIER)

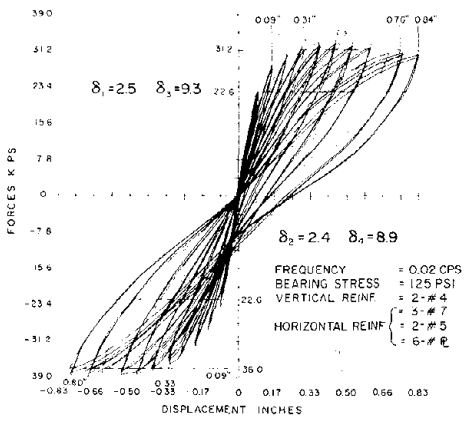

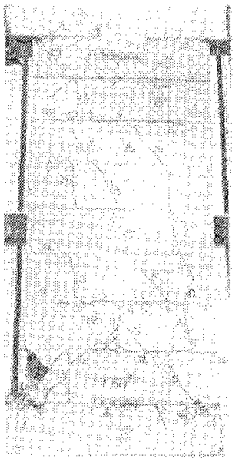

← + VE DIRECTION
MAX. + VE DISPL. & CORRES. FORCE : 0.52", 33 KIPS
MAX. – VE DISPL. & CORRES. FORCE : 0.47", 38 KIPS

FIGURE 4.15 HYSTERESIS LOOP TEST 15. (RIGHT SIDE PIER)

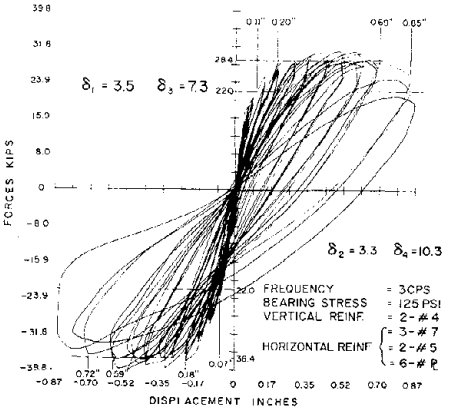

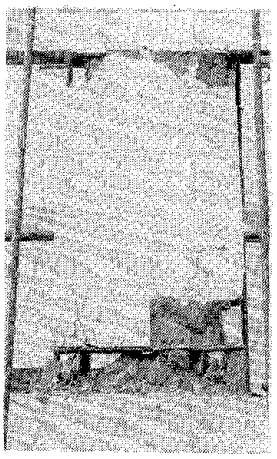

← + VE DIRECTION
MAX. + VE DISPL. & CORRES. FORCE : 0.58", 31 KIPS
MAX. – VE DISPL. & CORRES. FORCE : 0.51", 40 KIPS

FIGURE 4.16 HYSTERESIS LOOP TEST 16. (RIGHT SIDE PIER)

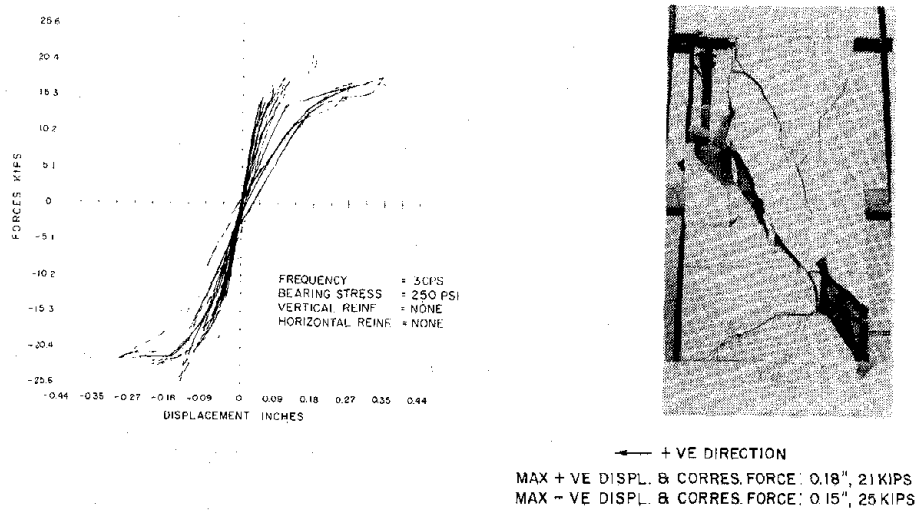

FIGURE 4.17 HYSTERESIS LOOP TEST 17 (RIGHT SIDE PIER)

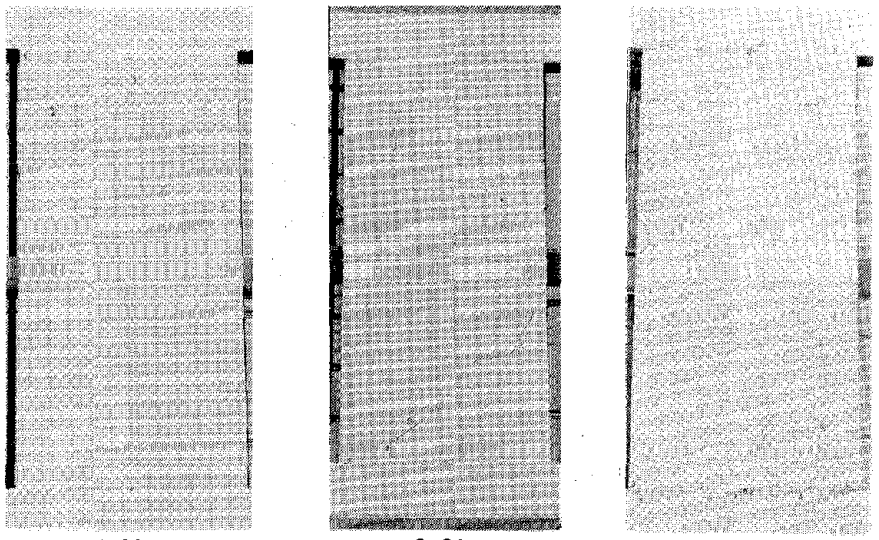

TEST NO.; LOAD (KIPS)	1; 20	2; 28	3; 21
SHEAR STRENGTH (PSI)	140	146	109

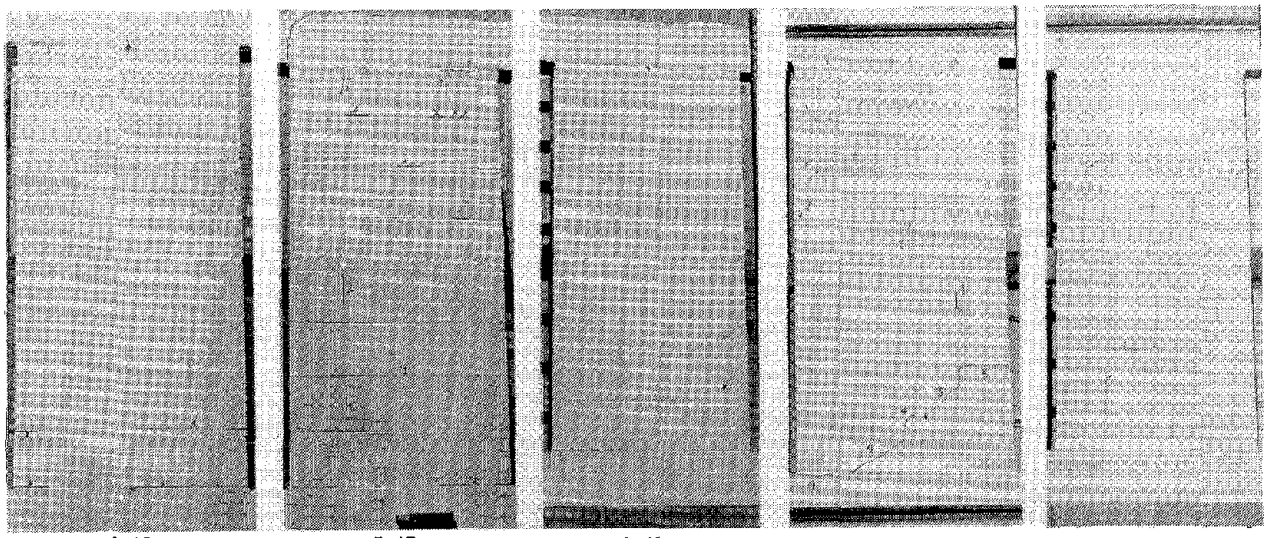

4; 18	5; 15	6; 19	7; 33	8; 33
94	78	99	178	172

FIGURE 4.18 CRACKED STATE OF PIERS AT THE SUGGESTED WORKING ULTIMATE STRENGTHS.

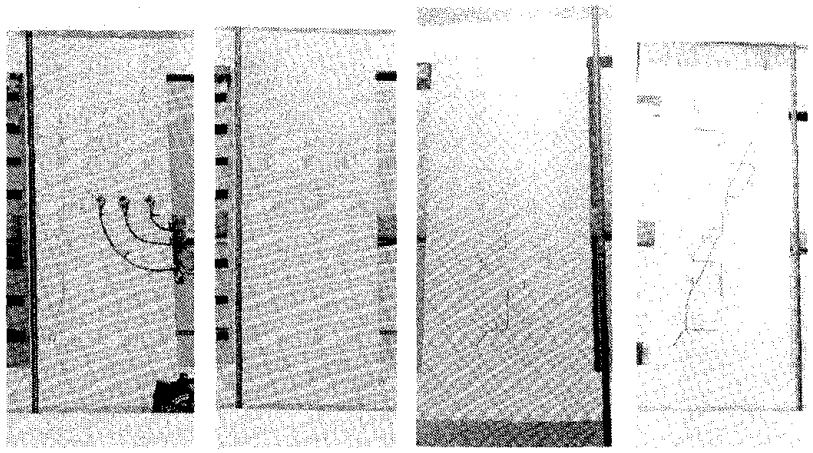

TEST NO. ; LOAD (KIPS)	9 ; 29	10 ; 28	11 ; 17	12 ; 18
SHEAR STRENGTH (PSI)	152	146	113	119

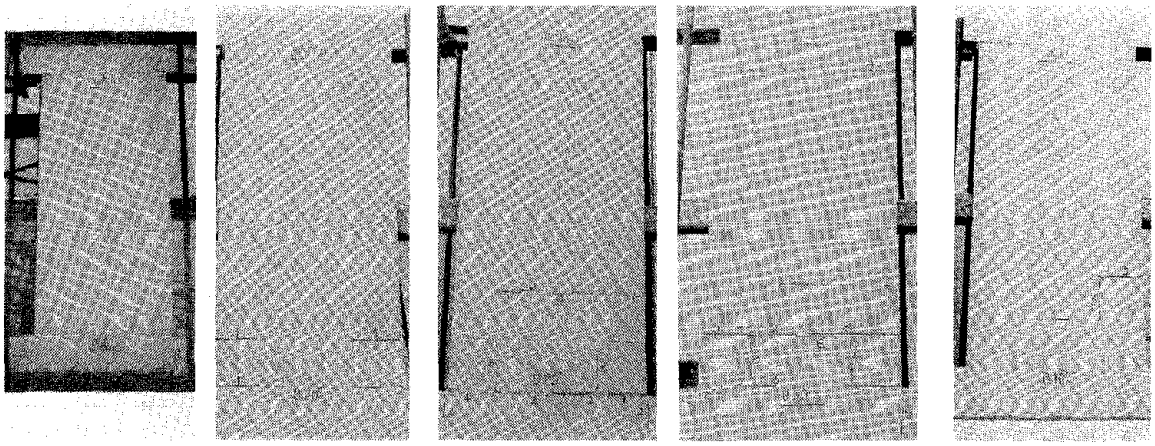

13 ; 18	14 ; 19	15 ; 23	16 ; 22	17 ; 17
95	101	118	115	89

FIGURE 4.18 (CONTINUE)

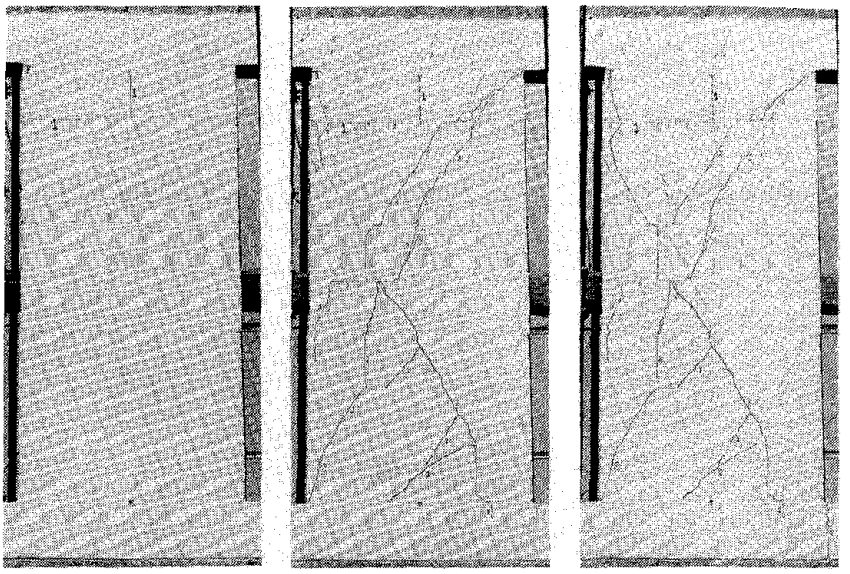

←— +VE DIRECTION
+VE LATERAL DISPL. CORRES.
SHEAR FORCE AND SHEAR STRESS
−VE LATERAL DISPL. CORRES.
SHEAR FORCE AND SHEAR STRESS

0.093"; 25.5 KIPS
130 PSI

0.113"; 25.1 KIPS
128 PSI

0.16"; 20.7 KIPS
106 PSI

0.19"; 20.3 KIPS
104 PSI

0.22"; 20.2 KIPS
103 PSI

0.25"; 15.7 KIPS
80 PSI

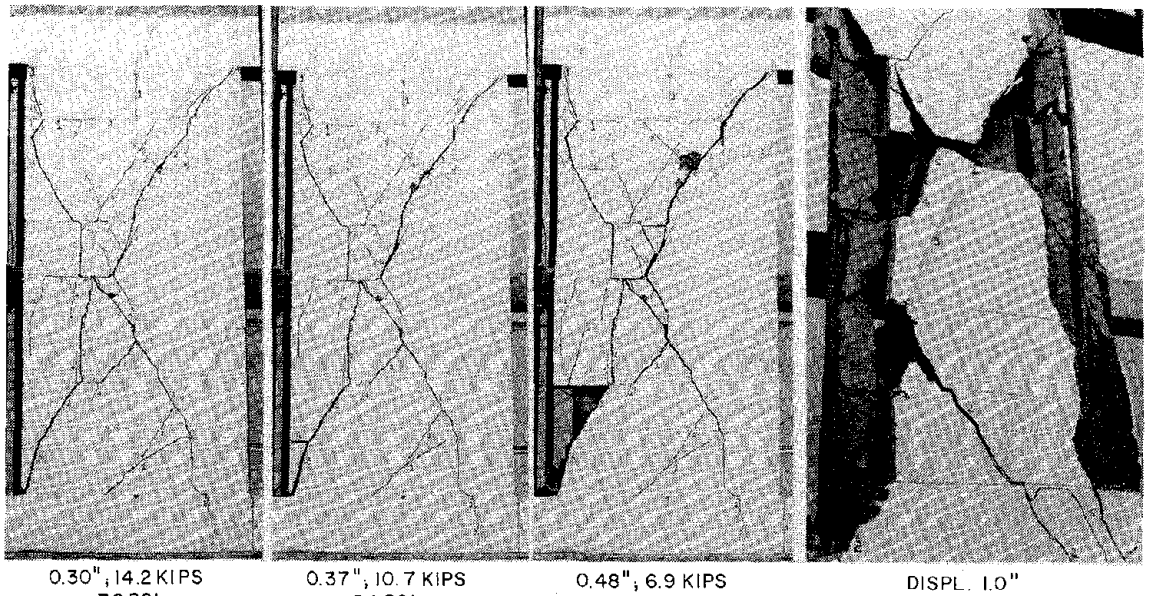

0.30"; 14.2 KIPS
72 PSI

0.33"; 6.1 KIPS
31 PSI

0.37"; 10.7 KIPS
54 PSI

0.38"; 4.4 KIPS
22 PSI

0.48"; 6.9 KIPS
35 PSI

0.50"; 1.9 KIPS
9 PSI

DISPL. 1.0"

DISPL. 1.0"

FIGURE 4.19 SUCCESSIVE CRACK FORMATION TEST 1. (RIGHT SIDE PIER)

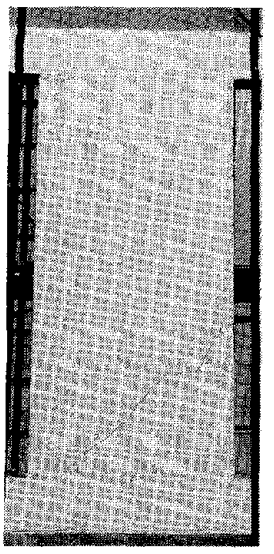

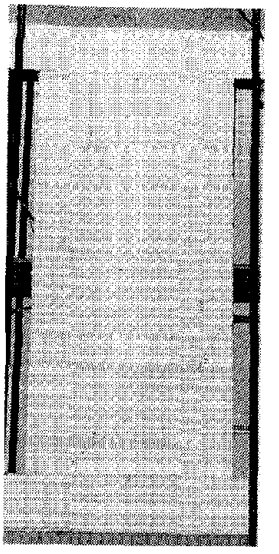

←— +VE DIRECTION
+VE LATERAL DISPL. CORRES.
SHEAR FORCE AND SHEAR STRESS
−VE LATERAL DISPL. CORRES.
SHEAR FORCE AND SHEAR STRESS

0.14"; 29.7 KIPS
149 PSI

0.15"; 29.7 KIPS
152 PSI

0.19"; 30.1 KIPS
154 PSI

0.23"; 25.1 KIPS
128 PSI

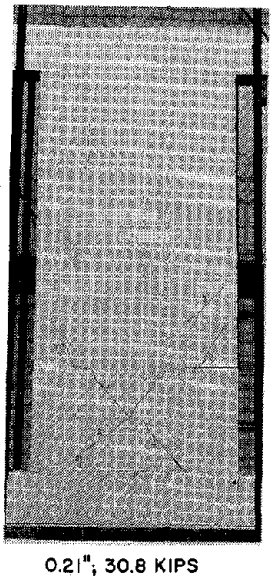

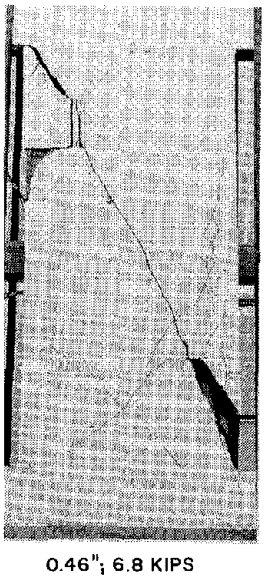

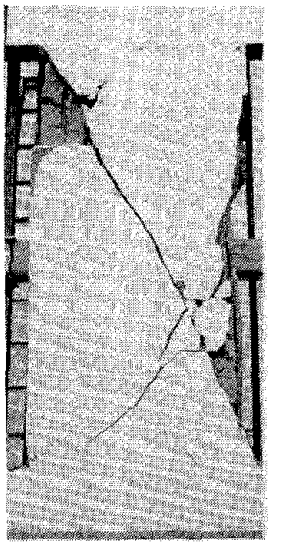

0.21"; 30.8 KIPS
157 PSI

0.23"; 26.5 KIPS
135 PSI

0.46"; 6.8 KIPS
34 PSI

0.47"; 7.2 KIPS
36 PSI

FIGURE 4.20 SUCCESSIVE CRACK FORMATION TEST 2. (RIGHT SIDE PIER)

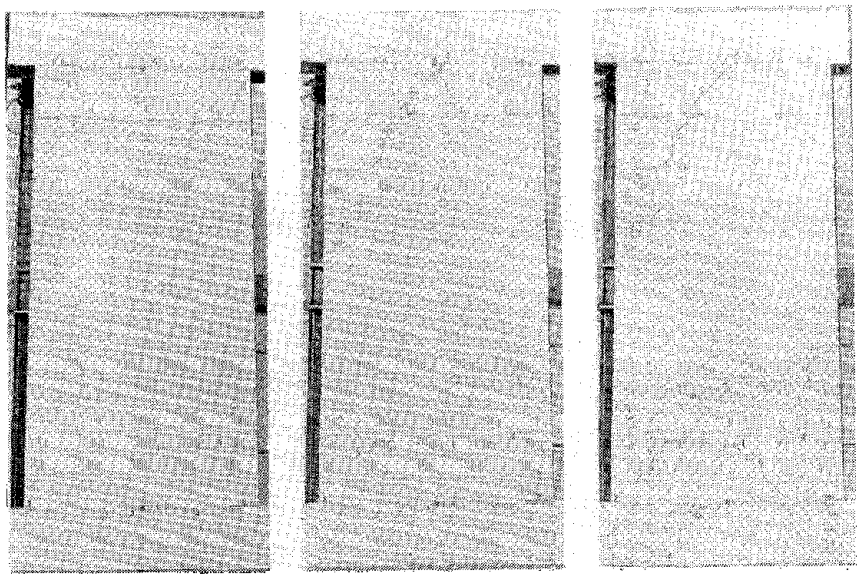

← + VE DIRECTION

+ VE LATERAL DISPL., CORRES. SHEAR FORCE AND SHEAR STRESS	0.11" ; 20.0 KIPS 102 PSI	0.18"; 24.0 KIPS 122 PSI	0.26"; 26.9 KIPS 137 PSI
− VE LATERAL DISPL., CORRES. SHEAR FORCE AND SHEAR STRESS	0.13"; 21.6 KIPS 110 PSI	0.22"; 23.0 KIPS 117 PSI	0.31"; 25.3 KIPS 129 PSI

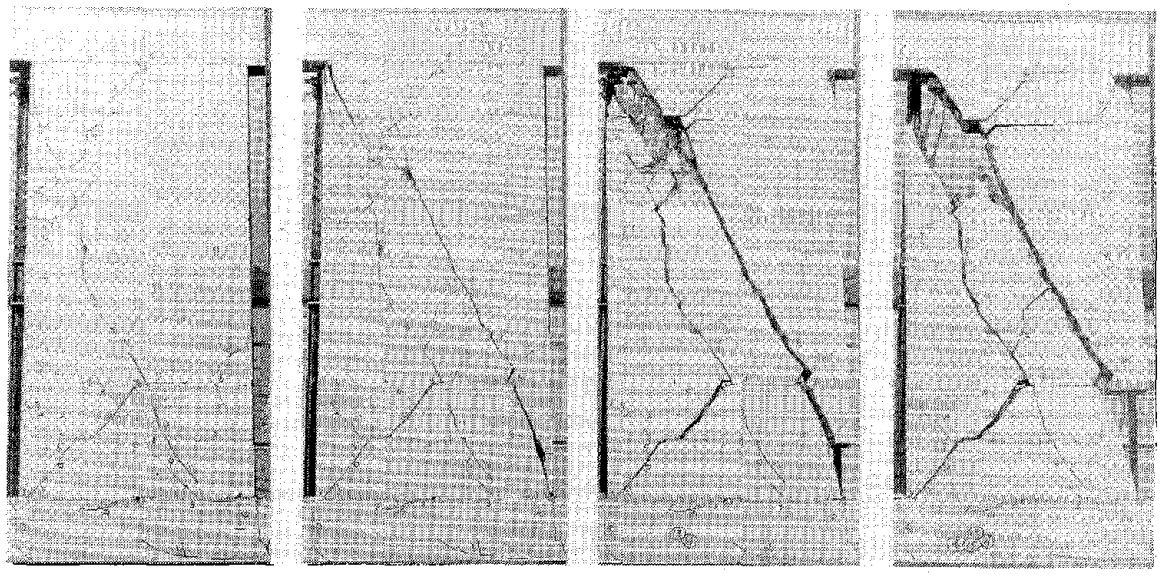

0.33"; 24.7 KIPS 126 PSI	0.45"; 14.5 KIPS 74 PSI	0.54"; 10.8 KIPS 55 PSI	DISPL. 1.0"
0.36"; 25.1 KIPS 128 PSI	0.46"; 22.2 KIPS 113 PSI	0.60"; 14.7 KIPS 75 PSI	DISPL. 1.0"

FIGURE 4.21 SUCCESSIVE CRACK FORMATION TEST 3. (RIGHT SIDE PIER)

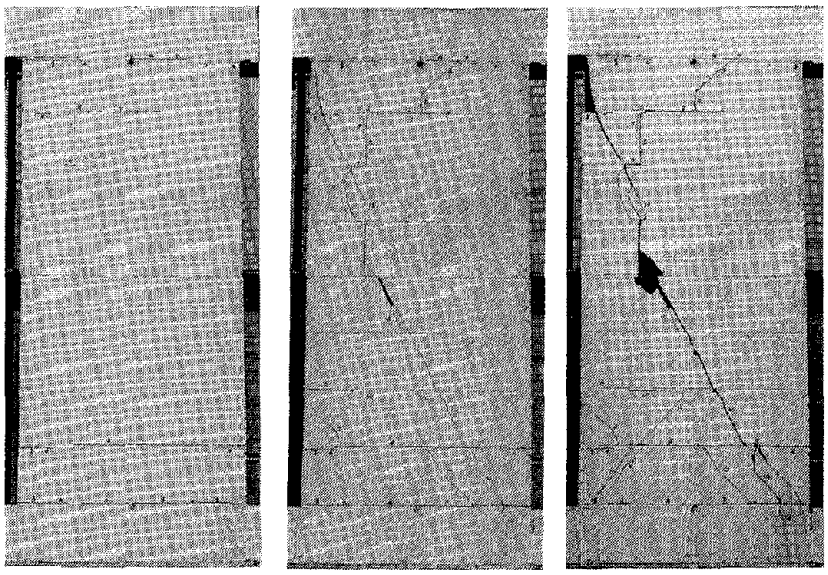

← +VE DIRECTION

+ VE LATERAL DISPL. CORRES.	0.18", 22.3 KIPS	0.31", 23.9 KIPS	0.35", 23.9 KIPS
SHEAR FORCE AND SHEAR STRESS	116 PSI	124 PSI	124 PSI
-VE LATERAL DISPL. CORRES.	0.15", 23.5 KIPS	0.26", 26.2 KIPS	0.36", 16.0 KIPS
SHEAR FORCE AND SHEAR STRESS	122 PSI	136 PSI	83 PSI

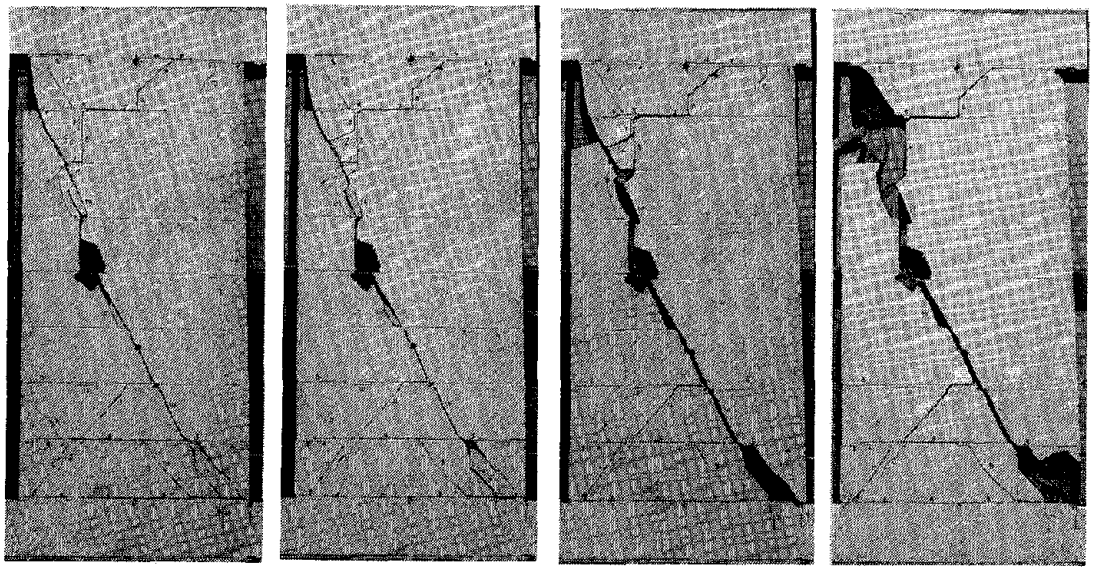

0.46", 19.2 KIPS	0.54", 15.8 KIPS	DISPL. 0.70"	DISPL. 1.0"
100 PSI	82 PSI		
0.43", 16.3 KIPS	0.49", 17.9 KIPS	DISPL. 0.70"	DISPL. 1.0"
85 PSI	93 PSI		

FIGURE 4.22 SUCCESSIVE CRACK FORMATION TEST 4. (RIGHT SIDE PIER)

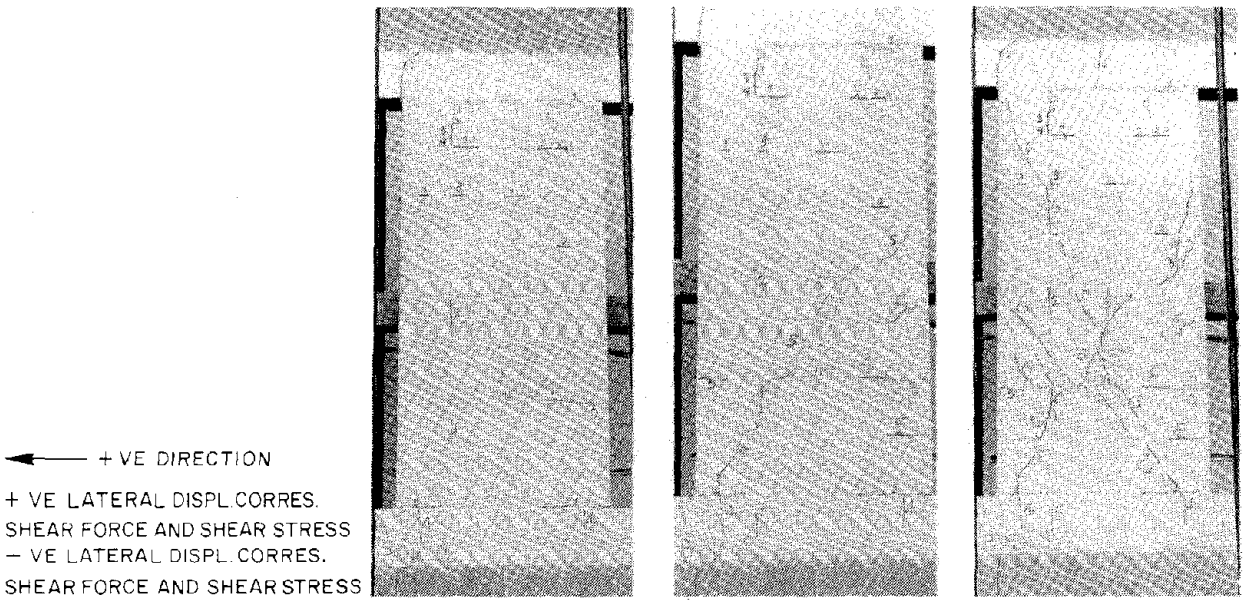

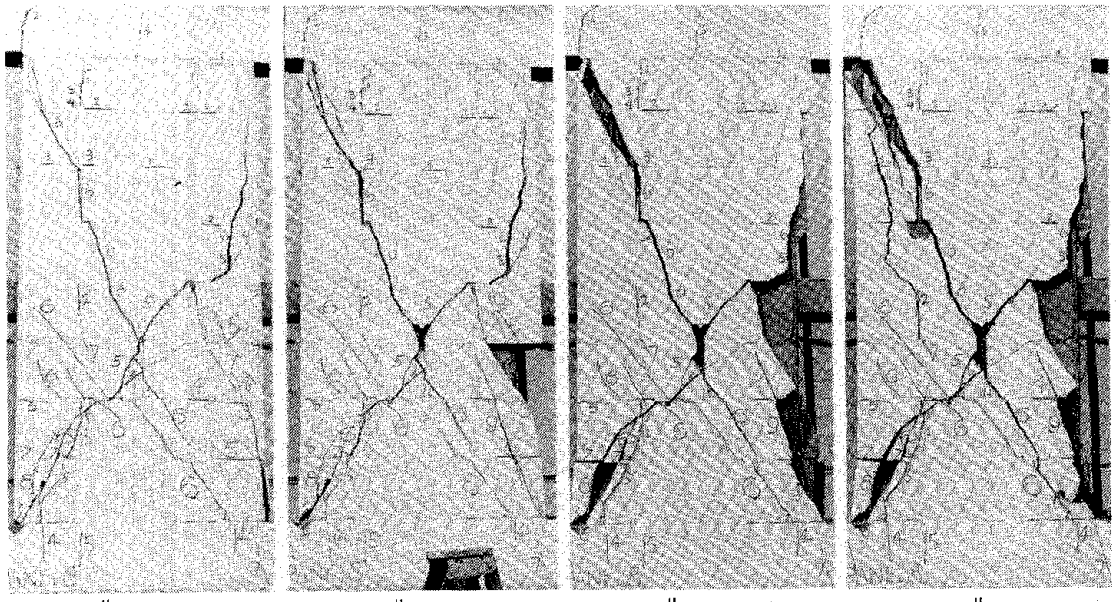

FIGURE 4.23 SUCCESSIVE CRACK FORMATION TEST 5. (RIGHT SIDE PIER)

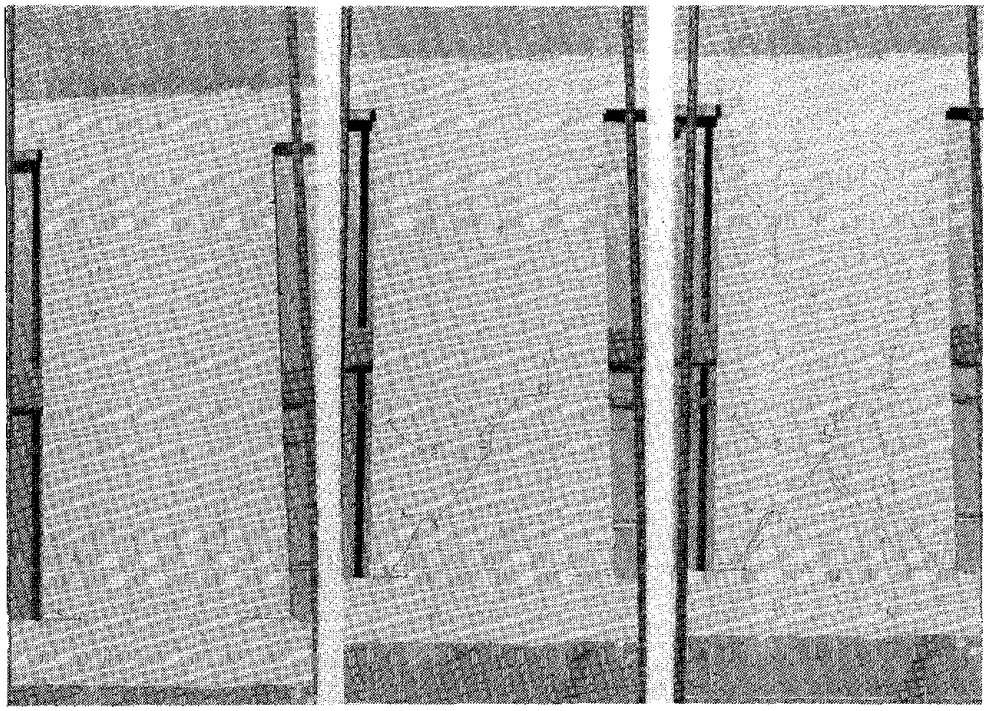

← + VE DIRECTION
+ VE LATERAL DISPL. CORRES.
SHEAR FORCE AND SHEAR STRESS
– VE LATERAL DISPL. CORRES.
SHEAR FORCE AND SHEAR STRESS

0.16"; 23.0 KIPS 120 PSI	0.29"; 18.8 KIPS 98 PSI	0.32"; 19.9 KIPS 104 PSI
0.13"; 20.1 KIPS 150 PSI	0.18"; 21.7 KIPS 113 PSI	0.24"; 19.1 KIPS 99 PSI

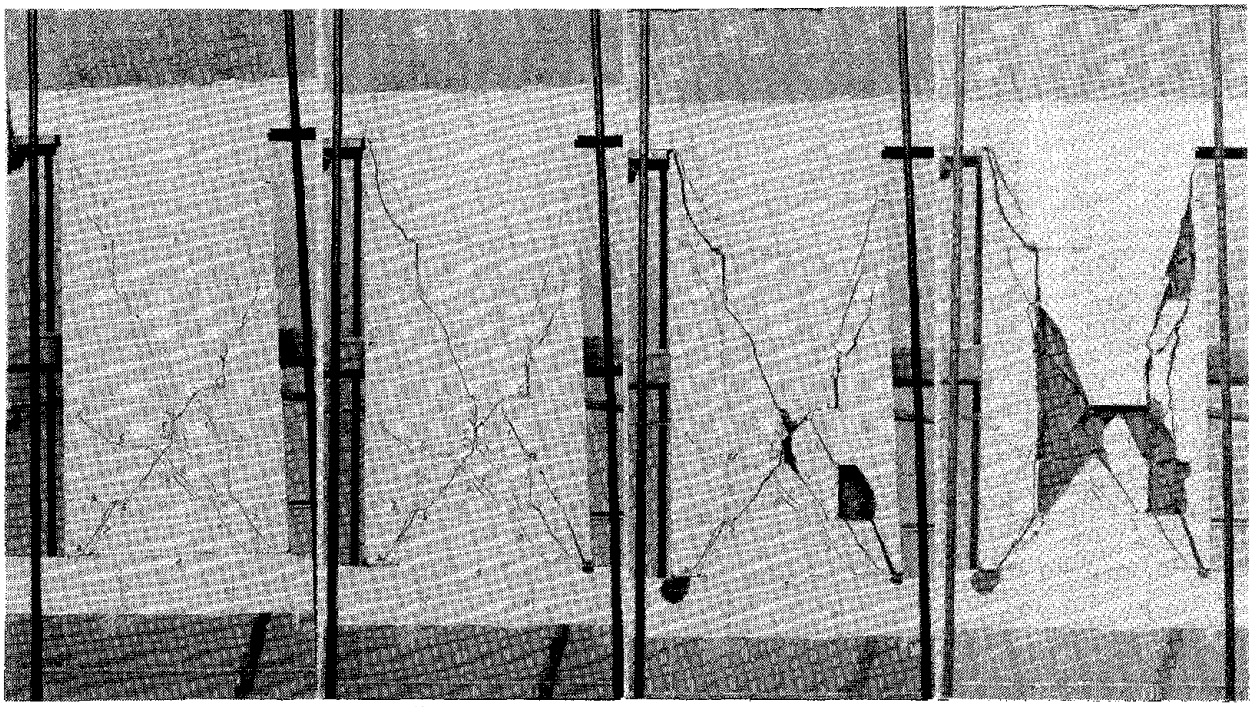

0.37"; 19.9 KIPS 104 PSI	0.51"; 10.5 KIPS 55 PSI	0.7"	1"
0.28"; 19.7 KIPS 102 PSI	0.41"; 13.6 KIPS 71 PSI	0.7"	1"

FIGURE 4.24 SUCCESSIVE CRACK FORMATION TEST 6. (RIGHT SIDE PIER)

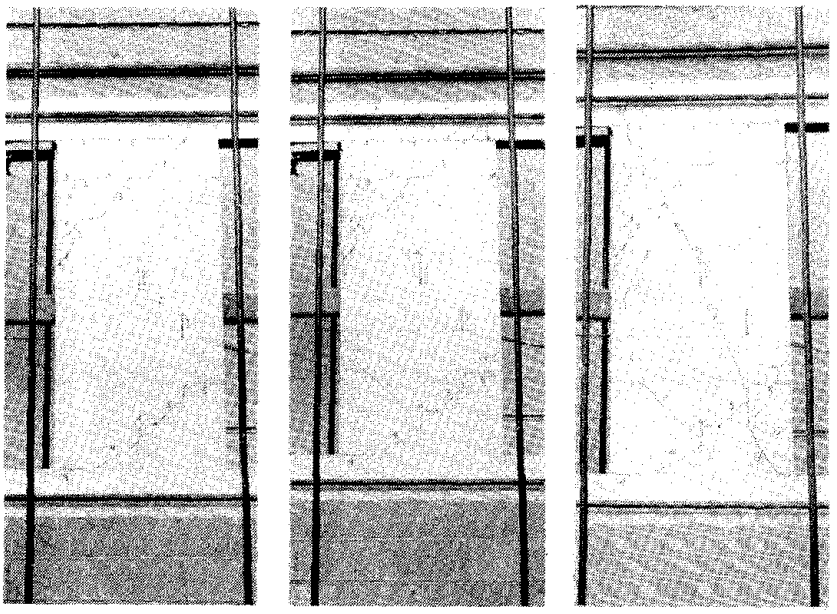

← + VE DIRECTION

+ VE LATERAL DISPL. CORRES.
SHEAR FORCE AND SHEAR STRESS
– VE LATERAL DISPL. CORRES.
SHEAR FORCE AND SHEAR STRESS

0.14"; 32.8 KIPS
171 PSI
0.11"; 31.5 KIPS
164 PSI

0.21"; 36.0 KIPS
188 PSI
0.18"; 36.4 KIPS
190 PSI

0.25"; 38.1 KIPS
198 PSI
0.22"; 38.9 KIPS
203 PSI

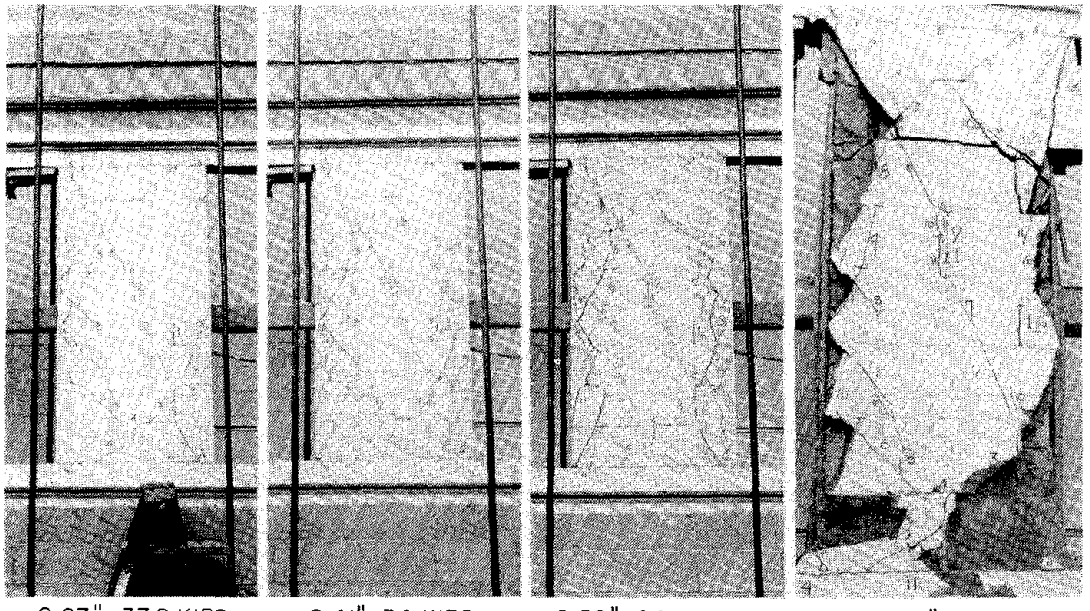

0.27"; 37.8 KIPS
197 PSI
0.26"; 39.7 KIPS
207 PSI

0.41"; 34 KIPS
177 PSI
0.46"; 31.6 KIPS
166 PSI

0.50"; 24.9 KIPS
130 PSI
0.60"; 27.8 KIPS
145 PSI

1"

1"

FIGURE 4.25 SUCCESSIVE CRACK FORMATION TEST 7. (RIGHT SIDE PIER)

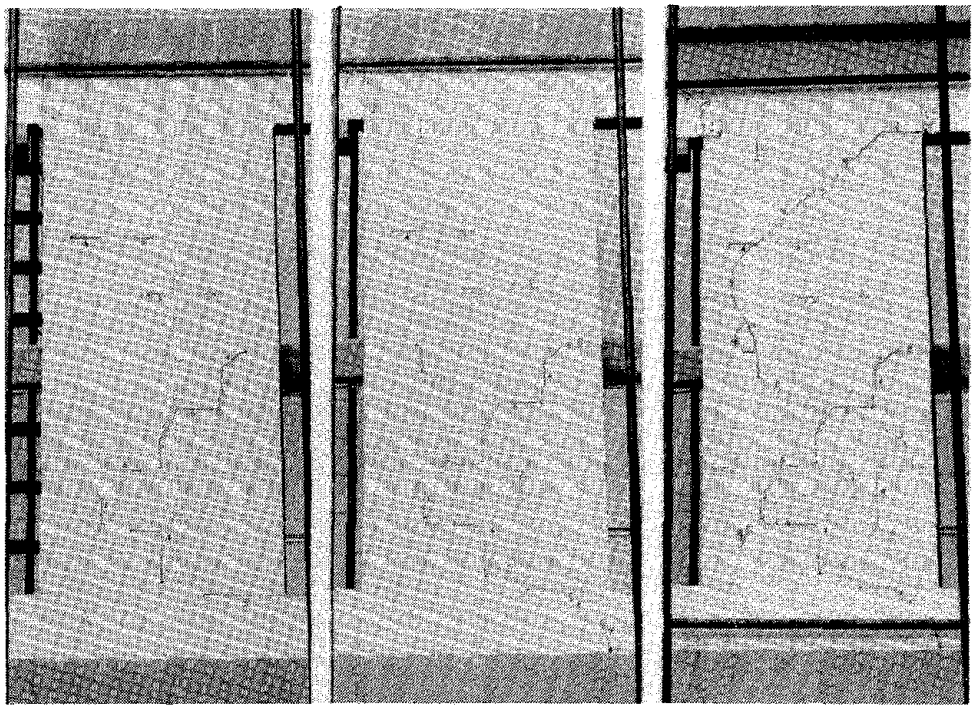

← + VE DIRECTION
+ VE LATERAL DISPL. CORRES.
SHEAR FORCE AND SHEAR STRESS
– VE LATERAL DISPL. CORRES.
SHEAR FORCE AND SHEAR STRESS

0.21"; 32.5 KIPS
169 PSI
0.19"; 32.0 KIPS
167 PSI

0.29"; 36.0 KIPS
187 PSI
0.26"; 37.0 KIPS
193 PSI

0.39"; 39.9 KIPS
208 PSI
0.35"; 42.2 KIPS
220 PSI

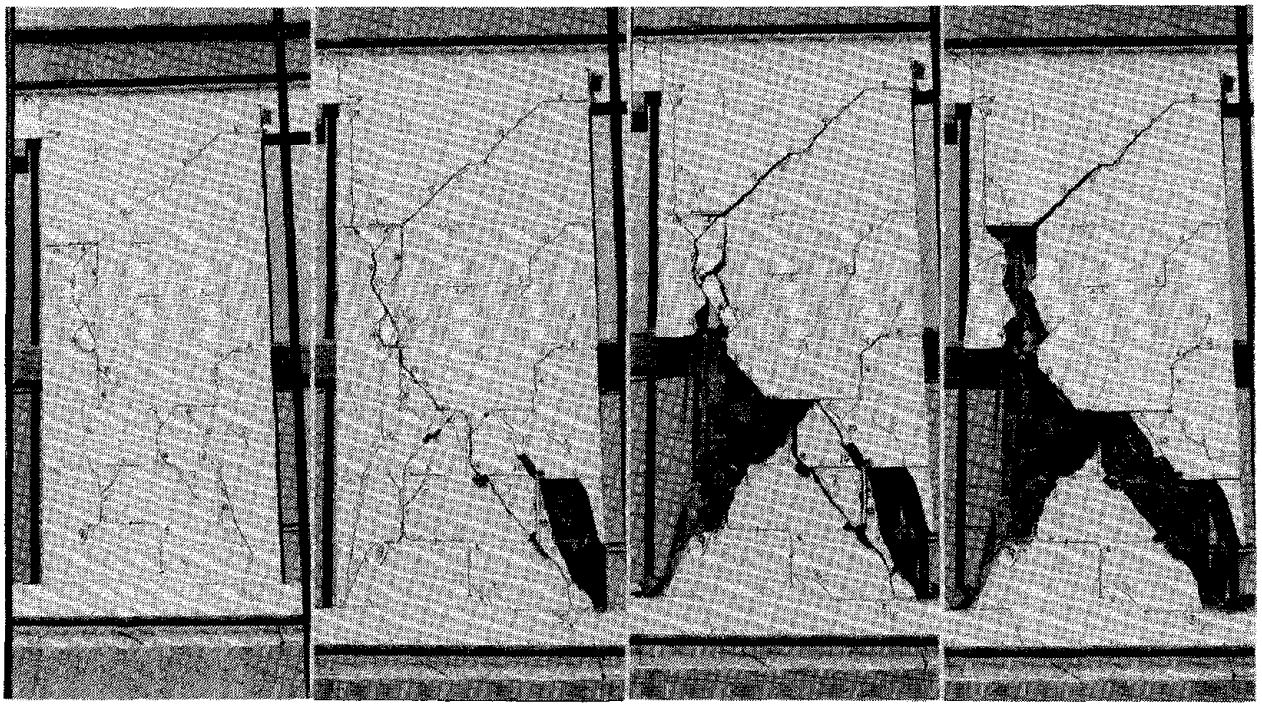

0.44"; 39.8 KIPS
207 PSI
0.39"; 43.4 KIPS
226 PSI

0.58"; 40.5 KIPS
211 PSI
0.63"; 29.4 KIPS
153 PSI

0.80"; 9.2 KIPS
48 PSI
0.86"; 6.9 KIPS
36 PSI

FIGURE 4.26 SUCCESSIVE CRACK FORMATION TEST 8. (RIGHT SIDE PIER)

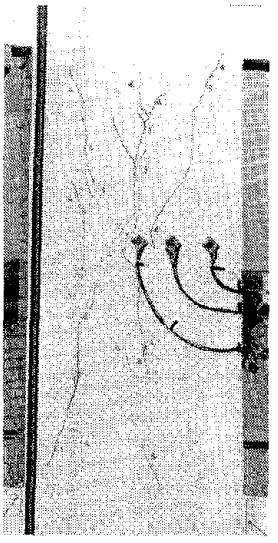

← + VE DIRECTION

+ VE LATERAL DISPL.CORRES. SHEAR FORCE AND SHEAR STRESS

0.12"; 26.2 KIPS
136 PSI

0.15"; 27.4 KIPS
143 PSI

- VE LATERAL DISPL.CORRES. SHEAR FORCE AND SHEAR STRESS

0.09"; 27.8 KIPS
145 PSI

0.14"; 28.7 KIPS
149 PSI

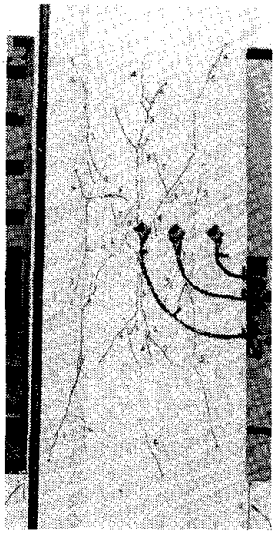

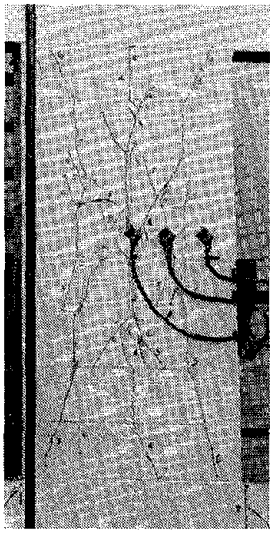

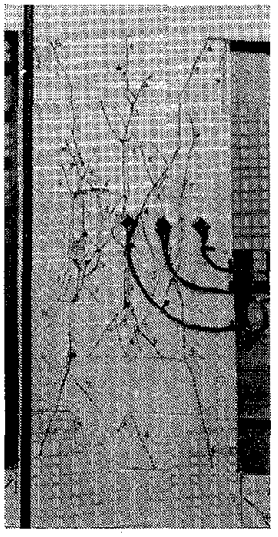

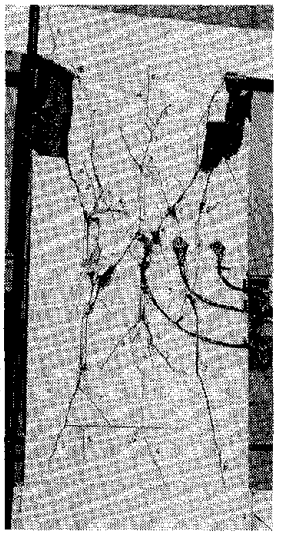

0.19"; 23.6 KIPS
123 PSI
0.21"; 26.5 KIPS
138 PSI

0.20"; 21.2 KIPS
110 PSI
0.27"; 26.2 KIPS
136 PSI

0.23"; 18.0 KIPS
94 PSI
0.32"; 23.7 KIPS
123 PSI

0.30"; 17.0 KIPS
89 PSI
0.31"; 20.9 KIPS
109 PSI

FIGURE 4.27 SUCCESSIVE CRACK FORMATION TEST 9. (RIGHT SIDE PIER)

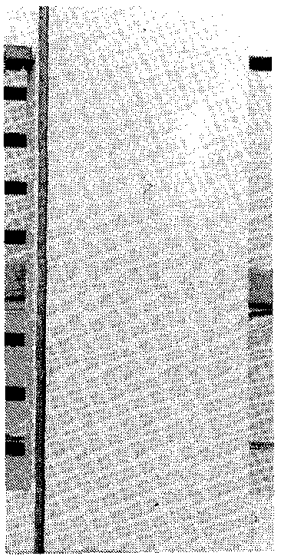

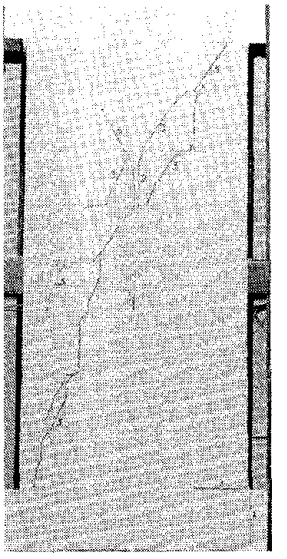

← + VE DIRECTION

+ VE LATERAL DISPL.CORRES. SHEAR FORCE AND SHEAR STRESS

0.08"; 32.3 KIPS
168 PSI

0.09"; 35.2 KIPS
183 PSI

– VE LATERAL DISPL.CORRES. SHEAR FORCE AND SHEAR STRESS

0.06"; 28.8 KIPS
150 PSI

0.08"; 31.8 KIPS
166 PSI

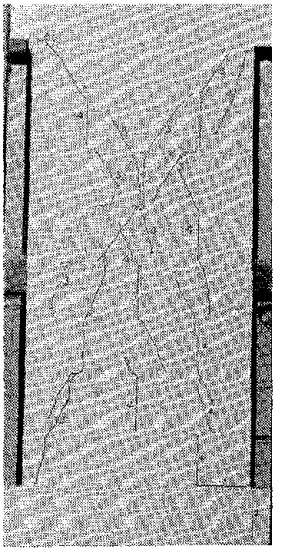

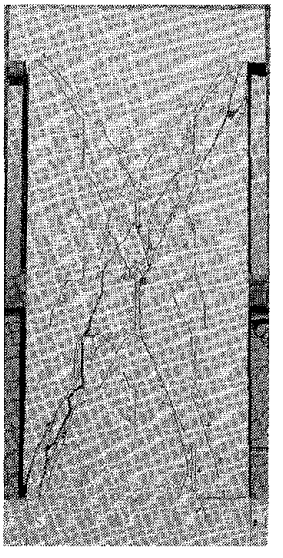

0.17"; 32.9 KIPS
171 PSI

0.13"; 33.0 KIPS
172 PSI

0.27"; 33.5 KIPS
174 PSI

0.22"; 33.7 KIPS
176 PSI

0.33"; 29.2 KIPS
152 PSI

0.27"; 32.9 KIPS
171 PSI

0.38"; 4.5 KIPS
23 PSI

0.45"; 89 KIPS
36 PSI

FIGURE 4.28 SUCCESSIVE CRACK FORMATION TEST 10.(RIGHT SIDE PIER)

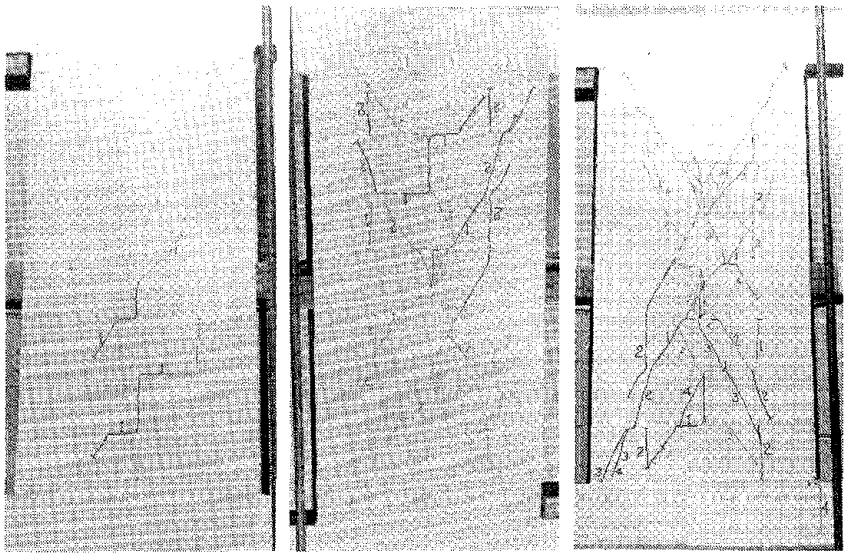

← + VE DIRECTION

+ VE LATERAL DISPL.CORRES.	0.07"; 17.2 KIPS	0.11"; 15.1 KIPS	0.20"; 17.4 KIPS
SHEAR FORCE AND SHEAR STRESS	113 PSI	99.3 PSI	114 PSI
- VE LATERAL DISPL.CORRES.	0.06"; 16.9 KIPS	0.10"; 16.6 KIPS	0.18"; 18.9 KIPS
SHEAR FORCE AND SHEAR STRESS	111 PSI	109 PSI	124 PSI

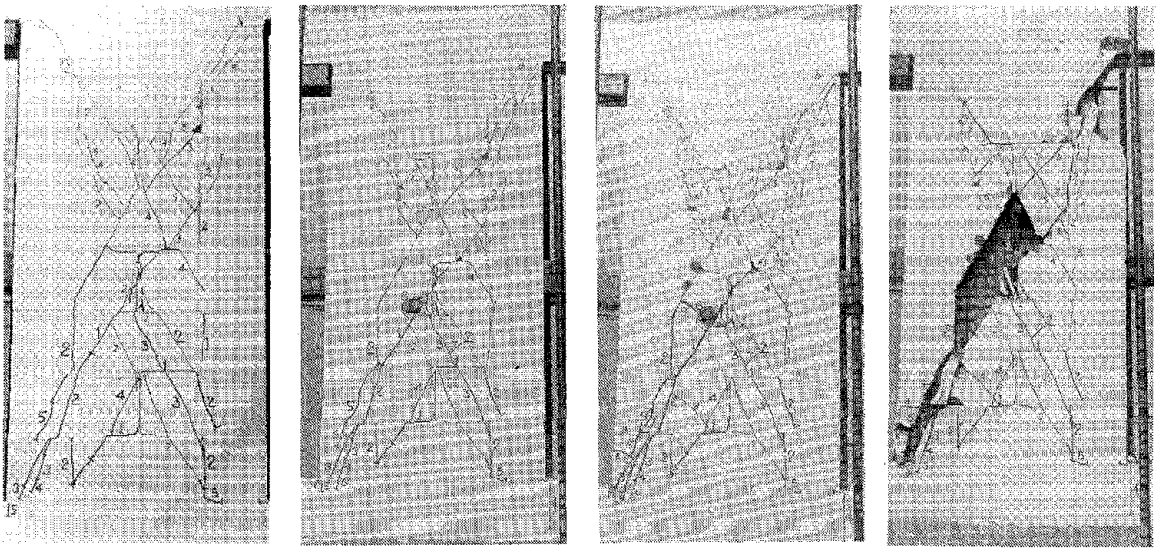

0.26"; 17.4 KIPS	0.34"; 16.9 KIPS	0.43"; 10.7 KIPS	0.51"; 4.7 KIPS
114 PSI	111 PSI	70 PSI	31 PSI
0.25"; 19.8 KIPS	0.33"; 21.1 KIPS	0.39"; 15.4 KIPS	0.41"; 9.1 KIPS
130 PSI	139 PSI	101 PSI	60 PSI

FIGURE 4.29 SUCCESSIVE CRACK FORMATION TEST 11.(RIGHT SIDE PIER)

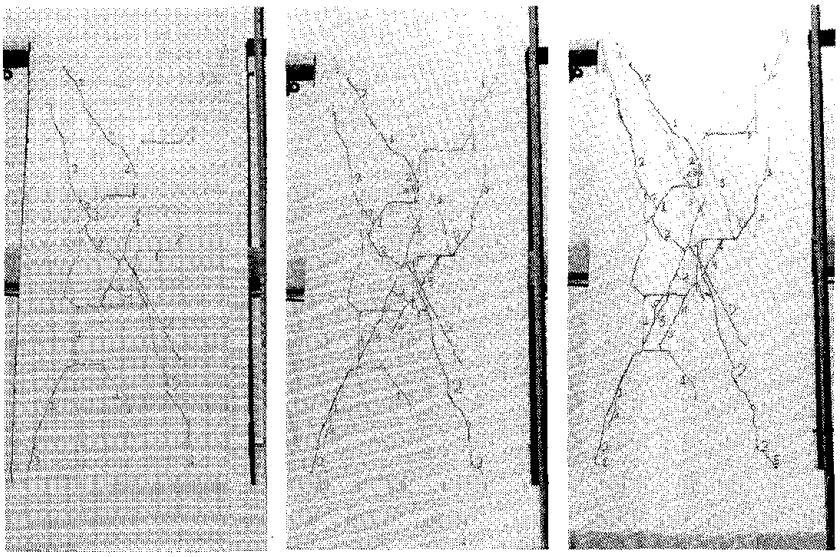

← + VE DIRECTION

+ VE LATERAL DISPL.CORRES.	0.14"; 19.1 KIPS	0.22"; 19.0 KIPS	0.27"; 19.7 KIPS
SHEAR FORCE AND SHEAR STRESS	126 PSI	125 PSI	130 PSI
- VE LATERAL DISPL.CORRES.	0.10"; 17.0 KIPS	0.21"; 19.4 KIPS	0.26"; 19.9 KIPS
SHEAR FORCE AND SHEAR STRESS	112 PSI	128 PSI	131 PSI

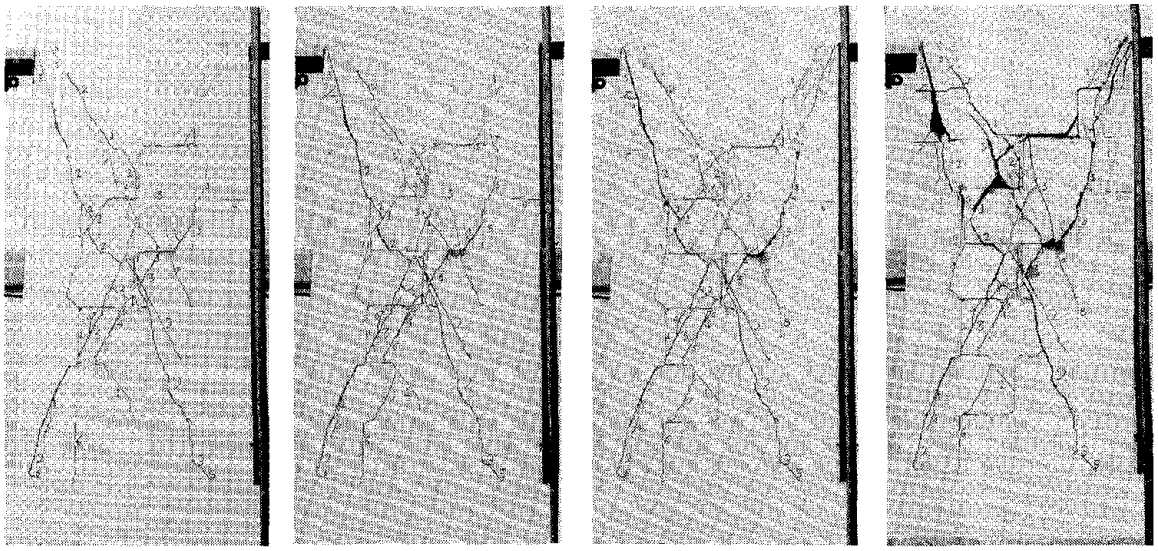

0.31"; 16.7 KIPS	0.36"; 18.5 KIPS	0.44"; 10.3 KIPS	0.51"; 7.3 KIPS
110 PSI	122 PSI	68 PSI	48 PSI
0.31"; 19.9 KIPS	0.35"; 18.1 KIPS	0.45"; 13.7 KIPS	0.51"; 9.8 KIPS
131 PSI	119 PSI	90 PSI	64 PSI

FIGURE 4.30 SUCCESSIVE CRACK FORMATION TEST 12. (RIGHT SIDE PIER)

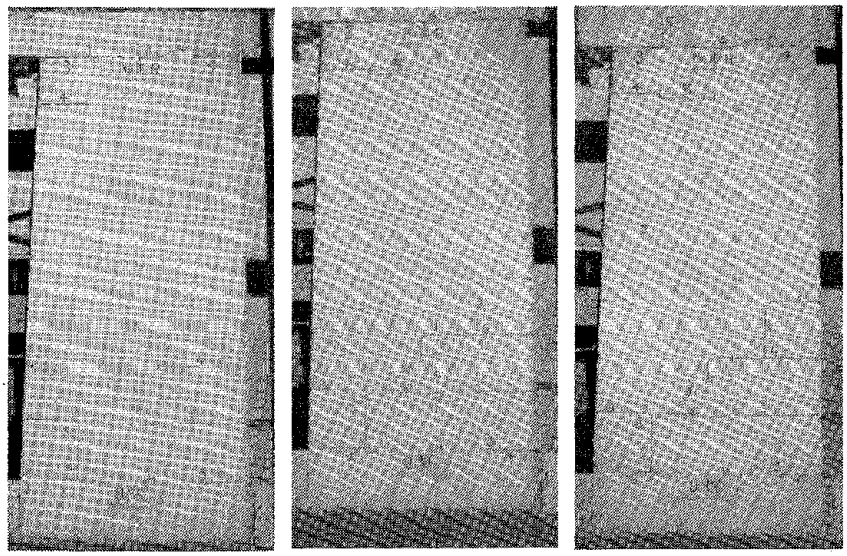

← + VE DIRECTION

+ VE LATERAL DISPL.CORRES.	0.14"; 23.7 KIPS	0.19"; 23.7 KIPS	0.22"; 24.9 KIPS
SHEAR FORCE AND SHEAR STRESS	123 PSI	123 PSI	130 PSI
- VE LATERAL DISPL.CORRES.	0.13"; 23.5 KIPS	0.14"; 25.7 KIPS	0.19"; 27.4 KIPS
SHEAR FORCE AND SHEAR STRESS	122 PSI	134 PSI	143 PSI

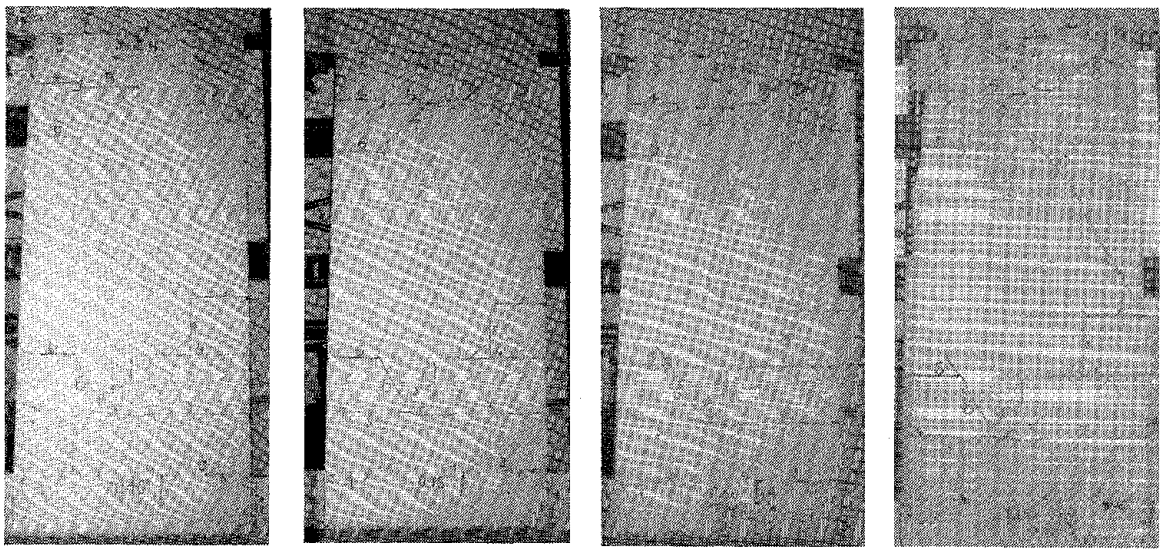

0.26"; 25.2 KIPS	0.29"; 26.0 KIPS	0.42"; 26.8 KIPS	DISPL. 1.0"
131 PSI	135 PSI	140 PSI	
0.19"; 28.2 KIPS	0.25"; 28.8 KIPS	0.35"; 31.3 KIPS	DISPL. 1.0"
147 PSI	150 PSI	163 PSI	

FIGURE 4.31 SUCCESSIVE CRACK FORMATION TEST 13. (RIGHT SIDE PIER)

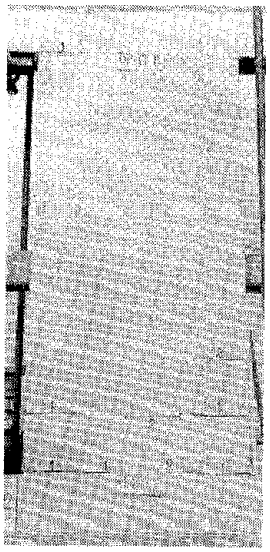

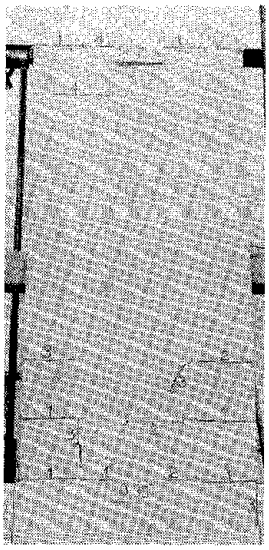

← + VE DIRECTION

+ VE LATERAL DISPL. CORRES.	0.12"; 21.2 KIPS	0.15"; 21.2 KIPS	0.18"; 23.3 KIPS
SHEAR FORCE AND SHEAR STRESS	110 PSI	110 PSI	121 PSI
- VE LATERAL DISPL. CORRES.	0.11"; 21.7 KIPS	0.14"; 23.4 KIPS	0.16"; 26.3 KIPS
SHEAR FORCE AND SHEAR STRESS	113 PSI	122 PSI	137 PSI

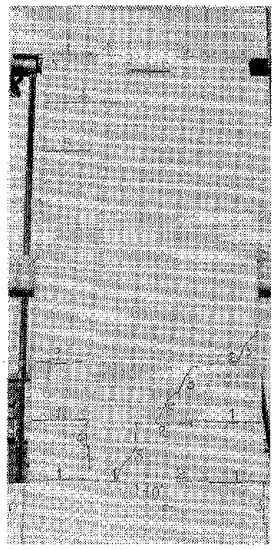

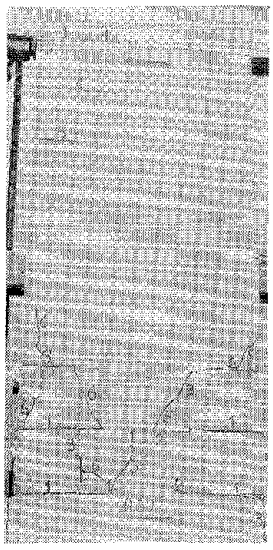

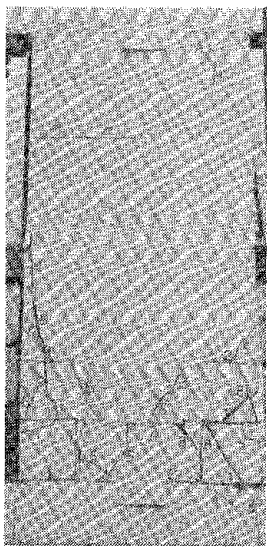

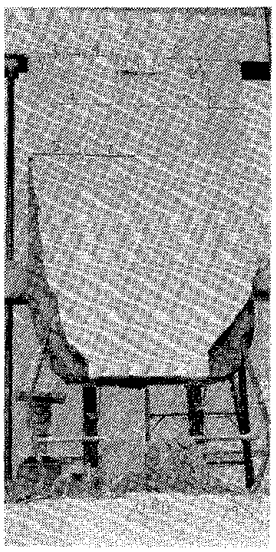

0.21"; 24.5 KIPS	0.29"; 24.6 KIPS	0.54"; 15.8 KIPS	DISPL. 0.9"
128 PSI	128 PSI	82 PSI	
0.19"; 26.4 KIPS	0.25"; 27.5 KIPS	0.44"; 17.9 KIPS	DISPL. 0.9"
137 PSI	143 PSI	93 PSI	

FIGURE 4.32 SUCCESSIVE CRACK FORMATION TEST 14. (RIGHT SIDE PIER)

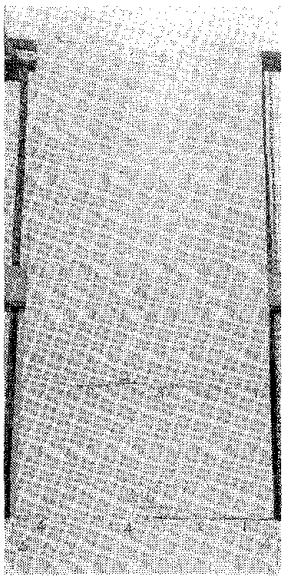

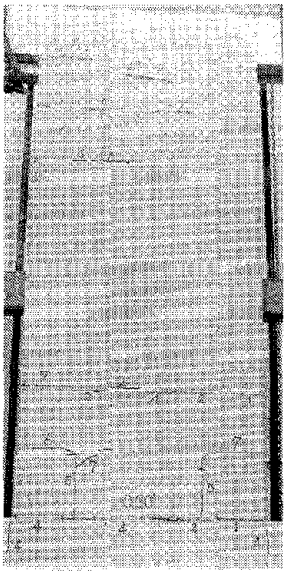

← + VE DIRECTION

+ VE LATERAL DISPL.CORRES.	0.08"; 20.0 KIPS	0.16"; 28.3 KIPS
SHEAR FORCE AND SHEAR STRESS	104 PSI	147 PSI
- VE LATERAL DISPL.CORRES.	0.08"; 21.3 KIPS	0.14"; 28.9 KIPS
SHEAR FORCE AND SHEAR STRESS	111 PSI	151 PSI

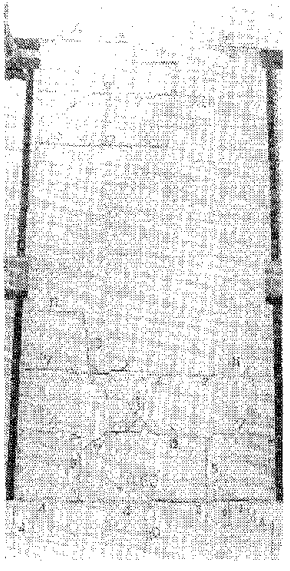

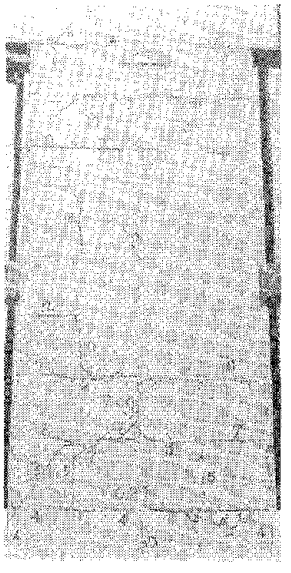

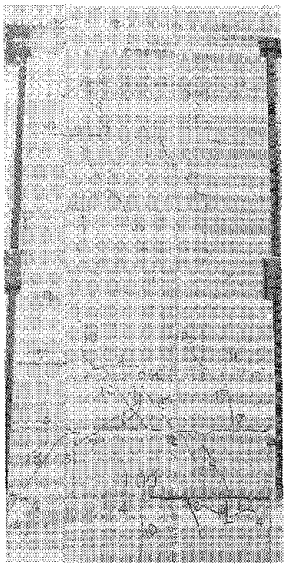

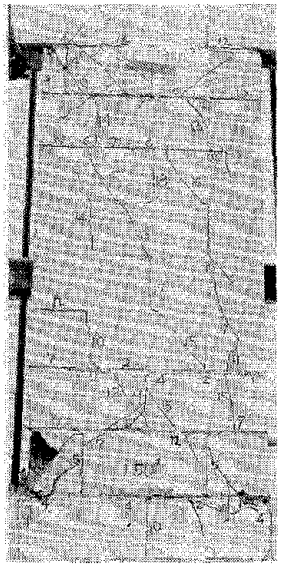

0.34"; 32.9 KIPS	0.52"; 33.0 KIPS	0.69"; 30.8 KIPS	DISPL. 1.5"
171 PSI	172 PSI	160 PSI	
0.32"; 36.2 KIPS	0.47"; 38.1 KIPS	0.63"; 38.1 KIPS	DISPL. 1.5"
189 PSI	200 PSI	198 PSI	

FIGURE 4.33 SUCCESSIVE CRACK FORMATION TEST 15. (RIGHT SIDE PIER)

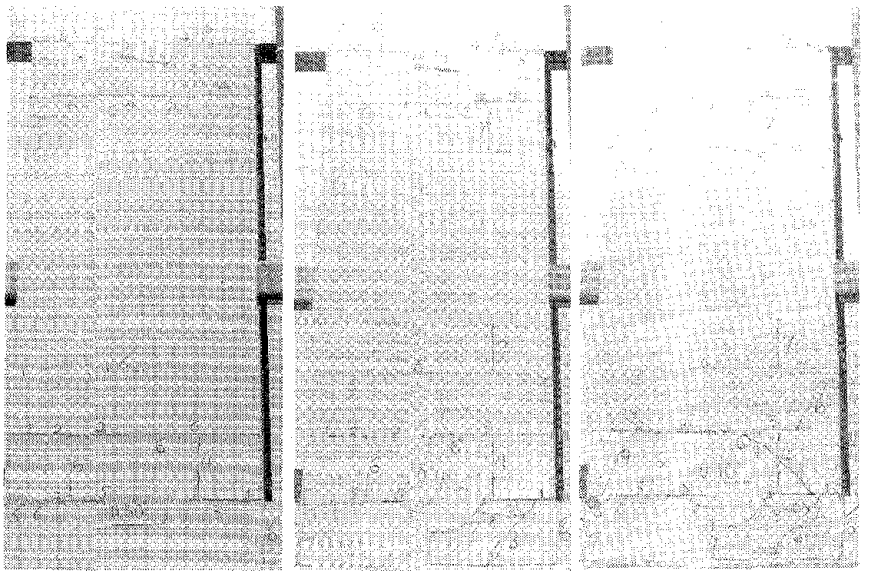

← + VE DIRECTION

+ VE LATERAL DISPL.CORRES.	0.28"; 28.3 KIPS	0.43"; 28.9 KIPS	0.52"; 28.5 KIPS
SHEAR FORCE AND SHEAR STRESS	147 PSI	151 PSI	148 PSI
- VE LATERAL DISPL.CORRES.	0.24"; 36.4 KIPS	0.35"; 37.2 KIPS	0.44"; 37.6 KIPS
SHEAR FORCE AND SHEAR STRESS	190PSI	194 PSI	196 PSI

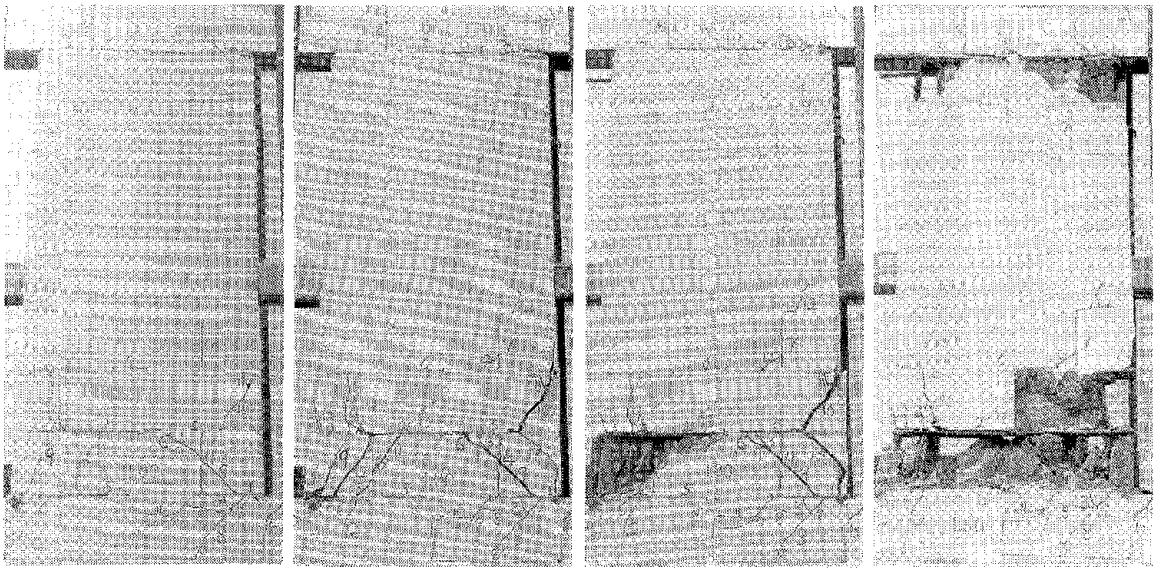

0.62"; 28.8 KIPS	0.78"; 20.9 KIPS	DISPL. 1.30"	DISPL. 1.50"
150 PSI	109 PSI		
0.58"; 37.6 KIPS	0.62"; 33.9 KIPS	DISPL. 1.30"	DISPL. 1.50"
196 PSI	177 PSI		

FIGURE 4.34 SUCCESSIVE CRACK FORMATION TEST 16. (RIGHT SIDE PIER)

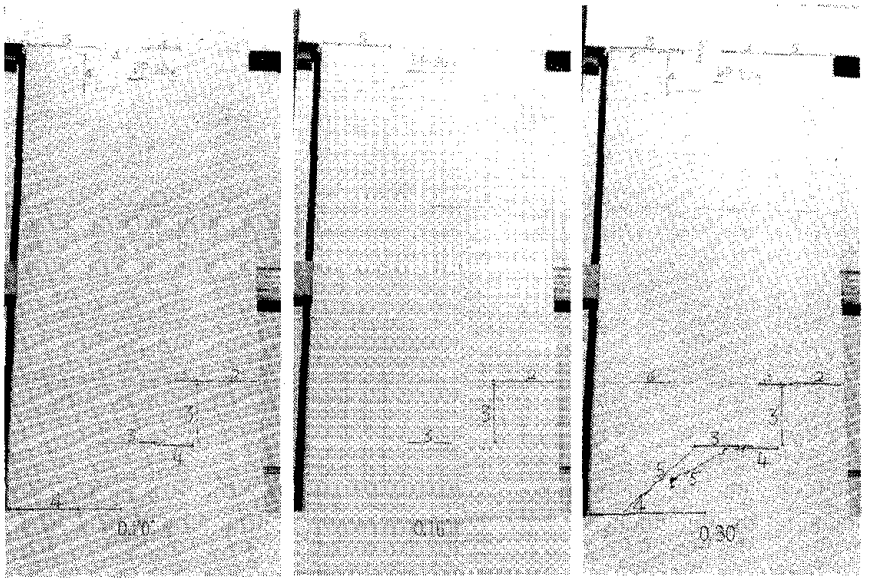

← + VE DIRECTION

+ VE LATERAL DISPL.CORRES.	0.08"; 16.6 KIPS	0.10"; 17.1 KIPS	0.17"; 22.2 KIPS
SHEAR FORCE AND SHEAR STRESS	86 PSI	89 PSI	166 PSI
- VE LATERAL DISPL.CORRES.	0.07"; 16.4 KIPS	0.09"; 17.8KIPS	0.14"; 22.9KIPS
SHEAR FORCE AND SHEAR STRESS	85 PSI	93 PSI	119 PSI

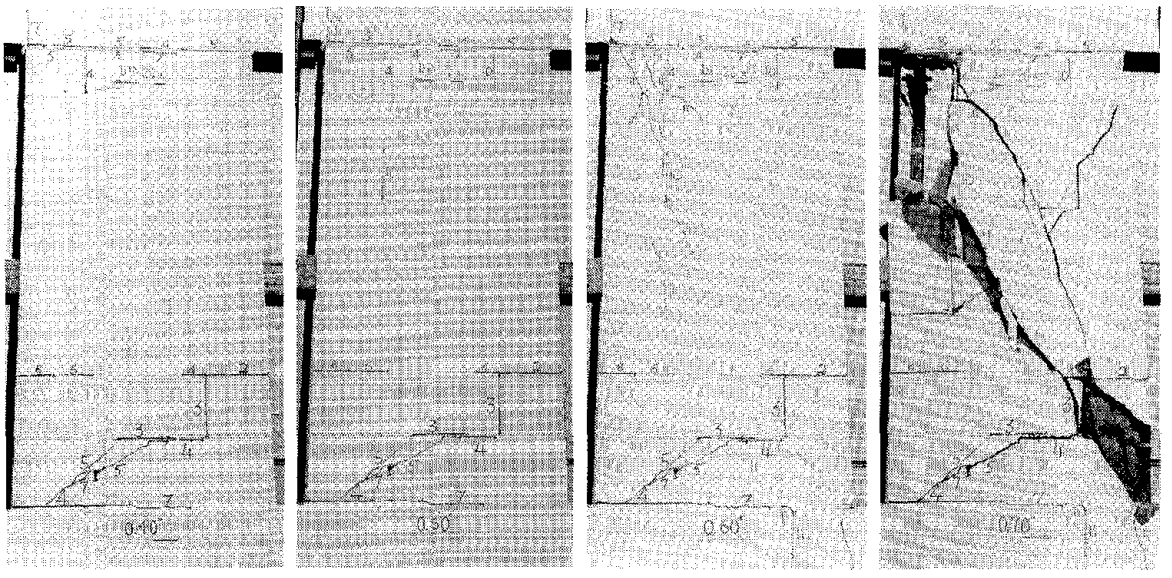

0.26"; 16.7 KIPS	0.35"; 18.1 KIPS	0.37"; 18.1KIPS	DISPL. 0.70"
87 PSI	94 PSI	94 PSI	
0.22"; 22.9KIPS	0.30"; 22.0KIPS	0.33"; 22.5KIPS	DISPL. 0.70"
119 PSI	115 PSI	117 PSI	

FIGURE 4.35 SUCCESSIVE CRACK FORMATION TEST 17.(RIGHT SIDE PIER)

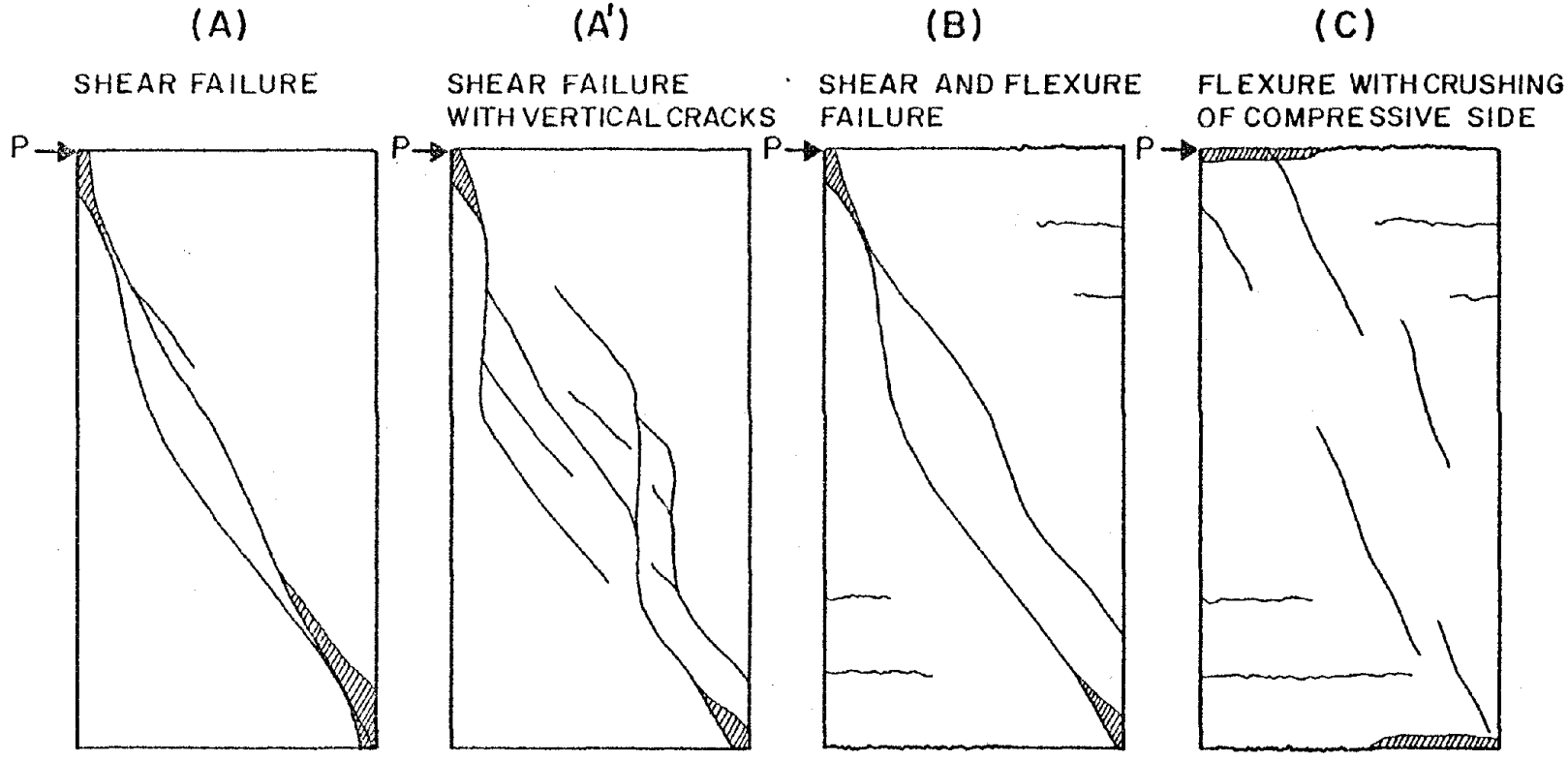

FIGURE 4.36 CLASSIFICATION OF MODE OF FAILURE

(a) Peak Ultimate Loads - P_{u1} and P_{u2}.

These are the maximum loads, in each direction, that were attained during a test.

(b) Average Ultimate Loads - P_1 and P_2.

The loads P_1 and P_2, in each direction, are approximately 90% of the mean of the peak ultimate loads; they were maintained for more than one cycle of input displacement.

(c) Working Ultimate Load - P_3.

P_3 was chosen as the load at which the first visible cracks formed in the piers. P_3 varied between 70 and 80% of the mean of the peak ultimate loads.

(d) Ductility Indicators - δ_1 to δ_4.

Ductility indicators associated with P_1, P_2 and P_3 were defined to give an indication of the displacement range over which loads P_1, P_2 and P_3 were maintained. δ_1 and δ_2 are associated with the average ultimate strengths P_1 and P_2, and are defined as the ratio of the displacement at which the pier can no longer withstand the lateral load P_1 or P_2 to the displacement at which P_1 or P_2 is first attained. δ_3 and δ_4 are similar ratios, in each direction, associated with the load P_3.

P_{u1}, P_{u2}, P_1, P_2 and P_3 are indicated in Figure 4.41. The mean of the loads P_{u1} and P_{u2}, the mean of the loads P_1 and P_2, and P_3 and their respective shear strengths based on the gross area of 192 sq. in. are listed in Table 4.1. δ_1 to δ_4 are defined as $\delta_1 = \frac{d_3}{d_2}$; $\delta_2 = \frac{d_7}{d_6}$; $\delta_3 = \frac{d_4}{d_1}$ and $\delta_4 = \frac{d_8}{d_5}$ where d_1 to d_8 are

indicated in Figure 4.41. The mean of δ_1 and δ_2, and the mean of δ_3 and δ_4 are listed in Table 4.1.

To give an indication of the envelope of the hysteresis loops, the shear stress and lateral displacement for each of the three (3) cycles at a given input displacement were averaged (i.e. the average of the absolute values of the forces and displacements) and plotted. The plots shown in Figures 4.37 to 4.40, demonstrate the effects of bearing stress, reinforcement and partial grouting on these curves.

4.4 Stiffness Degradation

To give an indication of the stiffness degradation occurring between different sequences of loading, a stiffness coefficient (K_I) defined as

$$K_I = \frac{\text{Maximum +ve force - Maximum -ve force}}{\text{Corresponding +ve displ. - Corresponding -ve displ.}} \quad (4.1)$$

was calculated for each cycle of loading. K_I for the right-side pier was plotted against the average lateral displacement and shear force for each cycle of loading - Figures 4.42 and 4.43. On each of these graphs a line indicating the first cracks visible to the eye and a line indicating the formation of the first major crack are also plotted.

4.5 Energy Dissipation

The energy dissipated per cycle of loading was expressed in terms of a dimensionless ratio EDT. EDT is defined as the ratio of the energy dissipated to the total stored strain energy per cycle and is diagrammatically shown in Figure 4.44.

$$EDT = \frac{\text{Energy Dissipated/cycle}}{\text{Total Stored Energy/cycle}} \quad (4.2)$$

EDT is plotted against the average lateral displacement for the right-side pier for each cycle of loading in Fig. 4.44.

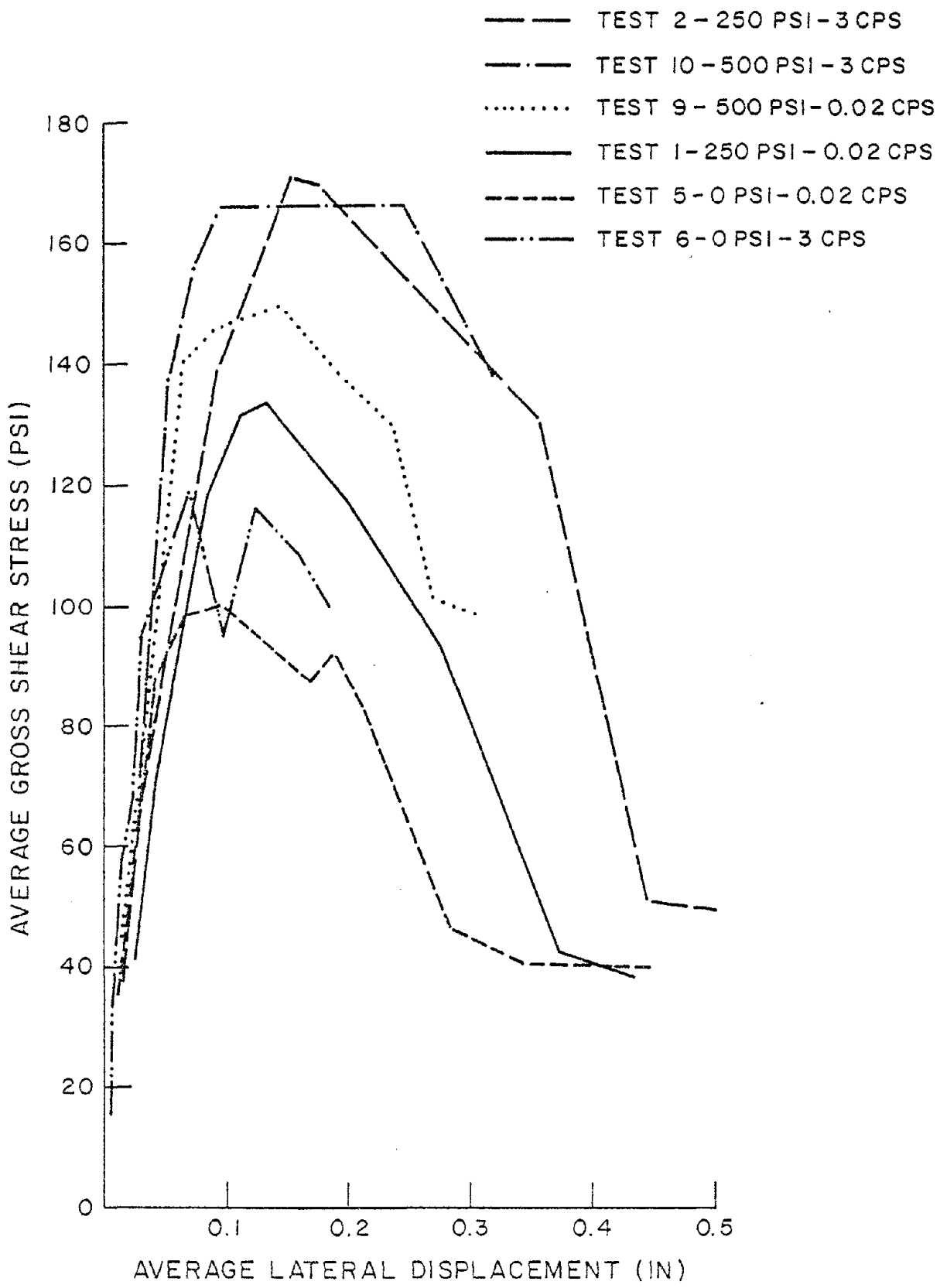

FIGURE 4.37 HYSTERESIS ENVELOPE (EFFECT OF BEARING STRESS)

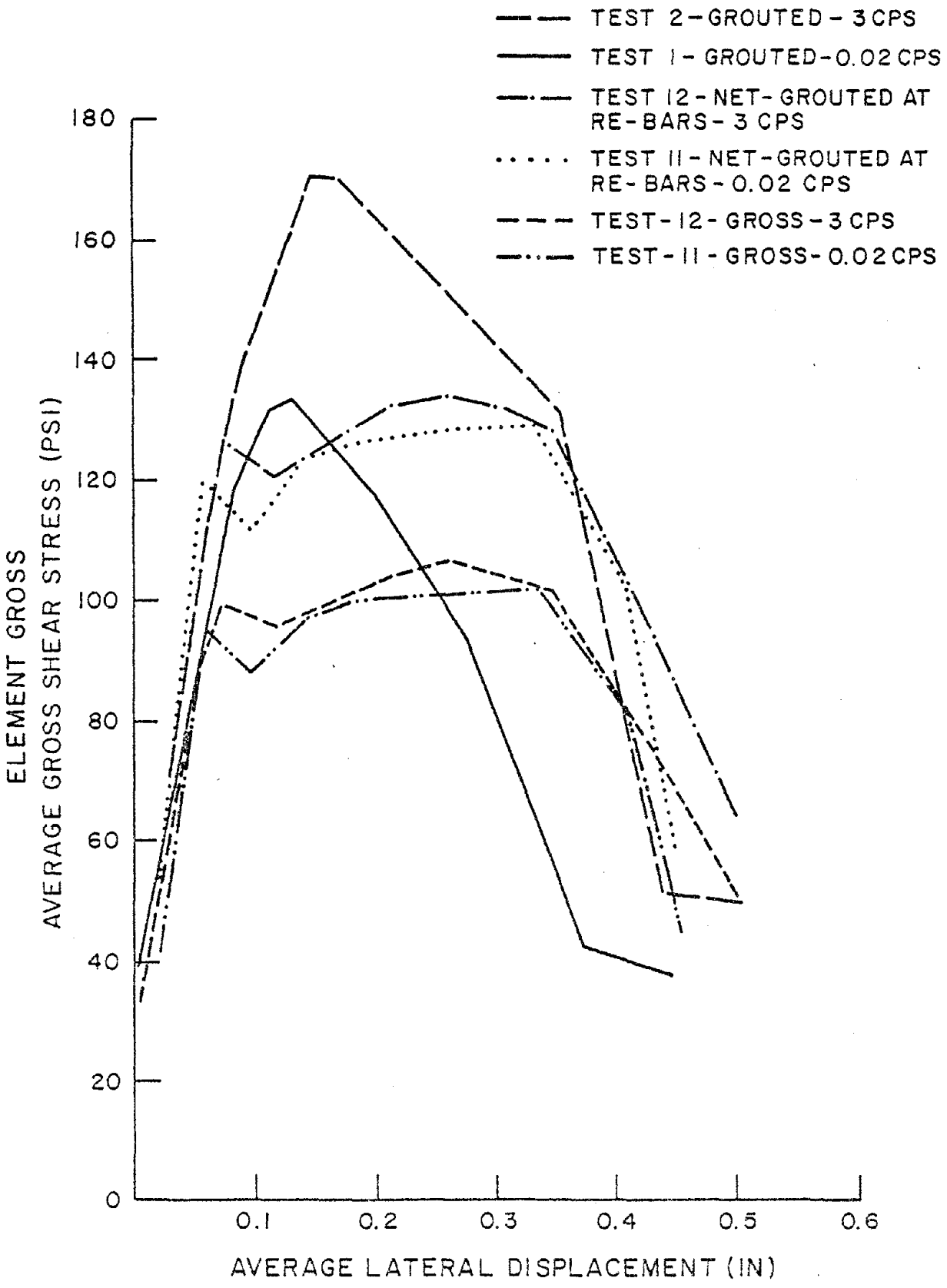

FIGURE 4.38 HYSTERESIS ENVELOPE (EFFECT OF PARTIAL GROUTING)

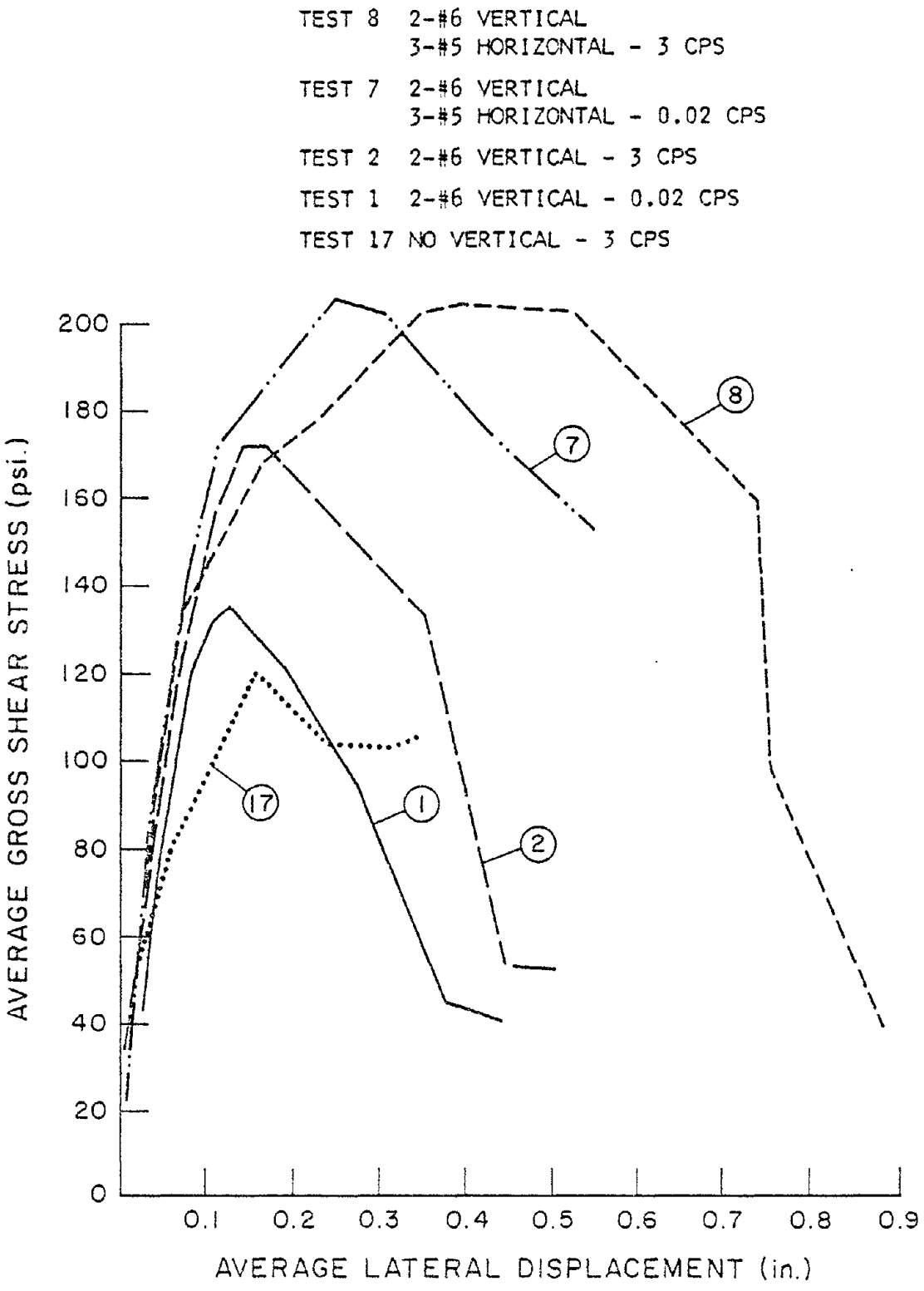

FIGURE 4.39 HYSTERESIS ENVELOPE (EFFECT OF REINFORCEMENT)

ALL 2-#4 VERTICAL, 125 PSI BEARING STRESS

TEST 3 NO HORIZONTAL 0.02 CPS (S)
TEST 4 NO HORIZONTAL 3.0 CPS (D)
TEST 13 2-#5, 3-#7 HORIZONTAL (S)
TEST 14 2-#5, 3-#7 HORIZONTAL (D)
TEST 15 2-#5, 3-#7 6-R HORIZONTAL (S)
TEST 16 2-#5, 3-#7 6-R HORIZONTAL (D)

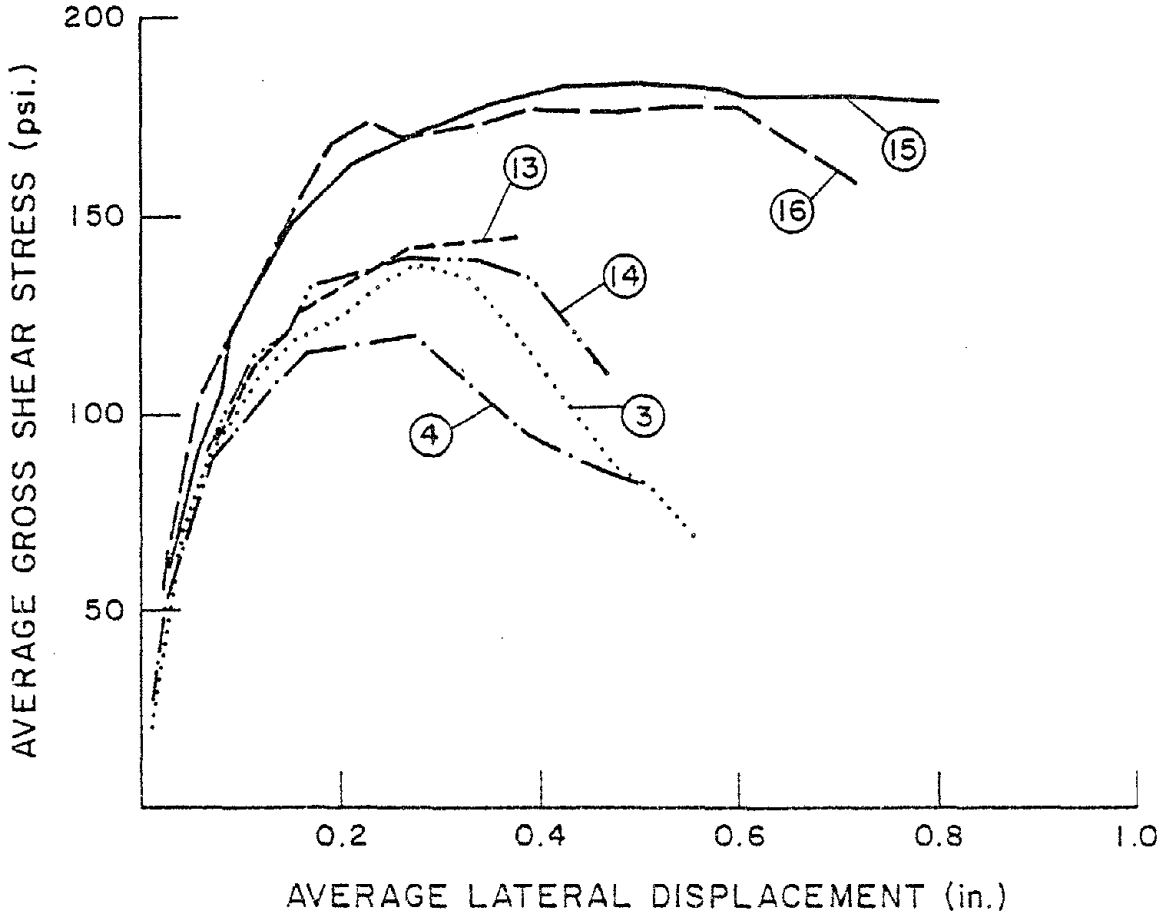

FIGURE 4.40 HYSTERESIS ENVELOPE (EFFECT OF HORIZONTAL REINFORCEMENT)

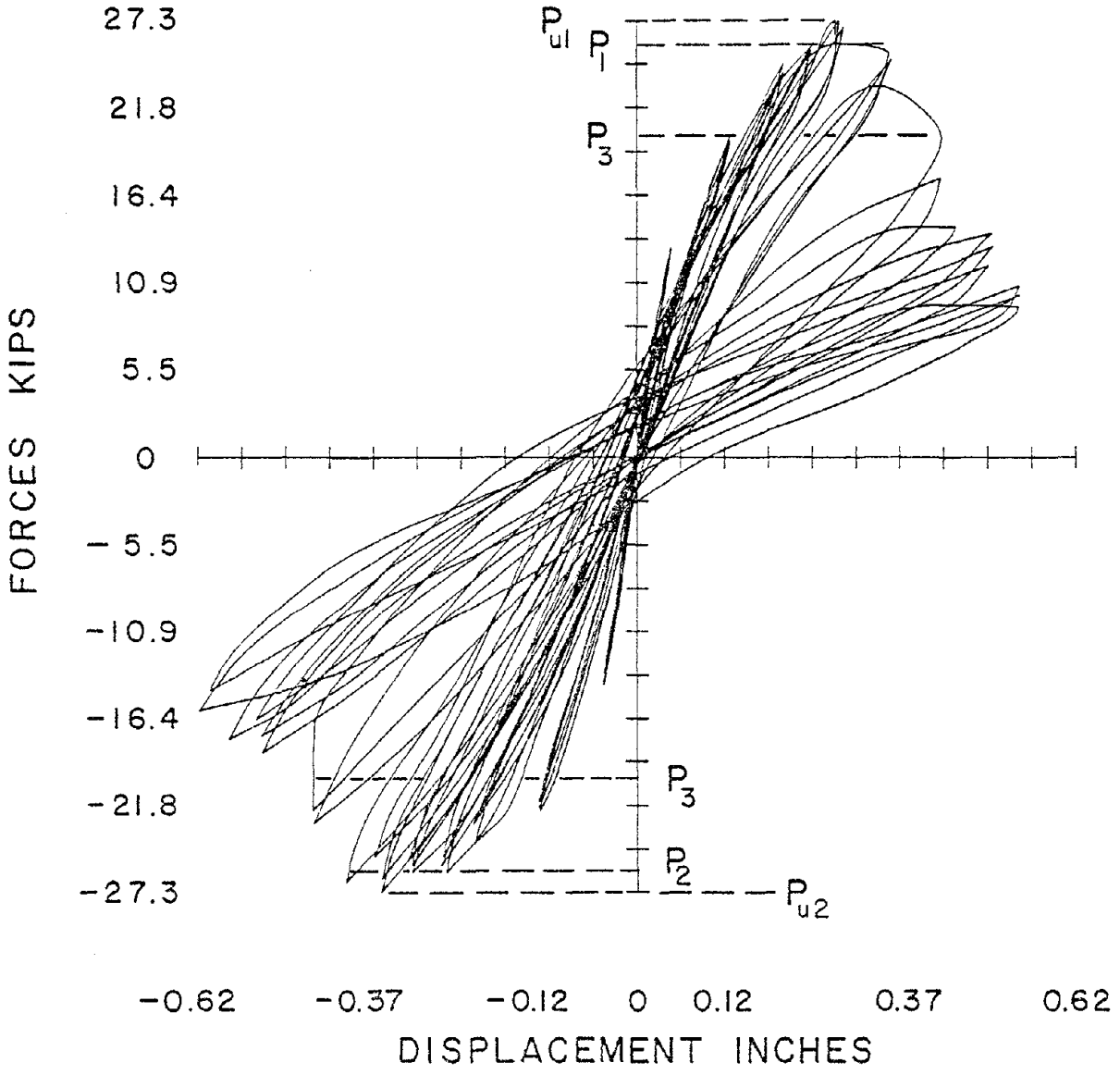

P_{u1} , P_{u2} – PEAK ULTIMATE STRENGTHS

P_1 , P_2 – AVERAGE ULTIMATE STRENGTHS APPROXIMATELY 90% OF P_{u1} , P_{u2}

P_3 – WORKING ULTIMATE STRENGTH APPROXIMATELY 70-80% OF P_{u1} , P_{u2}

FIGURE 4.41(1) DEFINITION OF ULTIMATE STRENGTH

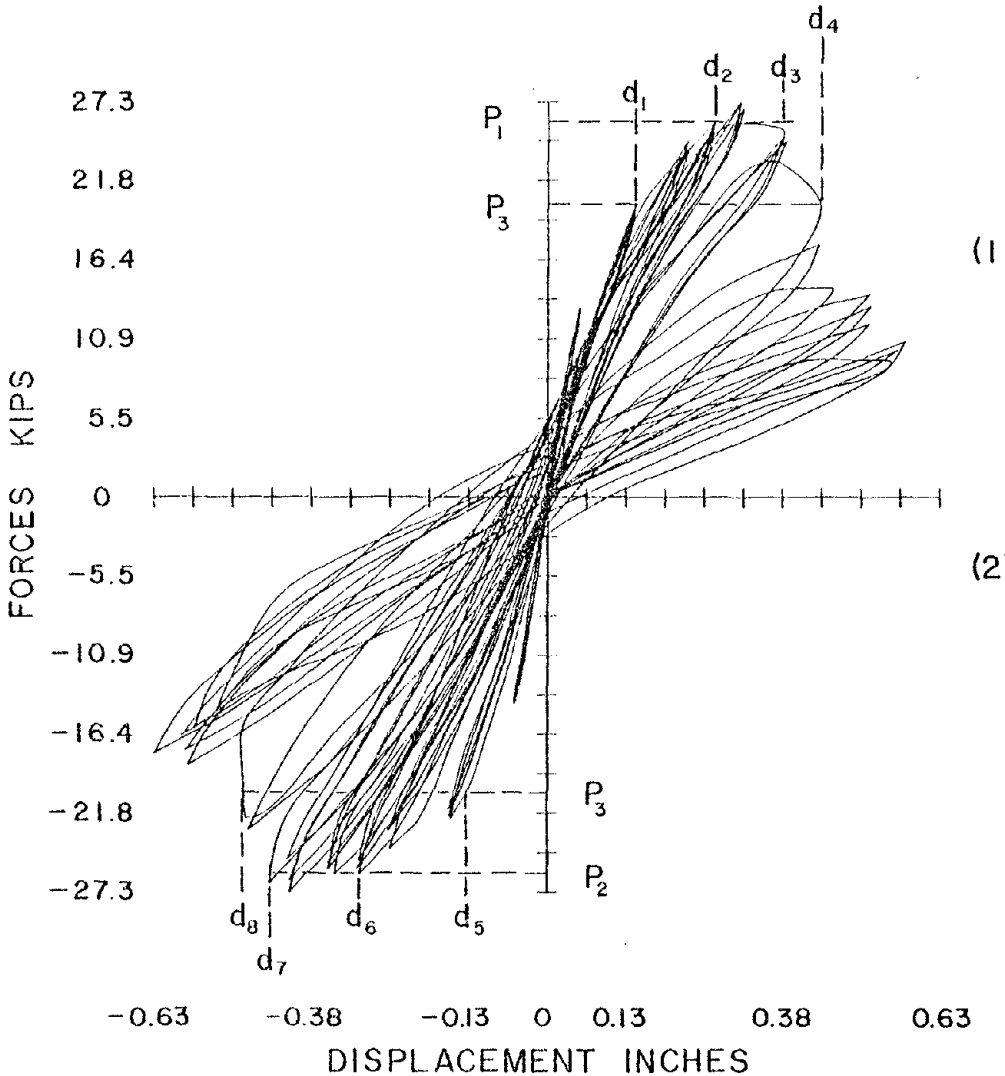

DUCTILITY INDICATORS

(1) AT AVERAGE ULTIMATE STRENGTH - P_1, P_2

$$\delta_1 = \frac{d_3}{d_2} \qquad \delta_2 = \frac{d_7}{d_6}$$

VARIED BETWEEN
1.45 — 5.1

(2) AT WORKING ULTIMATE STRENGTH - P_3

$$\delta_3 = \frac{d_4}{d_1} \qquad \delta_4 = \frac{d_8}{d_5}$$

VARIED BETWEEN
2.4 — 8.1

FIGURE 4.41(2) DEFINITION OF DUCTILITY INDICATORS

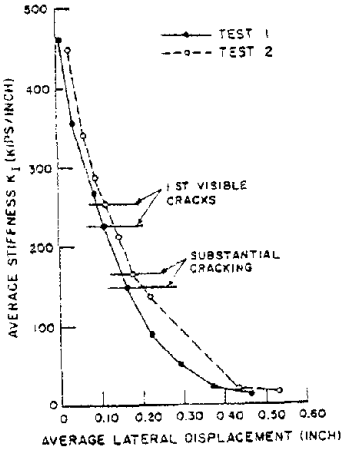

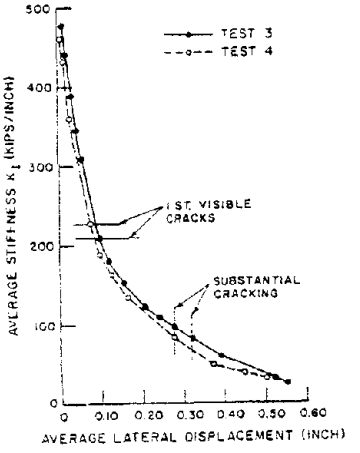

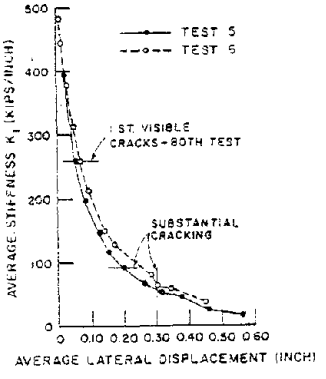

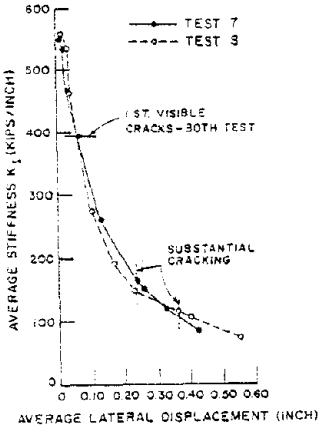

FIGURE 4.42 STIFFNESS DEGRADATION VS. LATERAL DISPLACEMENT

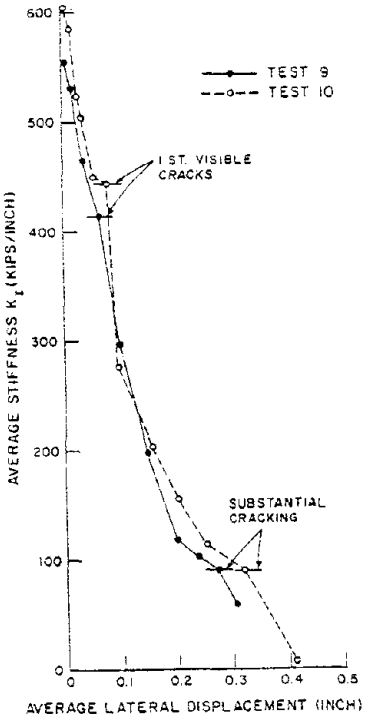

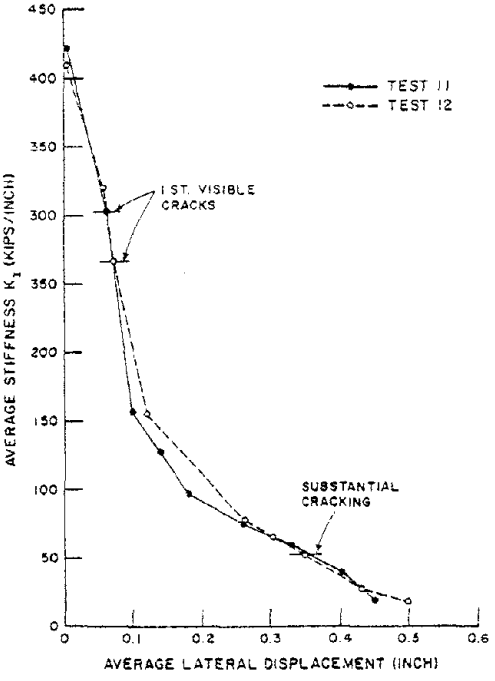

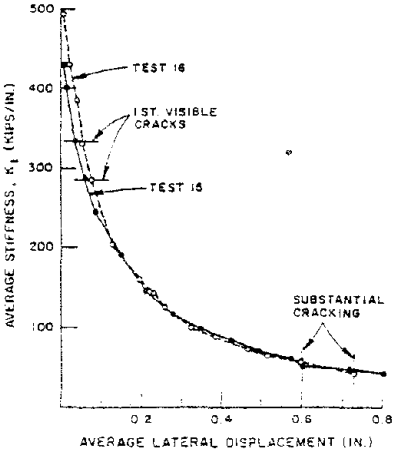

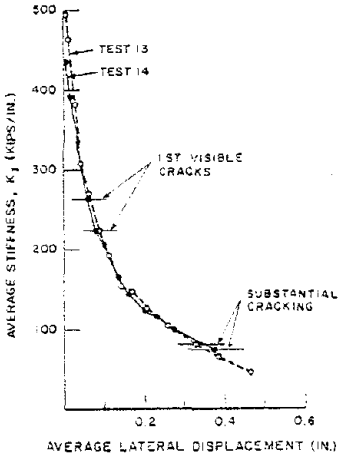

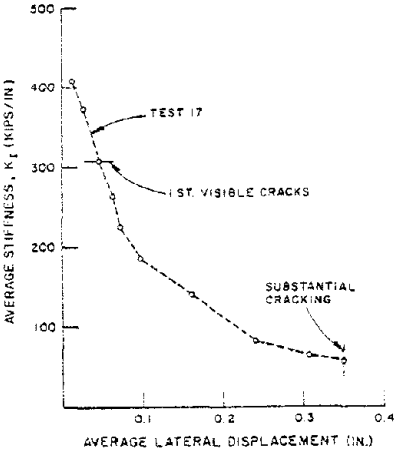

FIGURE 4.42 CONTINUE

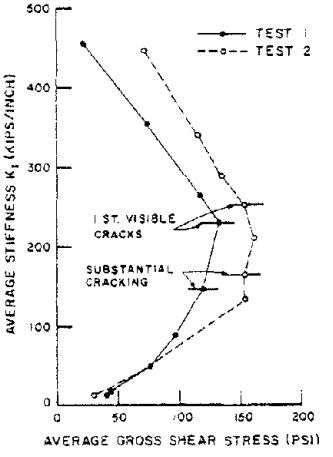

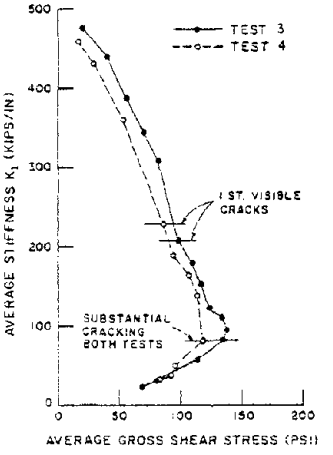

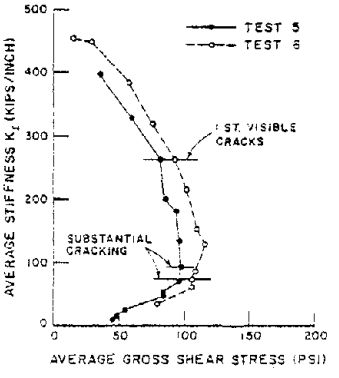

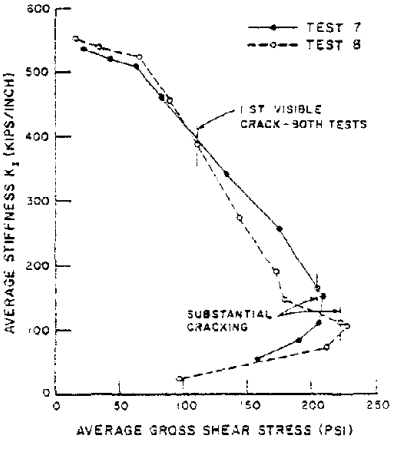

FIGURE 4.43 STIFFNESS DEGRADATION VS. SHEAR STRESS

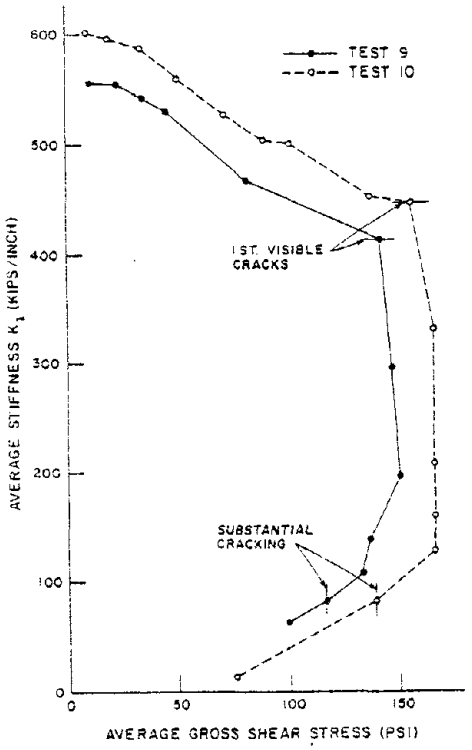

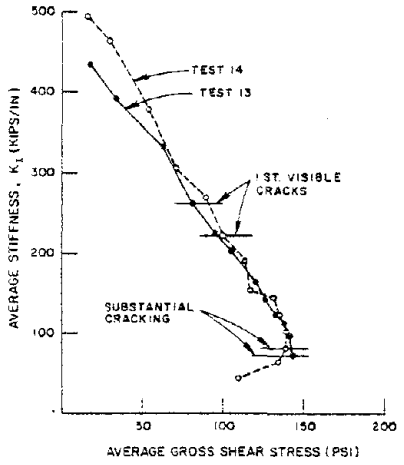

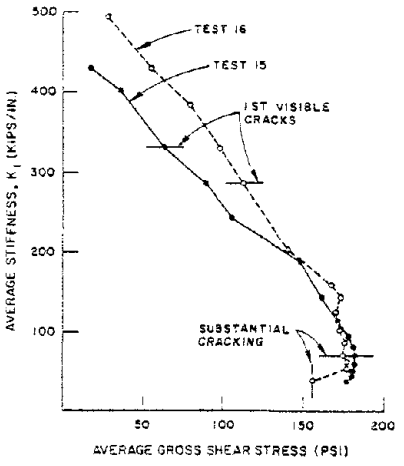

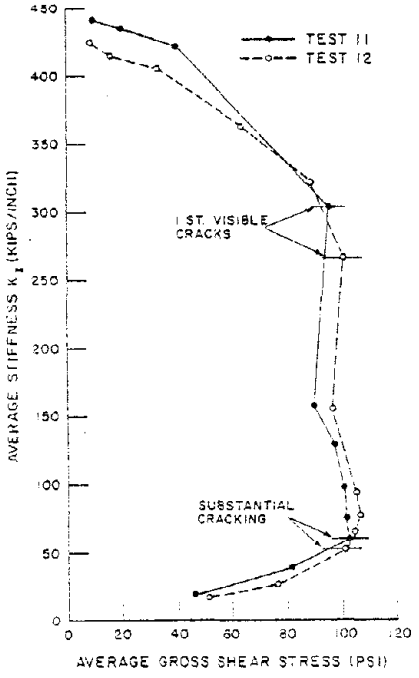

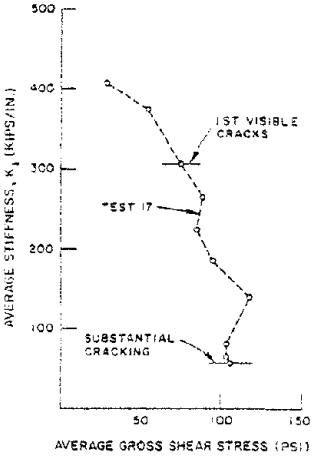

FIGURE 4.43 CONTINUE

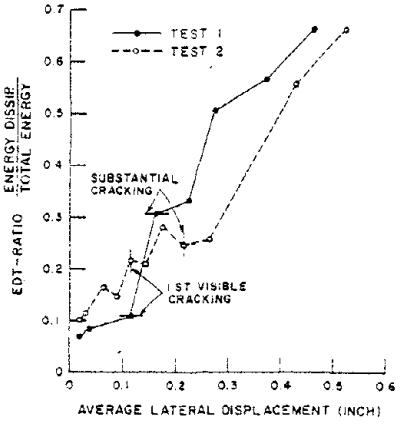

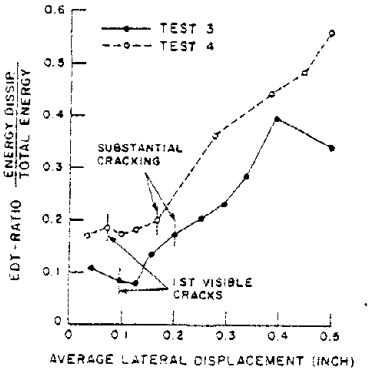

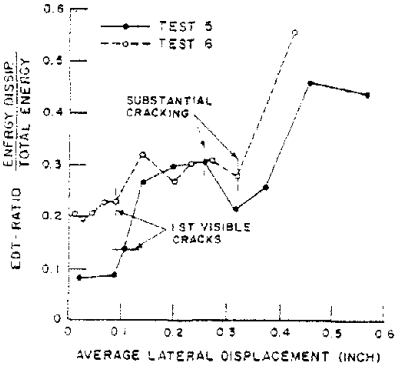

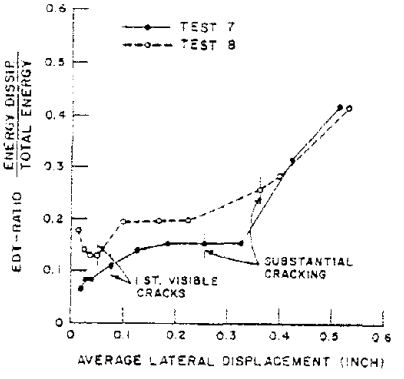

FIGURE 4.44 EDT - RATIO VS. LATERAL DISPLACEMENT

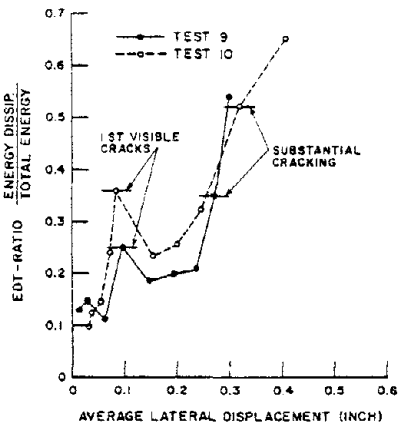

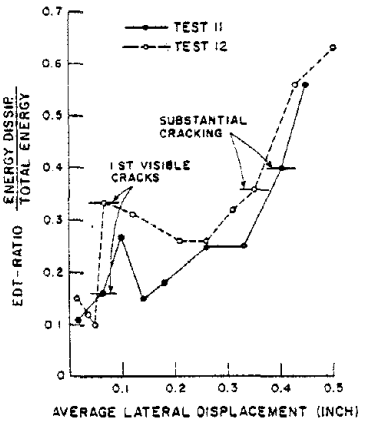

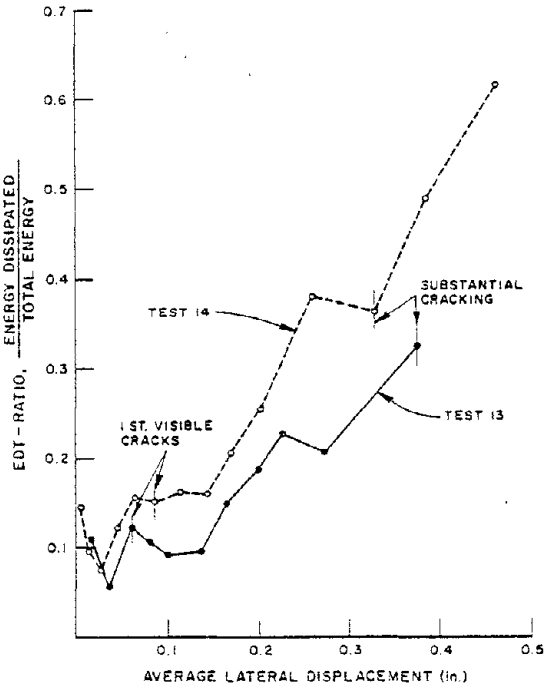

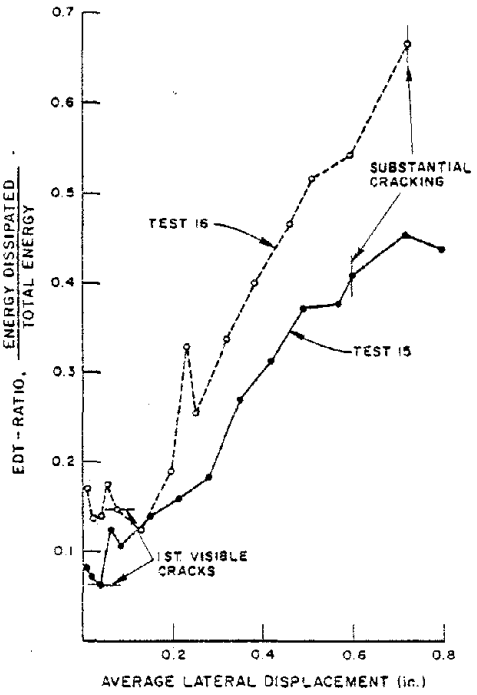

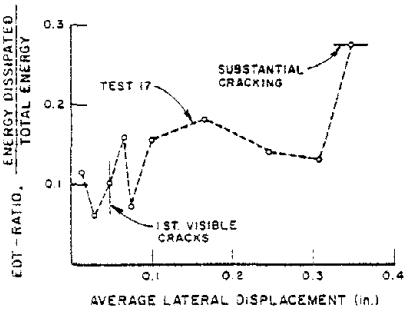

FIGURE 4.44 CONTINUE

5. DISCUSSION OF THE DOUBLE-PIER TEST RESULTS

5.1 Introduction

In order to categorize the effects of the various parameters on the dynamic properties and inelastic characteristics of the piers, the results of the seventeen tests are discussed under the following headings:

5.2 Ductility

5.3 Ultimate Strength

5.4 Stiffness Degradation

5.5 Energy Dissipation

5.6 Loading Sequence

A comparison of the theoretically predicted ultimate strengths and the observed test results is included in EERC Report No. 76-16. This comparison is of two-fold importance. First, test series such as those discussed here must be directed toward correlation of test results with theoretical methods of predicting the ultimate strength. Secondly, and more importantly, the test results are being used in an attempt to develop an ultimate strength design concept for masonry piers.

In considering these results, it is well to recall the earlier comment that Panels 1 and 2, 5-12, and 17 failed in the shear mode, Panels 3 and 4 failed in a combination of the shear and flexural modes, while Panels 13-16 failed in the flexural (secondary compression) mode.

5.2 Ductility

From the hysteresis loops and envelopes plotted in Figures 4.1 to 4.17 it is clear that almost all of the piers exhibit a ductile type of behavior. However, it is difficult to quantify and compare the ductility

in the various cases. From the hysteresis envelopes plotted in Figures 4.37 to 4.40 two distinct types of behavior are evident. The first is typified by Test 1 in Figure 4.37 where the hysteresis envelope reaches a maximum load, and then as the lateral displacement increases the load gradually decreases. The second is typified by Tests 11 and 15 in Figures 4.38 and 4.40 where the hysteresis envelope reaches a maximum load, and then as the lateral displacement increases this load is maintained up to a critical displacement at which point the load decreases. This is somewhat similar to an elasto-plastic force-deflection relationship. The first type of behavior is characterized by low values of the parameter $\frac{\delta_1 + \delta_2}{2}$ (approximately 1.5) and larger values of the parameter $\frac{\delta_3 + \delta_4}{2}$ (in the range of 2 to 6) whereas the corresponding values for the second type of behavior are in the range of 2-5 and 4-10, respectively.

A note of caution is made at this point with respect to the ductility indicators, in that they cannot be considered in isolation when evaluating the inelastic performance of the piers. First, the initial displacement at which the ductility indicators are measured $\frac{d_2 + d_6}{2}$ for $\frac{\delta_1 + \delta_2}{2}$ and $\frac{d_1 + d_5}{2}$ for $\frac{\delta_3 + \delta_4}{2}$ (see Figure 4.41 for the definition of d_1, d_2, d_5 and d_6), must be used in order to evaluate the displacement range over which the ductility indicators are valid. For example, Tests 1 and 8 have the same values of $\frac{\delta_1 + \delta_2}{2}$ and $\frac{\delta_3 + \delta_4}{2}$ but from the hysteresis envelopes shown in Figure 4.39, Test 8 obviously has a much more desirable inelastic behavior. Secondly, the maximum displacement the piers can withstand before failure is also important. For example,Tests 9 and 10 have reasonably large values of $\frac{\delta_1 + \delta_2}{2}$ and $\frac{\delta_3 + \delta_4}{2}$ compared to Tests 1 and 2, but the piers of 9 and

10 completely collapsed at a lateral displacement of only 0.5" whereas Tests 1 and 2 did not collapse until displacing 1.0". These two factors illustrate the limitations of the ductility indicators and demonstrate the necessity of including with the ductility indicators, the displacement range over which they are valid and the maximum lateral displacement the piers can withstand, in characterizing the ductility of the piers.

Another question to be considered is what constitutes desirable inelastic behavior. It is difficult to answer this question in quantitative terms but Figures 5.1, a, b and c are useful for a qualitative discussion of three different aspects of the behavior encountered in the test program. Figure 5.1(a) shows a set of four force-deflection relationships each with the same ultimate strength (F_1). Obviously the inelastic force-deflection relationship becomes more desirable in passing from curves A through D. Figure 5.1(b) shows a set of four force-deflection relationships with different ultimate strengths. The relative desirability of these curves is more difficult to evaluate as it is a function of the imposed interstory deflection. If the interstory deflection never exceeds d_1 then piers with the force-deflection relationships given by B, C and A are preferable to those of D. If the interstory deflection increases to d_2 then B C and D are preferable to A, and finally if the interstory deflection increases to d_3 then the order of increasing preference is A, B, C and D. Hence the relative desirability of the force-deflection relationships in Fig. 5.1b depends on the intensity of the expected earthquake. For a moderate earthquake where the interstory deflection is not expected to exceed d_1, the order of increasing preference would be D, C, A and

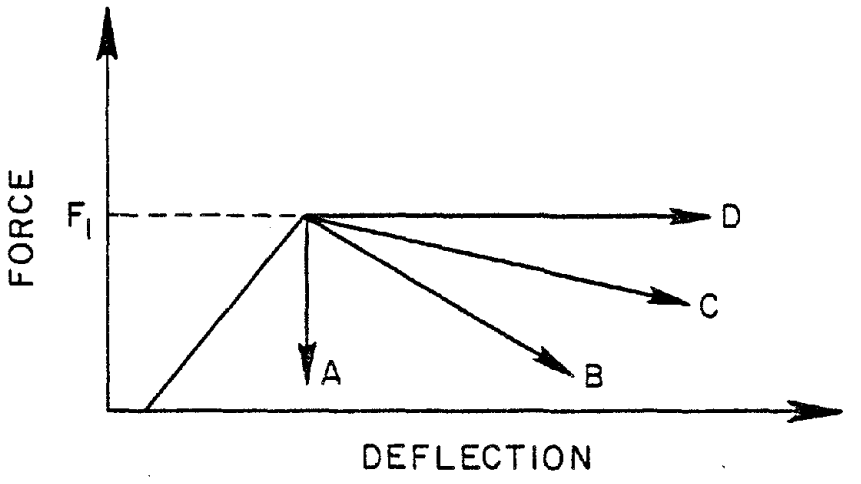

(A)

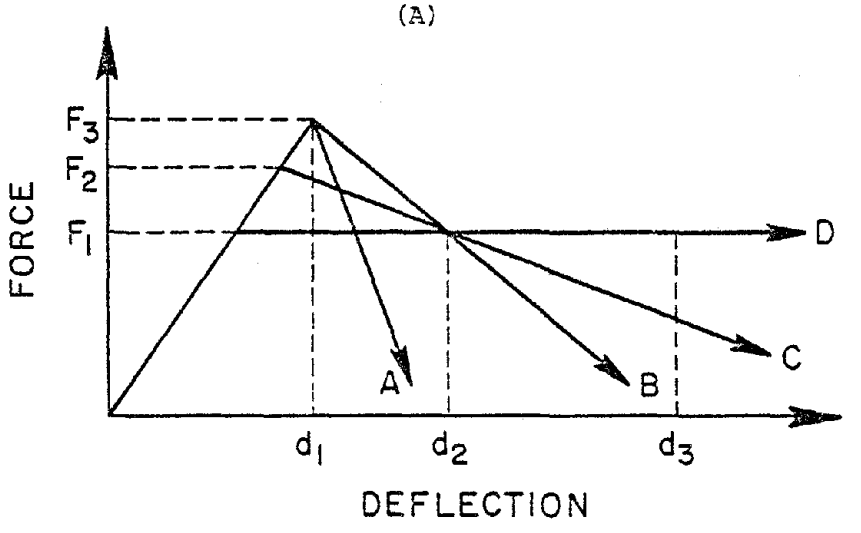

(B)

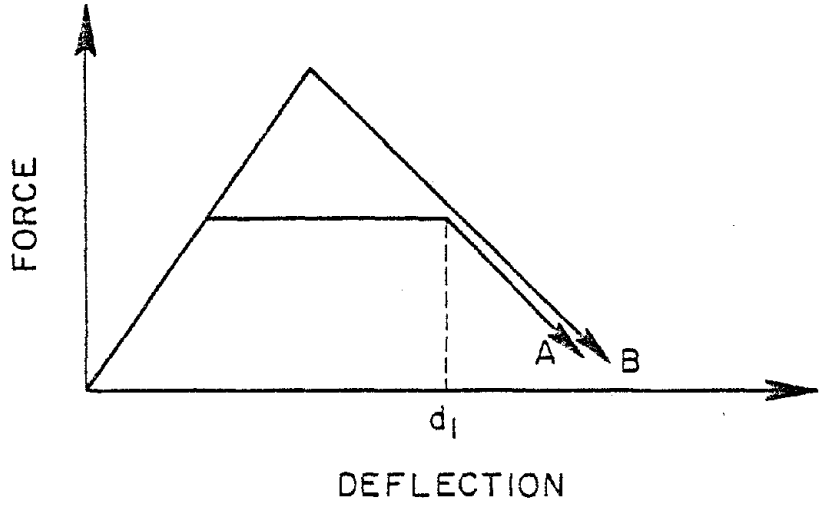

(C)

FIGURE 5.1 IDEALIZED HYSTERESIS ENVELOPES

B. If,however, a large earthquake is considered, where the interstory deflection could be expected to be of the order of d_3, the order of increasing preference would be A, B, C and D.

For the two force-deflection relationships given by Figure 5.1(c) obviously B is preferable to A as it is able to resist a greater lateral force and has the same characteristics when the interstory deflection exceeds d_1. With the foregoing discussion in mind the effect of the various test parameters on the ductility of the piers will be discussed.

The effect of bearing stress on the ductility of the piers is somewhat inconclusive. Evaluating the hysteresis envelopes of Figure 4.37 and the ductility indicators of Table 4.1, there is a trend towards a more ductile behavior as the bearing stress increases, however this is offset by the fact that the piers with a bearing stress of 500 psi can only withstand a maximum lateral displacement of 0.5" as opposed to 1.0" for the 0 and 250 psi piers. If the maximum displacement of 0.5" is not critical, then an increase in bearing stress could be considered to have a desirable effect on the ductility of the piers for the tests performed. However, because the number of tests is limited and because this finding conflicts with the conclusion of other investigators (see EERC Report No. 76-16), this parameter obviously requires further investigation.

The effect of partial grouting (Tests 1, 2, 11 and 12) on the ductility of the piers is also inconclusive. From the hysteresis envelopes of Figure 4.38, partial grouting produces a tendency towards an elasto-plastic type of force-deflection behavior and when compared to the fully grouted pseudo-static test (Test 1) the overall effect is significantly more desirable. However when compared to the fully grouted dynamic test the force-deflection curves are similar to those of

Figure 5.1(c) and, as explained previously, the fully grouted pier must be considered to have more desirable ductile behavior. In addition, both the partially grouted piers collapsed at a lateral displacement of 0.5" as opposed to 1.0" for the fully grouted walls. Because of the limited number of tests performed and the lack of any definite trend in the results it is clear that further tests are required.

Horizontal reinforcement has a very desirable effect on the shear mode of failure (Tests 1, 2, 7 and 8). As seen from the hysteresis envelopes of Figure 4.39 and the ductility indicators of Table 4.1, horizontal reinforcement substantially increases the overall ductility of the piers, with the dynamic test having a better performance than the pseudo-static test.

The performance in the flexural mode of failure was evaluated in Tests 3, 4 and 13-16 with hysteresis envelopes plotted in Figure 4.40. The basic difference between Tests 3, 4 and 13, 14 was the inclusion of horizontal reinforcement in Tests 13 and 14 to ensure that a pure flexural mode of failure was obtained. As expected, Tests 3 and 4 had characteristics of both the shear and flexural modes of failure, showing a more sudden drop in load carrying capacity at larger lateral displacements. Tests 13 and 14 show that the force-deflection relationship of the flexural mode of failure tends towards elasto-plastic characteristics. The most significant result determined in this series of tests was the effect of the joint reinforcement included in Tests 15 and 16 (Figures 2.4 and 2.5). The addition of the perforated steel plates in the mortar joints substantially increased both sets of ductility indicators as well as the maximum displacement that the piers could withstand, leading to extremely desirable inelastic behavior.

In summary, it is clear that more research is required to define the effect of bearing stress and partial grouting on the ductility of the piers although trends were indicated by the tests performed. However, it is concluded that it is possible to reinforce masonry piers so as to produce desirable ductile behavior. First, for piers failing in the shear mode, the addition of a sufficient amount of horizontal reinforcement produces a more ductile type of inelastic behavior. Second, piers failing in the flexural mode can be designed to have desirable ductile characteristics; moreover these characteristics can be improved still further with the addition of joint reinforcement.

5.3 Ultimate Strength

From the results presented in Table 4.1 it is clear that the ultimate strength of the piers is affected by the quantity and distribution of horizontal and vertical reinforcement, the bearing stress, the rate of loading and partial grouting. The effect of each of these parameters on the ultimate strength will be discussed separately and in qualitative terms. A quantitative correlation of the test results with theoretical predictions is presented in EERC Report No. 76-16.

5.3.1 Effect of Reinforcement

The effect of reinforcement on the ultimate strength is considered in conjunction with the various modes of failure, in the following paragraphs.

a) Shear Mode of Failure: Tests 1, 2, 7 and 8 indicate the effect of horizontal reinforcement on the shear mode of failure. As seen from Table 4.1, horizontal reinforcement substantially increased the ultimate strength of the piers. The ultimate strength shown by the dynamic test

is almost equal to the area of steel multiplied by the yield strength of the steel. If this result is substantiated by future tests, it is an important finding for design. In addition, if this behavior is coupled with desirable ductility, as it appears from the test results, then an adequate ultimate strength design concept can be developed for this mode of failure. However, a note of caution must be added in that this observation has not been substantiated by other investigators - see EERC Report No. 76-16.

b) Flexural Mode of Failures: Tests 3, 4 and 13-16 all failed in flexure. Several investigators have shown that the ultimate strength in this mode of failure can be predicted with reasonable accuracy. Priestley and Bridgeman[17] showed that if joint reinforcement is not present then the yield strength of the re-bars should be used to calculate the ultimate strength of the piers. However, if joint reinforcement is present then the ultimate strength of the re-bar should be used in predicting the ultimate strength of the piers. From the results shown in Table 4.1, this finding appears to be valid for the present tests because the ultimate strength of the piers with joint reinforcement is greater than for those without. The quantitative correlation with respect to this parameter is presented in EERC Report No. 76-16.

5.3.2 Effect of Bearing Load

The results of Tests 1, 5 and 9 indicate that, for a pseudo-static test, an increase in bearing stress from 0 to 250 to 500 psi causes a corresponding increase in the peak ultimate strength. For the corresponding dynamic (3 cps) Tests 2, 6 and 10, an increase in the peak

ultimate strength is obtained only as the bearing stress increases from 0 to 250 psi.

Figures 5.2(a) and (b) are plots of the bearing stress (based on net area) versus the working ultimate shear stress τ_3 (defined in Table 4.1) and the average peak ultimate shear stress $\frac{\tau_{u1} + \tau_{u2}}{2}$ for Tests 1, 2, 5, 6, 9 to 12 and 17, respectively. The linear dotted lines indicate that within experimental limits there appears to be a proportional relationship between the shear strength and increasing bearing stress. This factor is discussed in detail in EERC Report No. 76-16. Because each set of two test specimens was built at different times, the prism compressive strength (f'_m) of each pair varied over a range of 2110 psi to 2630 psi. In order to determine the effect of this variation, the shear strength was non-dimensionalized by dividing by f'_m and re-plotted against the bearing stress in Figures 5.3(a) and (b). Again the proportional trend is apparent.

5.3.3 Effect of Partial Grouting

The effect of partial grouting was evaluated in Tests 1, 8, 11, and 12. As expected there was a drop in the ultimate strengths based on gross area for the partially grouted walls. However if a comparison is made between the ultimate strengths based on net area, see Table 4.1, it can be seen that the net strengths for the pseudo-static tests are the same whereas for the dynamic test the fully grouted pier has a greater (25%) net ultimate strength than the partially grouted piers.

5.3.4 Effect of Rate of Loading

The effect of the rate of loading proved to be somewhat surprising. For piers failing in the shear or diagonal tension mode (Tests 1, 2, 5

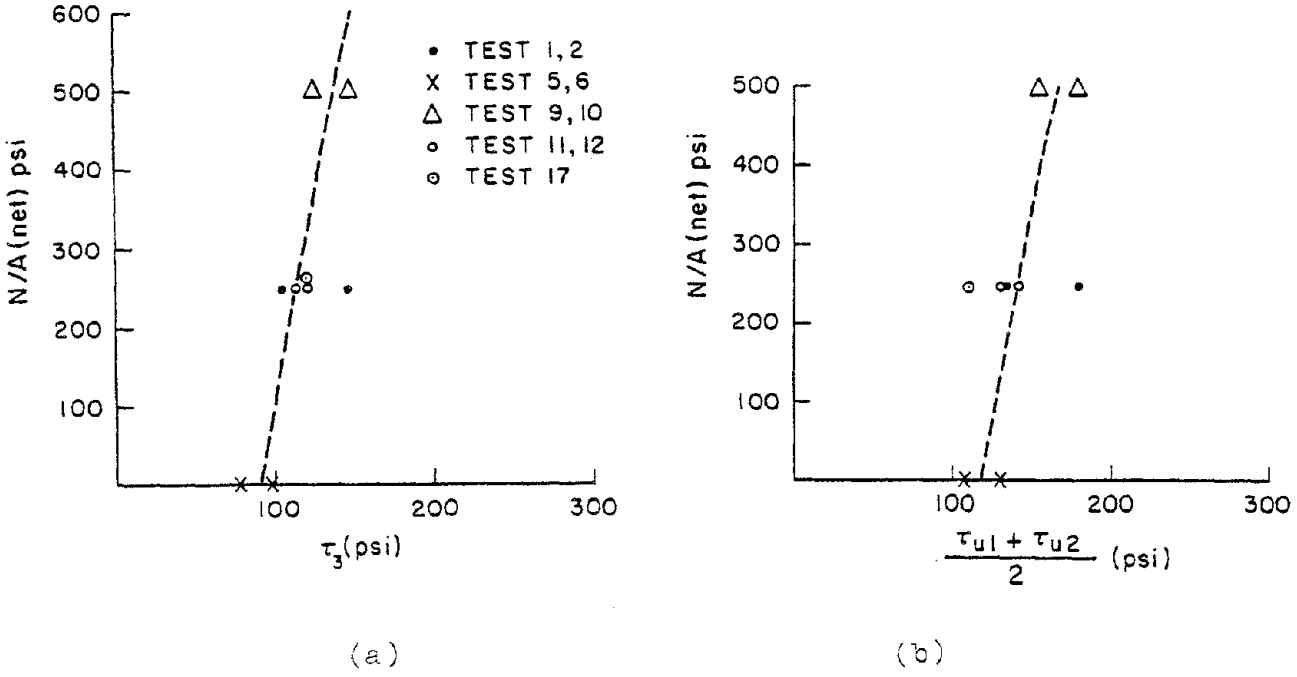

FIGURE 5.2 SHEAR STRESS VS. BEARING LOAD

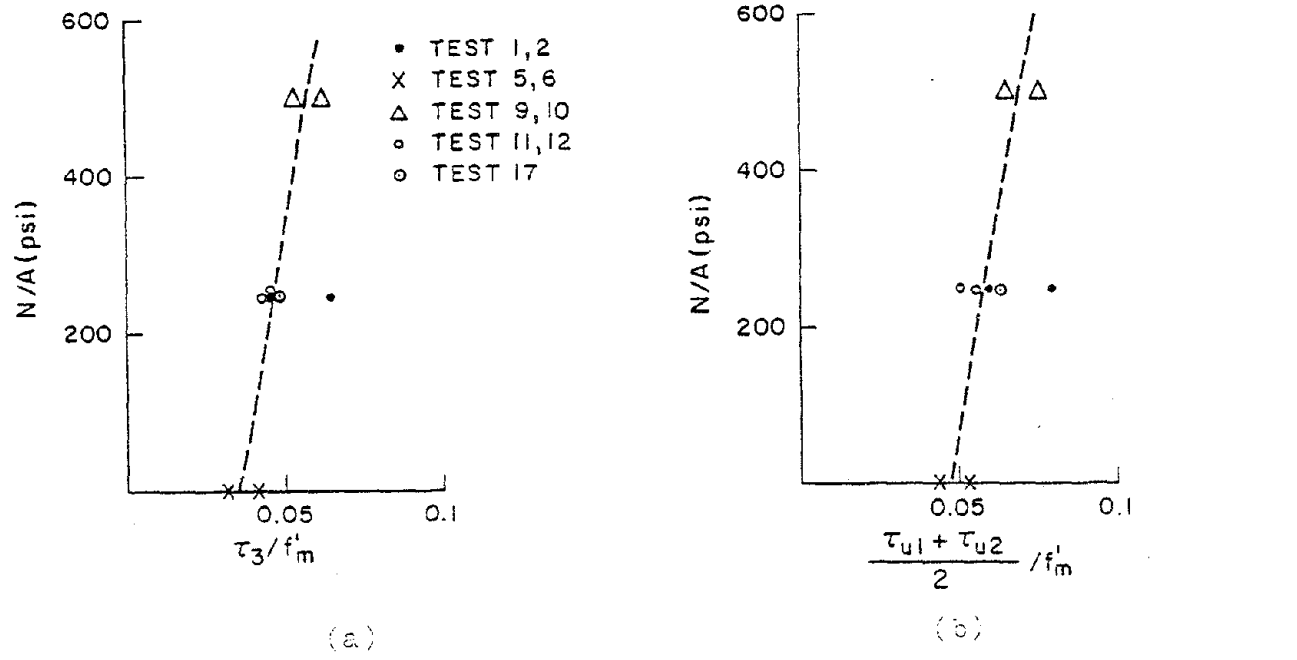

FIGURE 5.3 NONDIMENSIONALIZED SHEAR STRESS VS. BEARING LOAD

to 12) the peak and average strengths of the pseudo-static test were 8-23% less than those of the corresponding dynamic test. For piers failing in the flexural mode, the dynamic (3 Hz) values were either less than, or almost equal to, the pseudo-static strengths. For Tests 3 and 4 which failed in a combination of the shear and flexural modes, the pseudo-static peak ultimate strength was 5% greater than the dynamic strength. The corresponding difference for the average ultimate strength was 16%. For piers failing in the flexural mode, without joint reinforcement (Tests 13 and 14), the respective percentages were 1% and 8%. When joint reinforcement was added (Tests 15 and 16) the peak ultimate strength of the pseudo-static test was 3% greater than the dynamic strength while the average ultimate strength was 3.7% less.

Based on the limited number of tests performed, it appears that the ultimate strength obtained from the dynamic tests involving flexural failure is either less than or almost equal to the pseudo-static strengths. This result is somewhat surprising because for both concrete and steel members the effect of increasing the loading rate is to increase the ultimate strength; this same tendency was also found in the present tests involving the shear mode of failure. The implication of this conclusion (if substantiated by further tests) is that pseudo-static test results are non-conservative for the flexural mode of failure.

5.4 Stiffness Degradation

From Figures 4.42 and 4.43, it is clear that the piers suffer substantial stiffness degradation while being subjected to gradually increasing lateral displacements. The stiffness K_I at low (20 psi) shear stresses was affected by three of the basic test parameters:

bearing stress, rate of loading and partial grouting. The effect of horizontal reinforcement was not conclusive (Table 5.1).

An increase in the bearing stress from 0 to 250 to 500 psi increased K_I from 420 to 455 to 555 kips/in. for the 0.02 Hz tests and 450 to 510 to 605 kips/in. for the 3 Hz tests. In all tests except 3 and 4, an increase in the rate of loading caused an increase in K_I. This increase varied between 1.8% for Tests 7 and 8 and 18% for Tests 15 and 16. Partial grouting caused a decrease in K_I. The effect of horizontal reinforcement on Tests 1, 2, 7 and 8 caused a substantial increase in K_I, whereas for Tests 3, 4, and 13-16 the effect of horizontal reinforcement was negligible.

As the shear stress increased to 50 psi, the drop in K_I was between 8% and 19.6% in Tests 1 to 6 and 10 to 16, whereas with Tests 7 to 9 the maximum drop was 4.5%. It should be noted that at a shear stress of 50 psi there were no cracks visible to the eye. As the shear stress increased above 50 psi cracks became visible and the drop in stiffness was more severe.

The significance of these results, when evaluated from a theoretical point of view, is that a decrease in one or both of the apparent elastic moduli is indicated. The stiffness of the piers is a function of the shear modulus (G) and Young's modulus (E) of the non-homogeneous material, and as the measure of the stiffness (K_I) decreases with increasing lateral displacement, clearly E and/or G decreases in a similar manner.

With regard to the dynamic response of a masonry multistory building, these results indicate that the period of vibration of the building will increase as the amplitude of deformation increases. Depending upon the initial vibration period of the building and the nature of the earthquake

TABLE 5.1

THE EFFECT OF SHEAR STRESS AND OTHER PARAMETERS ON THE STIFFNESS COEFFICIENT K_I

TEST NO.	Frequency (cps)	Bearing Stress (psi)	Vertical Reinforcement	Horizontal Reinforcement	K_I at 20 psi (kips/in.)	K_I at 50 psi (kips/in.)	Percentage Decrease (%)
1	0.02	250	2 - #6	--	455	390	14.3
2	3	250	2 - #6	--	520 (est.)	465 (est.)	10.5
3	0.02	125	2 - #4	--	485	405	16.5
4	3	125	2 - #4	--	460	370	19.6
5	0.02	0	2 - #6	--	420 (est.)	350	16.7
6	3	0	2 - #6	--	450	400	11.1
7	0.02	250	2 - #6	1 - #5	545	525	3.7
8	3	250	2 - #6	1 - #5	555	540	2.7
9	0.02	500	2 - #6	--	555	520	4.5
10	3	500	2 - #6	--	605	560	7.4
11	0.02	250	2 - #6	--	415	380	8.4
12	3	250	2 - #6	--	435	400	8.0
13	0.02	125	2 - #4	3 - #7 2 - #5	430	360	16.3
14	3	125	2 - #4	3 - #7 2 - #5	485	395	18.6
15	0.02	125	2 - #4	3 - #7 2 - #5 6 - H	435	370	14.9
16	3	125	2 - #4	3 - #7 2 - #5 6 - H	515 (est.)	445	13.6
17	3	250	--	--	415 (est.)	380	8.4

excitation this behavior may or may not be desirable; however, in most cases the effect will be desirable in that the period shifts to a more favorable portion of the response spectrum.

5.5 Energy Dissipation

The energy dissipation characteristic expressed in terms of the EDT (strain energy) ratio (Equation 4.2 and plotted in Figure 4.43) is difficult to evaluate because in our view it is a function of the previous load history as discussed in the following section. However the trends of the plots indicate that when substantial cracking occurs there is a significant increase in the EDT ratio.

5.6 Effect of Loading Sequence

One of the most difficult decisions involved in an experimental investigation of this type is the choice of the loading sequence to be used. The objective of this test program was to evaluate the performance of the piers in multistory buildings when they are subjected to earthquake excitations. The actual loading sequence of a pier in a multistory building can be determined by calculating the time history of the interstory drift applied to the pier of interest. It is at this point that difficulties arise. The time histories of interstory drift are a function of both the multistory building properties and the earthquake excitation. Because of the large variability of both the earthquake excitation and the types of buildings, it is impossible to cover all types of possible loading sequences. However, as a gross generalization, the predominant nature of the interstory drift is sinusoidal with a frequency approximately equal to the fundamental frequency of the building.

The magnitude of the sinusoidal displacement is obviously a function of the ground motion and if the earthquake is characterized by early large amplitude motion then the amplitude of the interstory drift will build up to its maximum quickly and then slowly decrease. If, however, the earthquake is characterized by a gradual build up to its large amplitude motion then the amplitude at the interstory drift will gradually build up to its maximum amplitude and then decrease.

Because only a limited number of tests could be performed in this investigation, it was decided to used a sinusoidal controlled displacement with gradually increasing amplitude as the input. Until a comparison is made with other types of loading sequences, it is difficult to evaluate the effect of the loading sequence on the results; however the following opinions are presented. First, it is probable that the type of load sequence chosen will demonstrate the best possible ductility of the piers. If the piers had not been subjected to such a gradual build up in lateral displacement, the ductility might not have been as good as was demonstrated by these tests; however this observation must be verified in future test programs. Second, the energy dissipated per cycle of loading is probably lower in these tests than would be expected if a less extensive load history were used because the loading sequence used in this test series leads to a gradual breakdown in the energy dissipating mechanisms. Again, this opinion must be verified in future test programs.

6. CONCLUSIONS

The main conclusion of this report is that much more research is required on the shear strength of masonry piers. Trends of behavior were indicated in these results, but because an insufficient number of tests were performed definitive conclusions could not be made on many facets of the initial goals of the investigations. Nevertheless, the following definite trends could be identified from the results obtained.

1) The inclusion of a sufficient amount of horizontal reinforcement significantly enhances the ductile behavior of piers failing in the shear mode.

2) The inclusion of 1/8" plates in the horizontal mortar joints at the toes of the piers produces extremely desirable ductile behavior for piers failing in the flexural mode.

3) An increase in bearing stress produces a tendency towards a more ductile type of behavior for piers failing in the shear mode.

4) Partial grouting produces a tendency towards an elasto-plastic force-deflection relationship for piers failing in the shear mode. However, it is not clear whether partial grouting enhances the overall ductile behavior of the piers when compared to the behavior of fully grouted piers.

5) Piers that failed in the shear mode had pseudo-static ultimate strengths less than the corresponding dynamic strengths whereas piers that failed in the flexural mode had pseudo-static ultimate strengths greater or almost equal to the corresponding dynamic strengths.

6) The initial stiffness of the piers was increased significantly by increasing the bearing stress. All piers suffered substantial stiffness degradation as the lateral displacement increased.

REFERENCES

1. Blume, J. A. and Prolux, J., "Shear in Grouted Brick Masonry Wall Elements," Report to Western States Clay Products from J. A. Blume and Associates, August 1968.

2. Borchelt, J. G., "Analysis of Brick Walls Subjected to Axial Compression and in Plane Shear," Proceedings of Second International Brick Masonry Conference, Stoke-on-Trent, April 1970.

3. Greenley, D. G. and Cattaneo, L. E., "The Effect of Edge Load on the Racking Strength of Clay Masonry," Proceedings of Second International Brick Masonry Conference, Stoke-on-Trent, April 1970.

4. Haller, P., "Load Capacity of Brick Masonry," Designing, Engineering and Constructing with Masonry Products, Edited by F. B. Johnson, May 1969.

5. Kalita, U. C. and Hendry, A. W., "An Experimental and Theoretical Investigation of the Stresses and Deflections in Model Cross Wall Structures," Proceedings of the Second International Brick Masonry Conference, Stoke-on-Trent, April 1970.

6. Moss, P. J. and Scrivener, J. C., "Masonry Wall Panel Tests," New Zealand Concrete Construction, April 1968.

7. Pieper, K. and Trausch, W., "Shear Tests on Walls," Proceedings of Second International Brick Masonry Conference, Stoke-on-Trent, April 1970.

8. Schneider, R. R., "Lateral Load Tests on Reinforced Grouted Masonry Shear Walls," University of Southern California Engineering Center, Report No. 70-101, 1959.

9. Schneider, R. R., "Shear in Concrete Masonry Piers," California State Polytechnic College, Pomona, California, 1959.

10. Scrivener, J. C., "Concrete Masonry Wall Panel Tests with Predominant Flexural Effect," New Zealand Concrete Construction, July 1966.

11. Scrivener, J. C., "Static Racking Tests on Concrete Masonry Walls," Designing, Engineering and Constructing with Masonry Products, Edited by F. B. Johnson, May 1969.

12. Sinha, B. P., and Hendry, A. W., "Racking Tests on Story Height Shear Wall Structures with Openings, Subjected to Precompression," Designing, Engineering and Constructing with Masonry Products, Edited by F. B. Johnson, May 1969.

13. Sinha, B. P., Maurenbrecher, A. H. P. and Hendry, A. W., "Model and Full Scale Tests on a Five Story Cross Wall Structure under Lateral Loading," Proceedings of Second International Brick Masonry Conference, Stoke-on-Trent, April 1970.

14. Turnsek, V. and Cacovic, F., "Some Experimental Results on the Strength of Brick Masonry Walls," Proceedings of Second International Brick Masonry Conference, Stoke-on-Trent, April 1970.

15. Williams, D. W., "Seismic Behaviour of Reinforced Masonry Shear Walls," Ph.D. Thesis, University of Canterbury, Christchurch, New Zealand.

16. Meli, R., "Behaviour of Masonry Walls Under Lateral Loads," Proceedings Fifth World Conference on Earthquake Engineering, Rome, 1972.

17. Priestley, M. J. N. and Bridgeman, D. O., "Seismic Resistance of Brick Masonry Walls," Bulletin of the New Zealand National Society for Earthquake Engineering, Vol. 7, No. 4, December 1974.

18. Mayes, R. L. and Clough, R. W., "A Literature Survey - Compressive, Tensile, Bond and Shear Strength of Masonry," EERC Report No. 75-15, University of California, Berkeley, August 1975.

19. Mayes, R. L. and Clough, R. W., "State-Of-The-Art in Seismic Shear Strength of Masonry - An Evaluation and Review," EERC Report No. 75-21, University of California, Berkeley, October 1975.

20. 1974 Masonry Codes and Specifications, Published by Masonry Industry Advancement Committee, California, 1974.

EARTHQUAKE ENGINEERING RESEARCH CENTER REPORTS

EERC 67-1 "Feasibility Study Large-Scale Earthquake Simulator Facility," by J. Penzien, J. G. Bouwkamp, R. W. Clough and D. Rea - 1967 (PB 187 905)

EERC 68-1 Unassigned

EERC 68-2 "Inelastic Behavior of Beam-to-Column Subassemblages Under Repeated Loading," by V. V. Bertero - 1968 (PB 184 888)

EERC 68-3 "A Graphical Method for Solving the Wave Reflection-Refraction Problem," by H. D. McNiven and Y. Mengi 1968 (PB 187 943)

EERC 68-4 "Dynamic Properties of McKinley School Buildings," by D. Rea, J. G. Bouwkamp and R. W. Clough - 1968 (PB 187 902)

EERC 68-5 "Characteristics of Rock Motions During Earthquakes," by H. B. Seed, I. M. Idriss and F. W. Kiefer - 1968 (PB 188 338)

EERC 69-1 "Earthquake Engineering Research at Berkeley," - 1969 (PB 187 906)

EERC 69-2 "Nonlinear Seismic Response of Earth Structures," by M. Dibaj and J. Penzien - 1969 (PB 187 904)

EERC 69-3 "Probabilistic Study of the Behavior of Structures During Earthquakes," by P. Ruiz and J. Penzien - 1969 (PB 187 886)

EERC 69-4 "Numerical Solution of Boundary Value Problems in Structural Mechanics by Reduction to an Initial Value Formulation," by N. Distefano and J. Schujman - 1969 (PB 187 942)

EERC 69-5 "Dynamic Programming and the Solution of the Biharmonic Equation," by N. Distefano - 1969 (PB 187 941)

Note: Numbers in parenthesis are Accession Numbers assigned by the National Technical Information Service. Copies of these reports may be ordered from the National Technical Information Service, 5285 Port Royal Road, Springfield, Virginia, 22161. Accession Numbers should be quoted on orders for the reports (PB --- ---) and remittance must accompany each order. (Foreign orders, add $2.50 extra for mailing charges.) Those reports without this information listed are not yet available from NTIS. Upon request, EERC will mail inquirers this information when it becomes available to us.

EERC 69-6 "Stochastic Analysis of Offshore Tower Structures," by A. K. Malhotra and J. Penzien - 1969 (PB 187 903)

EERC 69-7 "Rock Motion Accelerograms for High Magnitude Earthquakes," by H. B. Seed and I. M. Idriss - 1969 (PB 187 940)

EERC 69-8 "Structural Dynamics Testing Facilities at the University of California, Berkeley," by R. M. Stephen, J. G. Bouwkamp, R. W. Clough and J. Penzien - 1969 (PB 189 111)

EERC 69-9 "Seismic Response of Soil Deposits Underlain by Sloping Rock Boundaries," by H. Dezfulian and H. B. Seed - 1969 (PB 189 114)

EERC 69-10 "Dynamic Stress Analysis of Axisymmetric Structures under Arbitrary Loading," by S. Ghosh and E. L. Wilson - 1969 (PB 189 026)

EERC 69-11 "Seismic Behavior of Multistory Frames Designed by Different Philosophies," by J. C. Anderson and V. V. Bertero - 1969 (PB 190 662)

EERC 69-12 "Stiffness Degradation of Reinforcing Concrete Structures Subjected to Reversed Actions," by V. V. Bertero, B. Bresler and H. Ming Liao - 1969 (PB 202 942)

EERC 69-13 "Response of Non-Uniform Soil Deposits to Travel Seismic Waves," by H. Dezfulian and H. B. Seed - 1969 (PB 191 023)

EERC 69-14 "Damping Capacity of a Model Steel Structure," by D. Rea, R. W. Clough and J. G. Bouwkamp - 1969 (PB 190 663)

EERC 69-15 "Influence of Local Soil Conditions on Building Damage Potential during Earthquakes," by H. B. Seed and I. M. Idriss - 1969 (PB 191 036)

EERC 69-16 "The Behavior of Sands under Seismic Loading Conditions," by M. L. Silver and H. B. Seed - 1969 (AD 714 982)

EERC 70-1 "Earthquake Response of Concrete Gravity Dams," by A. K. Chopra - 1970 (AD 709 640)

EERC 70-2 "Relationships between Soil Conditions and Building Damage in the Caracas Earthquake of July 29, 1967," by H. B. Seed, I. M. Idriss and H. Dezfulian - 1970 (PB 195 762)

EERC 70-3 "Cyclic Loading of Full Size Steel Connections," by E. P. Popov and R. M. Stephen - 1970 (PB 213 545)

EERC 70-4 "Seismic Analysis of the Charaima Building, Caraballeda, Venezuela," by Subcommittee of the SEAONC Research Committee: V. V. Bertero, P. F. Fratessa, S. A. Mahin, J. H. Sexton, A. C. Scordelis, E. L. Wilson, L. A. Wyllie, H. B. Seed and J. Penzien, Chairman - 1970 (PB 201 455)

EERC 70-5 "A Computer Program for Earthquake Analysis of Dams," by A. K. Chopra and P. Chakrabarti - 1970 (AD 723 994)

EERC 70-6 "The Propagation of Love Waves across Non-Horizontally Layered Structures," by J. Lysmer and L. A. Drake - 1970 (PB 197 896)

EERC 70-7 "Influence of Base Rock Characteristics on Ground Response," by J. Lysmer, H. B. Seed and P. B. Schnabel - 1970 (PB 197 897)

EERC 70-8 "Applicability of Laboratory Test Procedures for Measuring Soil Liquefaction Characteristics under Cyclic Loading," by H. B. Seed and W. H. Peacock - 1970 (PB 198 016)

EERC 70-9 "A Simplified Procedure for Evaluating Soil Liquefaction Potential," by H. B. Seed and I. M. Idriss - 1970 (PB 198 009)

EERC 70-10 "Soil Moduli and Damping Factors for Dynamic Response Analysis," by H. B. Seed and I. M. Idriss - 1970 (PB 197 869)

EERC 71-1 "Koyna Earthquake and the Performance of Koyna Dam," by A. K. Chopra and P. Chakrabarti - 1971 (AD 731 496)

EERC 71-2 "Preliminary In-Situ Measurements of Anelastic Absorption in Soils Using a Prototype Earthquake Simulator," by R. D. Borcherdt and P. W. Rodgers - 1971 (PB 201 454)

EERC 71-3 "Static and Dynamic Analysis of Inelastic Frame Structures," by F. L. Porter and G. H. Powell - 1971 (PB 210 135)

EERC 71-4 "Research Needs in Limit Design of Reinforced Concrete Structures," by V. V. Bertero - 1971 (PB 202 943)

EERC 71-5 "Dynamic Behavior of a High-Rise Diagonally Braced Steel Building," by D. Rea, A. A. Shah and J. G. Bouwkamp - 1971 (PB 203 584)

EERC 71-6 "Dynamic Stress Analysis of Porous Elastic Solids Saturated with Compressible Fluids," by J. Ghaboussi and E. L. Wilson - 1971 (PB 211 396)

EERC 71-7 "Inelastic Behavior of Steel Beam-to-Column Subassemblages," by H. Krawinkler, V. V. Bertero and E. P. Popov - 1971 (PB 211 335)

EERC 71-8 "Modification of Seismograph Records for Effects of Local Soil Conditions," by P. Schnabel, H. B. Seed and J. Lysmer - 1971 (PB 214 450)

EERC 72-1 "Static and Earthquake Analysis of Three Dimensional Frame and Shear Wall Buildings," by E. L. Wilson and H. H. Dovey - 1972 (PB 212 904)

EERC 72-2 "Accelerations in Rock for Earthquakes in the Western United States," by P. B. Schnabel and H. B. Seed - 1972 (PB 213 100)

EERC 72-3 "Elastic-Plastic Earthquake Response of Soil-Building Systems," by T. Minami - 1972 (PB 214 868)

EERC 72-4 "Stochastic Inelastic Response of Offshore Towers to Strong Motion Earthquakes," by M. K. Kaul - 1972 (PB 215 713)

EERC 72-5 "Cyclic Behavior of Three Reinforced Concrete Flexural Members with High Shear," by E. P. Popov, V. V. Bertero and H. Krawinkler - 1972 (PB 214 555)

EERC 72-6 "Earthquake Response of Gravity Dams Including Reservoir Interaction Effects," by P. Chakrabarti and A. K. Chopra - 1972 (AD 762 330)

EERC 72-7 "Dynamic Properties on Pine Flat Dam," by D. Rea, C. Y. Liaw and A. K. Chopra - 1972 (AD 763 928)

EERC 72-8 "Three Dimensional Analysis of Building Systems," by E. L. Wilson and H. H. Dovey - 1972 (PB 222 438)

EERC 72-9 "Rate of Loading Effects on Uncracked and Repaired Reinforced Concrete Members," by S. Mahin, V. V. Bertero, D. Rea and M. Atalay - 1972 (PB 224 520)

EERC 72-10 "Computer Program for Static and Dynamic Analysis of Linear Structural Systems," by E. L. Wilson, K.-J. Bathe, J. E. Peterson and H. H. Dovey - 1972 (PB 220 437)

EERC 72-11 "Literature Survey - Seismic Effects on Highway Bridges," by T. Iwasaki, J. Penzien and R. W. Clough - 1972 (PB 215 613)

EERC 72-12 "SHAKE-A Computer Program for Earthquake Response Analysis of Horizontally Layered Sites," by P. B. Schnabel and J. Lysmer - 1972 (PB 220 207)

EERC 73-1 "Optimal Seismic Design of Multistory Frames," by V. V. Bertero and H. Kamil - 1973

EERC 73-2 "Analysis of the Slides in the San Fernando Dams during the Earthquake of February 9, 1971," by H. B. Seed, K. L. Lee, I. M. Idriss and F. Makdisi - 1973 (PB 223 402)

EERC 73-3 "Computer Aided Ultimate Load Design of Unbraced Multistory Steel Frames," by M. B. El-Hafez and G. H. Powell - 1973

EERC 73-4 "Experimental Investigation into the Seismic Behavior of Critical Regions of Reinforced Concrete Components as Influenced by Moment and Shear," by M. Celebi and J. Penzien - 1973 (PB 215 884)

EERC 73-5 "Hysteretic Behavior of Epoxy-Repaired Reinforced Concrete Beams," by M. Celebi and J. Penzien - 1973

EERC 73-6 "General Purpose Computer Program for Inelastic Dynamic Response of Plane Structures," by A. Kanaan and G. H. Powell - 1973 (PB 221 260)

EERC 73-7 "A Computer Program for Earthquake Analysis of Gravity Dams Including Reservoir Interaction," by P. Chakrabarti and A. K. Chopra - 1973 (AD 766 271)

EERC 73-8 "Behavior of Reinforced Concrete Deep Beam-Column Subassemblages under Cyclic Loads," by O. Kustu and J. G. Bouwkamp - 1973

EERC 73-9 "Earthquake Analysis of Structure-Foundation Systems," by A. K. Vaish and A. K. Chopra - 1973 (AD 766 272)

EERC 73-10 "Deconvolution of Seismic Response for Linear Systems," by R. B. Reimer - 1973 (PB 227 179)

EERC 73-11 "SAP IV: A Structural Analysis Program for Static and Dynamic Response of Linear Systems," by K.-J. Bathe, E. L. Wilson and F. E. Peterson - 1973 (PB 221 967)

EERC 73-12 "Analytical Investigations of the Seismic Response of Long, Multiple Span Highway Bridges," by W. S. Tseng and J. Penzien - 1973 (PB 227 816)

EERC 73-13 "Earthquake Analysis of Multi-Story Buildings Including Foundation Interaction," by A. K. Chopra and J. A. Gutierrez - 1973 (PB 222 970)

EERC 73-14 "ADAP: A Computer Program for Static and Dynamic Analysis of Arch Dams," by R. W. Clough, J. M. Raphael and S. Majtahedi - 1973 (PB 223 763)

EERC 73-15 "Cyclic Plastic Analysis of Structural Steel Joints," by R. B. Pinkney and R. W. Clough - 1973 (PB 226 843)

EERC 73-16 "QUAD-4: A Computer Program for Evaluating the Seismic Response of Soil Structures by Variable Damping Finite Element Procedures," by I. M. Idriss, J. Lysmer, R. Hwang and H. B. Seed - 1973 (PB 229 424)

EERC 73-17 "Dynamic Behavior of a Multi-Story Pyramid Shaped Building," by R. M. Stephen and J. G. Bouwkamp - 1973

EERC 73-18 "Effect of Different Types of Reinforcing on Seismic Behavior of Short Concrete Columns," by V. V. Bertero, J. Hollings, O. Kustu, R. M. Stephen and J. G. Bouwkamp - 1973

EERC 73-19 "Olive View Medical Center Material Studies, Phase I," by B. Bresler and V. V. Bertero - 1973 (PB 235 986)

EERC 73-20 "Linear and Nonlinear Seismic Analysis Computer Programs for Long Multiple-Span Highway Bridges," by W. S. Tseng and J. Penzien - 1973

EERC 73-21 "Constitutive Models for Cyclic Plastic Deformation of Engineering Materials," by J. M. Kelly and P. P. Gillis - 1973 (PB 226 024)

EERC 73-22 "DRAIN - 2D User's Guide," by G. H. Powell - 1973 (PB 227 016)

EERC 73-23 "Earthquake Engineering at Berkeley - 1973" - 1973 (PB 226 033)

EERC 73-24 Unassigned

EERC 73-25 "Earthquake Response of Axisymmetric Tower Structures Surrounded by Water," by C. Y. Liaw and A. K. Chopra - 1973 (AD 773 052)

EERC 73-26 "Investigation of the Failures of the Olive View Stairtowers during the San Fernando Earthquake and Their Implications in Seismic Design," by V. V. Bertero and R. G. Collins - 1973 (PB 235 106)

EERC 73-27 "Further Studies on Seismic Behavior of Steel Beam-Column Subassemblages," by V. V. Bertero, H. Krawinkler and E. P. Popov - 1973 (PB 234 172)

EERC 74-1 "Seismic Risk Analysis," by C. S. Oliveira - 1974 (PB 235 920)

EERC 74-2 "Settlement and Liquefaction of Sands under Multi-Directional Shaking," by R. Pyke, C. K. Chan and H. B. Seed - 1974

EERC 74-3 "Optimum Design of Earthquake Resistant Shear Buildings," by D. Ray, K. S. Pister and A. K. Chopra - 1974 (PB 231 172)

EERC 74-4 "LUSH - A Computer Program for Complex Response Analysis of Soil-Structure Systems," by J. Lysmer, T. Udaka, H. B. Seed and R. Hwang - 1974 (PB 236 796)

EERC 74-5 "Sensitivity Analysis for Hysteretic Dynamic Systems: Applications to Earthquake Engineering," by D. Ray - 1974 (PB 233 213)

EERC 74-6 "Soil-Structure Interaction Analyses for Evaluating Seismic Response," by H. B. Seed, J. Lysmer and R. Hwang - 1974 (PB 236 519)

EERC 74-7 Unassigned

EERC 74-8 "Shaking Table Tests of a Steel Frame - A Progress Report," by R. W. Clough and D. Tang - 1974

EERC 74-9 "Hysteretic Behavior of Reinforced Concrete Flexural Members with Special Web Reinforcement," by V. V. Bertero, E. P. Popov and T. Y. Wang - 1974 (PB 236 797)

EERC 74-10 "Applications of Reliability-Based, Global Cost Optimization to Design of Earthquake Resistant Structures," by E. Vitiello and K. S. Pister - 1974 (PB 237 231)

EERC 74-11 "Liquefaction of Gravelly Soils under Cyclic Loading Conditions," by R. T. Wong, H. B. Seed and C. K. Chan - 1974

EERC 74-12 "Site-Dependent Spectra for Earthquake-Resistant Design," by H. B. Seed, C. Ugas and J. Lysmer - 1974

EERC 74-13 "Earthquake Simulator Study of a Reinforced Concrete Frame," by P. Hidalgo and R. W. Clough - 1974 (PB 241 944)

EERC 74-14 "Nonlinear Earthquake Response of Concrete Gravity Dams," by N. Pal - 1974 (AD/A006583)

EERC 74-15 "Modeling and Identification in Nonlinear Structural Dynamics, I - One Degree of Freedom Models," by N. Distefano and A. Rath - 1974 (PB 241 548)

EERC 75-1 "Determination of Seismic Design Criteria for the Dumbarton Bridge Replacement Structure, Vol. I: Description, Theory and Analytical Modeling of Bridge and Parameters," by F. Baron and S.-H. Pang - 1975

EERC 75-2 "Determination of Seismic Design Criteria for the Dumbarton Bridge Replacement Structure, Vol. 2: Numerical Studies and Establishment of Seismic Design Criteria," by F. Baron and S.-H. Pang - 1975

EERC 75-3 "Seismic Risk Analysis for a Site and a Metropolitan Area," by C. S. Oliveira - 1975

EERC 75-4 "Analytical Investigations of Seismic Response of Short, Single or Multiple-Span Highway Bridges," by Ma-chi Chen and J. Penzien - 1975 (PB 241 454)

EERC 75-5 "An Evaluation of Some Methods for Predicting Seismic Behavior of Reinforced Concrete Buildings," by Stephen A. Mahin and V. V. Bertero - 1975

EERC 75-6 "Earthquake Simulator Study of a Steel Frame Structure, Vol. I: Experimental Results," by R. W. Clough and David T. Tang - 1975 (PB 243 981)

EERC 75-7 "Dynamic Properties of San Bernardino Intake Tower," by Dixon Rea, C.-Y. Liaw, and Anil K. Chopra - 1975 (AD/A008406)

EERC 75-8 "Seismic Studies of the Articulation for the Dumbarton Bridge Replacement Structure, Vol. I: Description, Theory and Analytical Modeling of Bridge Components," by F. Baron and R. E. Hamati - 1975

EERC 75-9 "Seismic Studies of the Articulation for the Dumbarton Bridge Replacement Structure, Vol. 2: Numerical Studies of Steel and Concrete Girder Alternates," by F. Baron and R. E. Hamati - 1975

EERC 75-10 "Static and Dynamic Analysis of Nonlinear Structures," by Digambar P. Mondkar and Graham H. Powell - 1975 (PB 242 434)

EERC 75-11 "Hysteretic Behavior of Steel Columns," by E. P. Popov, V. V. Bertero and S. Chandramouli - 1975

EERC 75-12 "Earthquake Engineering Research Center Library Printed Catalog" - 1975 (PB 243 711)

EERC 75-13 "Three Dimensional Analysis of Building Systems," Extended Version, by E. L. Wilson, J. P. Hollings and H. H. Dovey - 1975 (PB 243 989)

EERC 75-14 "Determination of Soil Liquefaction Characteristics by Large-Scale Laboratory Tests," by Pedro De Alba, Clarence K. Chan and H. Bolton Seed - 1975

EERC 75-15 "A Literature Survey - Compressive, Tensile, Bond and Shear Strength of Masonry," by Ronald L. Mayes and Ray W. Clough - 1975

EERC 75-16 "Hysteretic Behavior of Ductile Moment Resisting Reinforced Concrete Frame Components," by V. V. Bertero and E. P. Popov - 1975

EERC 75-17 "Relationships Between Maximum Acceleration, Maximum Velocity, Distance from Source, Local Site Conditions for Moderately Strong Earthquakes," by H. Bolton Seed, Ramesh Murarka, John Lysmer and I. M. Idriss - 1975

EERC 75-18 "The Effects of Method of Sample Preparation on the Cyclic Stress-Strain Behavior of Sands," by J. Paul Mulilis, Clarence K. Chan and H. Bolton Seed - 1975

EERC 75-19 "The Seismic Behavior of Critical Regions of Reinforced Concrete Components as Influenced by Moment, Shear and Axial Force," by B. Atalay and J. Penzien - 1975

EERC 75-20 "Dynamic Properties of an Eleven Story Masonry Building," by R. M. Stephen, J. P. Hollings, J. G. Bouwkamp and D. Jurukovski - 1975

EERC 75-21 "State-of-the-Art in Seismic Shear Strength of Masonry - An Evaluation and Review," by Ronald L. Mayes and Ray W. Clough - 1975

EERC 75-22 "Frequency Dependencies Stiffness Matrices for Viscoelastic Half-Plane Foundations," by Anil K. Chopra, P. Chakrabarti and Gautam Dasgupta - 1975

EERC 75-23 "Hysteretic Behavior of Reinforced Concrete Framed Walls," by T. Y. Wong, V. V. Bertero and E. P. Popov - 1975

EERC 75-24 "Testing Facility for Subassemblages of Frame-Wall Structural Systems," by V. V. Bertero, E. P. Popov and T. Endo - 1975

EERC 75-25 "Influence of Seismic History of the Liquefaction Characteristics of Sands," by H. Bolton Seed, Kenji Mori and Clarence K. Chan - 1975

EERC 75-26 "The Generation and Dissipation of Pore Water Pressures during Soil Liquefaction," by H. Bolton Seed, Phillippe P. Martin and John Lysmer - 1975

EERC 75-27 "Identification of Research Needs for Improving a Seismic Design of Building Structures," by V. V. Bertero - 1975

EERC 75-28 "Evaluation of Soil Liquefaction Potential during Earthquakes," by H. Bolton Seed, I. Arango and Clarence K. Chan 1975

EERC 75-29 "Representation of Irregular Stress Time Histories by Equivalent Uniform Stress Series in Liquefaction Analyses," by H. Bolton Seed, I. M. Idriss, F. Makdisi and N. Banerjee 1975

EERC 75-30 "FLUSH - A Computer Program for Approximate 3-D Analysis of Soil-Structure Interaction Problems," by J. Lysmer, T. Udaka, C.-F. Tsai and H. B. Seed - 1975

EERC 75-31 "ALUSH - A Computer Program for Seismic Response Analysis of Axisymmetric Soil-Structure Systems," by E. Berger, J. Lysmer and H. B. Seed - 1975

EERC 75-32 "TRIP and TRAVEL - Computer Programs for Soil-Structure Interaction Analysis with Horizontally Travelling Waves," by T. Udaka, J. Lysmer and H. B. Seed - 1975

EERC 75-33 "Predicting the Performance of Structures in Regions of High Seismicity," by Joseph Penzien - 1975

EERC 75-34 "Efficient Finite Element Analysis of Seismic Structure - Soil - Direction," by J. Lysmer, H. Bolton Seed, T. Udaka, R. N. Hwang and C.-F. Tsai - 1975

EERC 75-35 "The Dynamic Behavior of a First Story Girder of a Three-Story Steel Frame Subjected to Earthquake Loading," by Ray W. Clough and Lap-Yan Li - 1975

EERC 75-36 "Earthquake Simulator Study of a Steel Frame Structure, Volume II - Analytical Results," by David T. Tang - 1975

EERC 75-37 "ANSR-I General Purpose Computer Program for Analysis of Non-Linear Structure Response," by Digambar P. Mondkar and Graham H. Powell - 1975

EERC 75-38 "Nonlinear Response Spectra for Probabilistic Seismic Design and Damage Assessment of Reinforced Concrete Structures," by Masaya Murakami and Joseph Penzien - 1975

EERC 75-39 "Study of a Method of Feasible Directions for Optimal Elastic Design of Framed Structures Subjected to Earthquake Loading," by N. D. Walker and K. S. Pister - 1975

EERC 75-40 "An Alternative Representation of the Elastic-Viscoelastic Analogy," by Gautam Dasgupta and Jerome L. Sackman - 1975

EERC 75-41 "Effect of Multi-Directional Shaking on Liquefaction of Sands," by H. Bolton Seed, Robert Pyke and Geoffrey R. Martin - 1975

EERC 76-1 "Strength and Ductility Evaluation of Existing Low-Rise Reinforced Concrete Buildings - Screening Method," by Tsuneo Okada and Boris Bresler - 1976

EERC 76-2 "Experimental and Analytical Studies on the Hysteretic Behavior of Reinforced Concrete Rectangular and T-Beams," by Shao-Yeh Marshall Ma, Egor P. Popov and Vitelmo V. Bertero - 1976

EERC 76-3 "Dynamic Behavior of a Multistory Triangular-Shaped Building," by J. Petrovski, R. M. Stephen, E. Gartenbaum and J. G. Bouwkamp - 1976

EERC 76-4 "Earthquake Induced Deformations of Earth Dams," by Norman Serff and H. Bolton Seed - 1976

EERC 76-5 "Analysis and Design of Tube-Type Tall Building Structures," by H. de Clercq and G. H. Powell - 1976

EERC 76-6 "Time and Frequency Domain Analysis of Three-Dimensional Ground Motions, San Fernando Earthquake," by Tetsuo Kubo and Joseph Penzien - 1976

EERC 76-7 "Expected Performance of Uniform Building Code Design Masonry Structures," by R. L. Mayes, Y. Omote, S. W. Chen and R. W. Clough - 1976

EERC 76-8 "Cyclic Shear Tests on Concrete Masonry Piers, Volume I Test Results," by R. L. Mayes, Y. Omote and R. W. Clough 1976